# Stress, strain, fracturing, deformation mechanisms, fluid pressure and fluid flow in folded-fractured reservoirs : what can we learn from integrated studies of natural analogues?

Sheep Mountain and Rattlesnake Mountain Anticlines (Wyoming, USA) as case studies

Olivier LACOMBE

UPMC SORBONNE UNIVERSITÉS

CNRS

Institut des Sciences de la Terre de Paris
ISTeP
SORBONNE UNIVERSITÉS

UMR 7193

The study of fold evolution has for long been based on geometrical models.

These models were used to investigate possible kinematic scenarios of folding, based on the present-day geometry of folded strata and geometrical assumptions (thickness and/or length preservation).
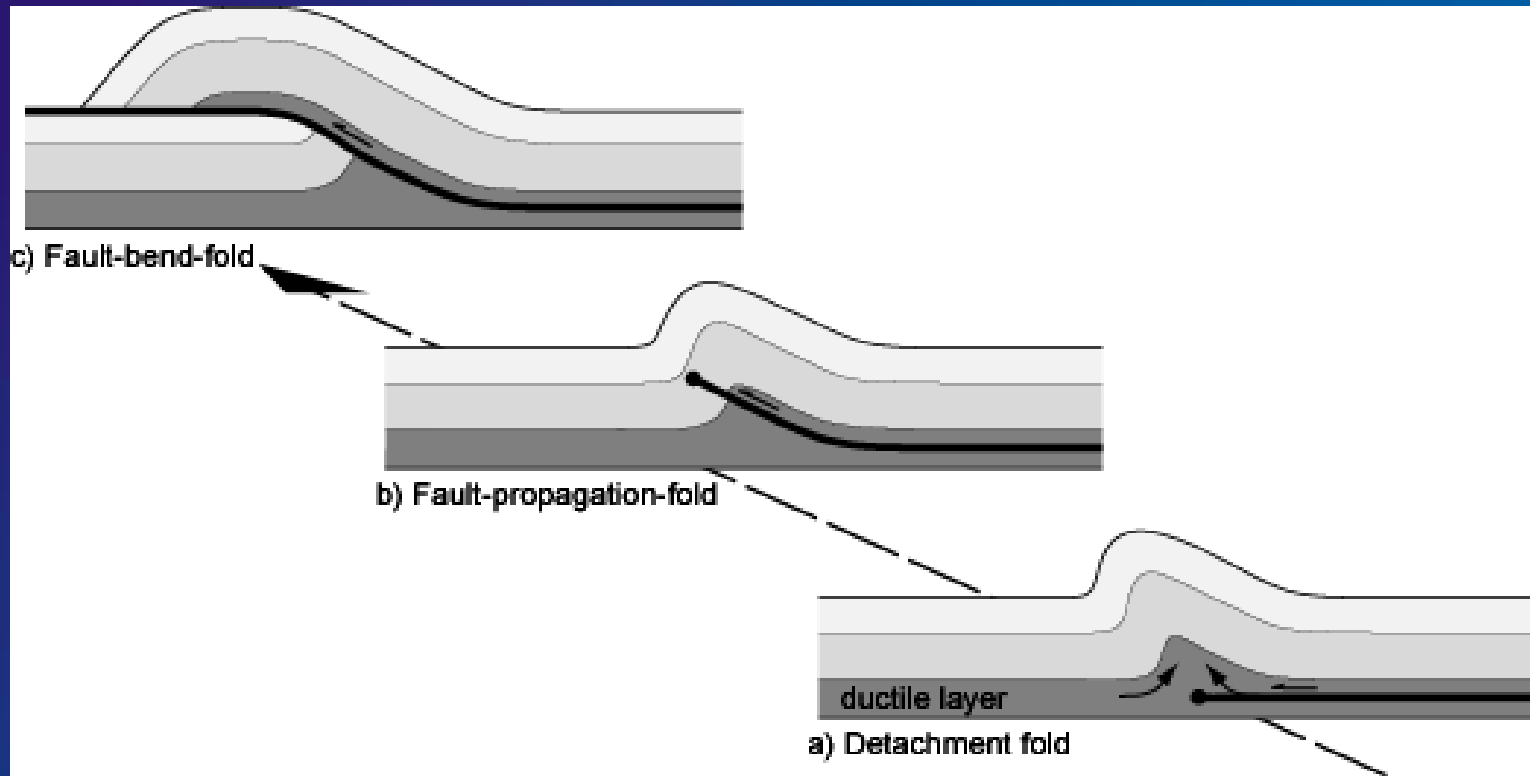

Unified model where folding modes may illustrate different stages of evolution of a single fold (Molinaro, 2004; Sherkati, 2004)
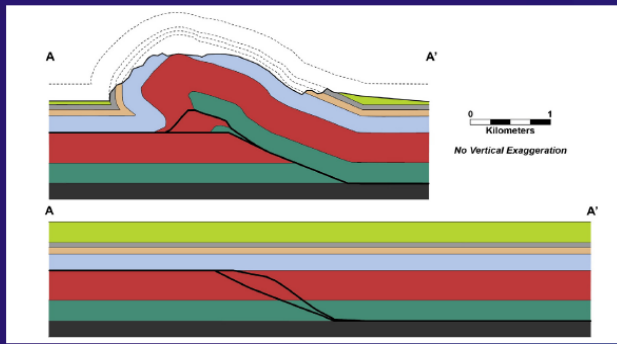
Geomechanical modeling can predict the onset of failure and the type and abundance of deformation features along with the orientations and magnitudes of stresses.

Forward models incorporate realistic mechanical stratigraphy, include faults and bedding-slip surfaces as frictional sliding interfaces, reproduce the overall geometry of the fold structures and allow tracking of stress and strain through the deformation history.

The use of inelastic constitutive relationships (e.g., elastic–plastic behavior) allows permanent strains to develop in response to loading.
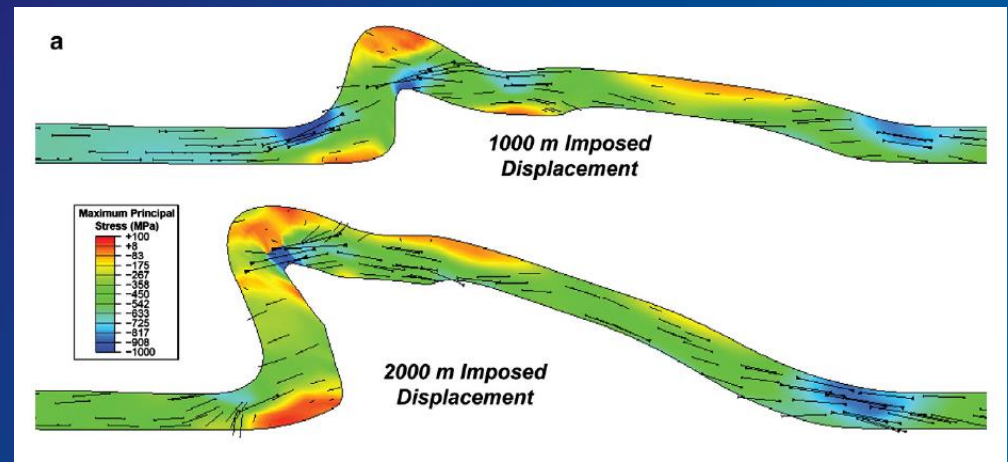
(Smart et al., 2012)
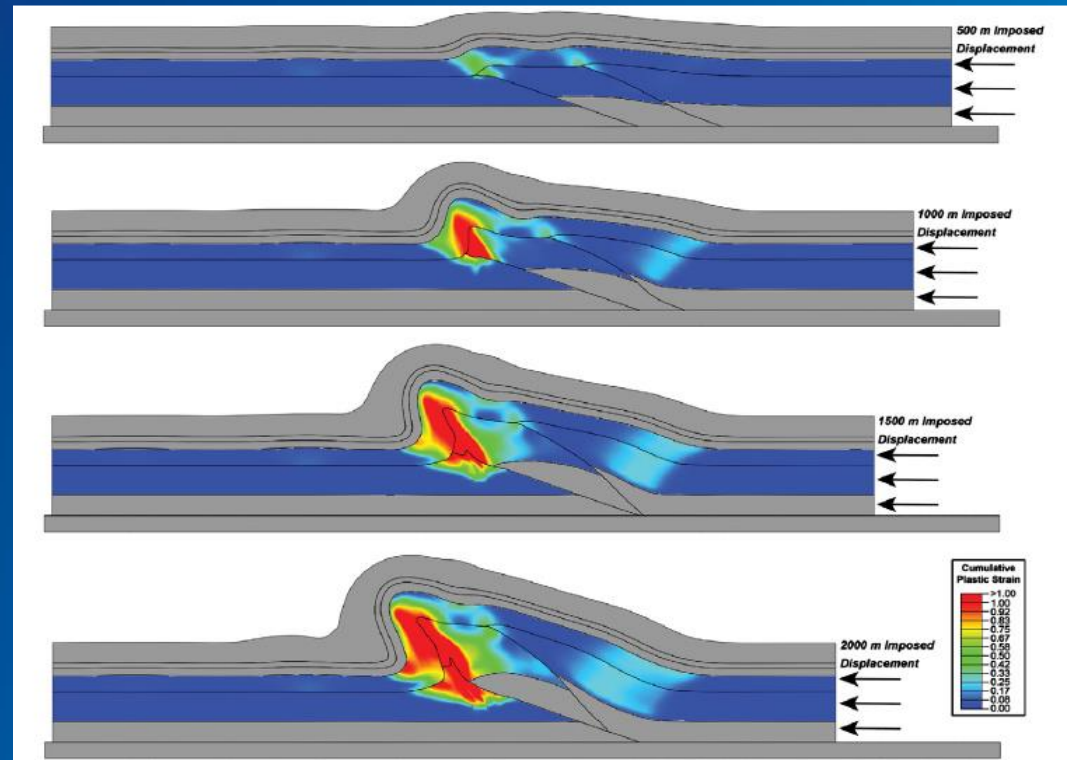
Only few works have attempted to bridge the gap between the macroscopic scale and the microscopic scale and to provide quantities like stress or strain to be compared with outputs of geomechanical models.
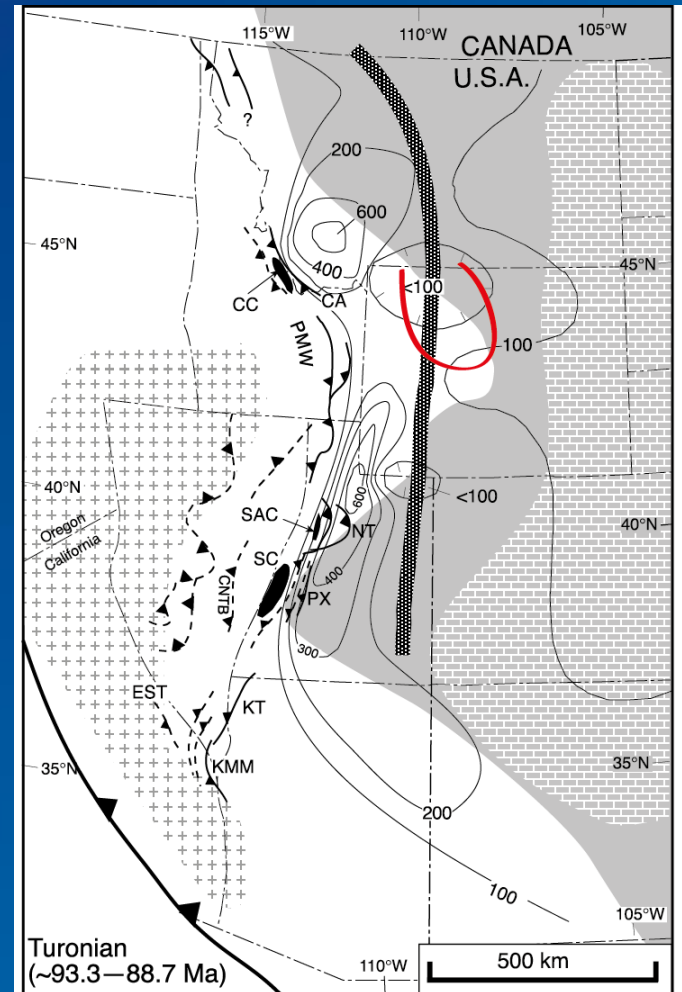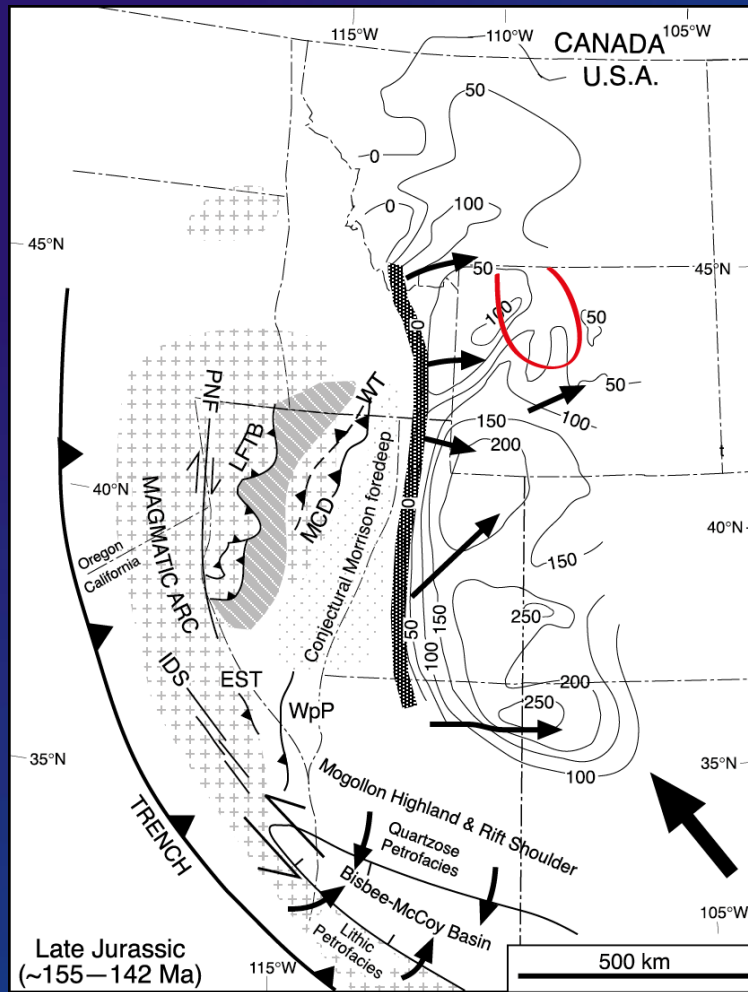
Changes in P-T-X conditions, fluid flow, fracture development as well as stress and strain pattern within folded strata are
still to be more properly linked to the geometric/kinematic macroscopic evolution of folds.

Advances in understanding deformation processes and history of folded rocks have important socio-economic implications :
accurate description and simulation of geological reservoirs for resources or waste require a good knowledge of the mechanical/hydraulical behavior of rocks when they are folded, faulted and fractured.
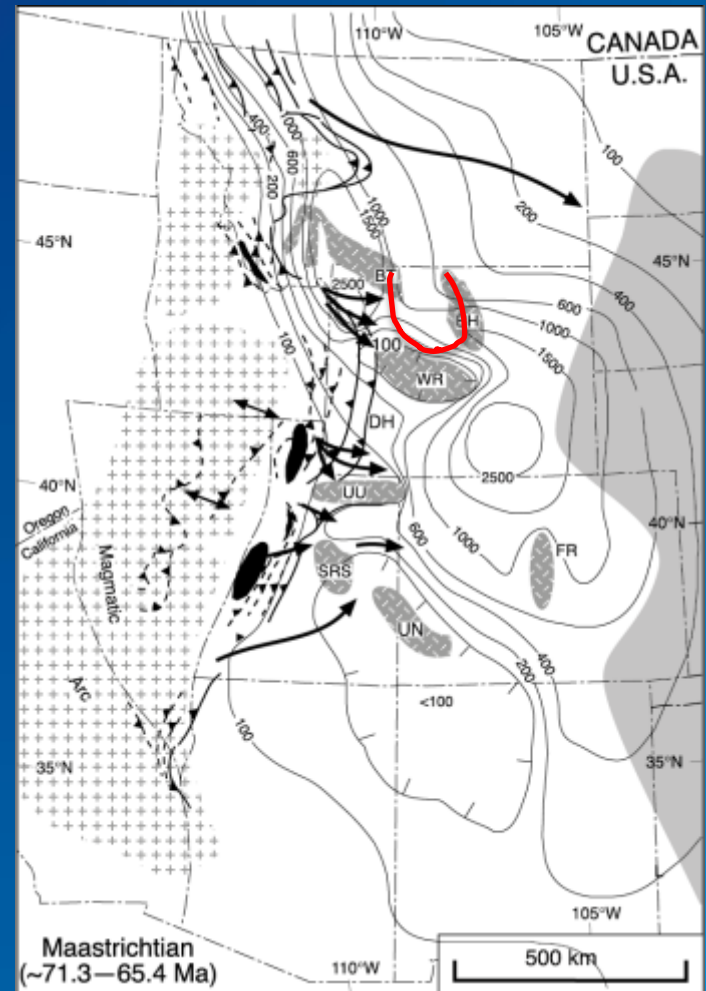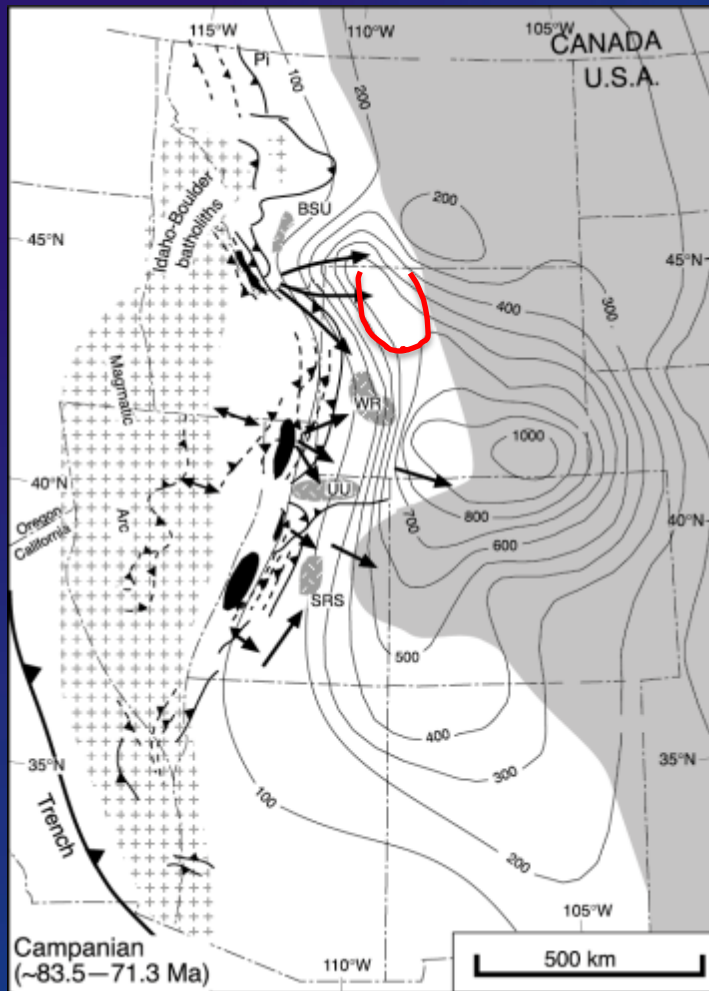
The Bighorn Basin
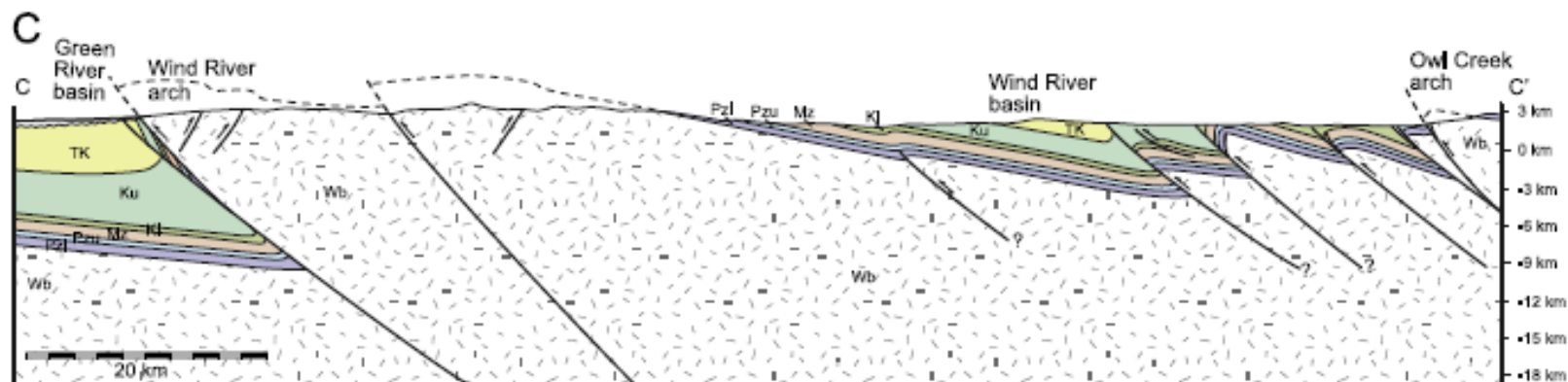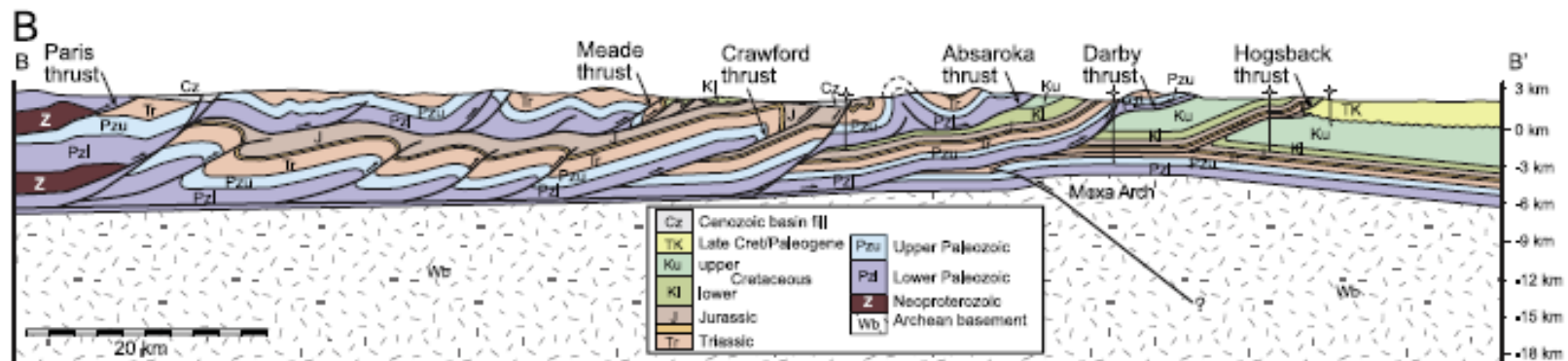# and the Sevier and Laramide orogenies
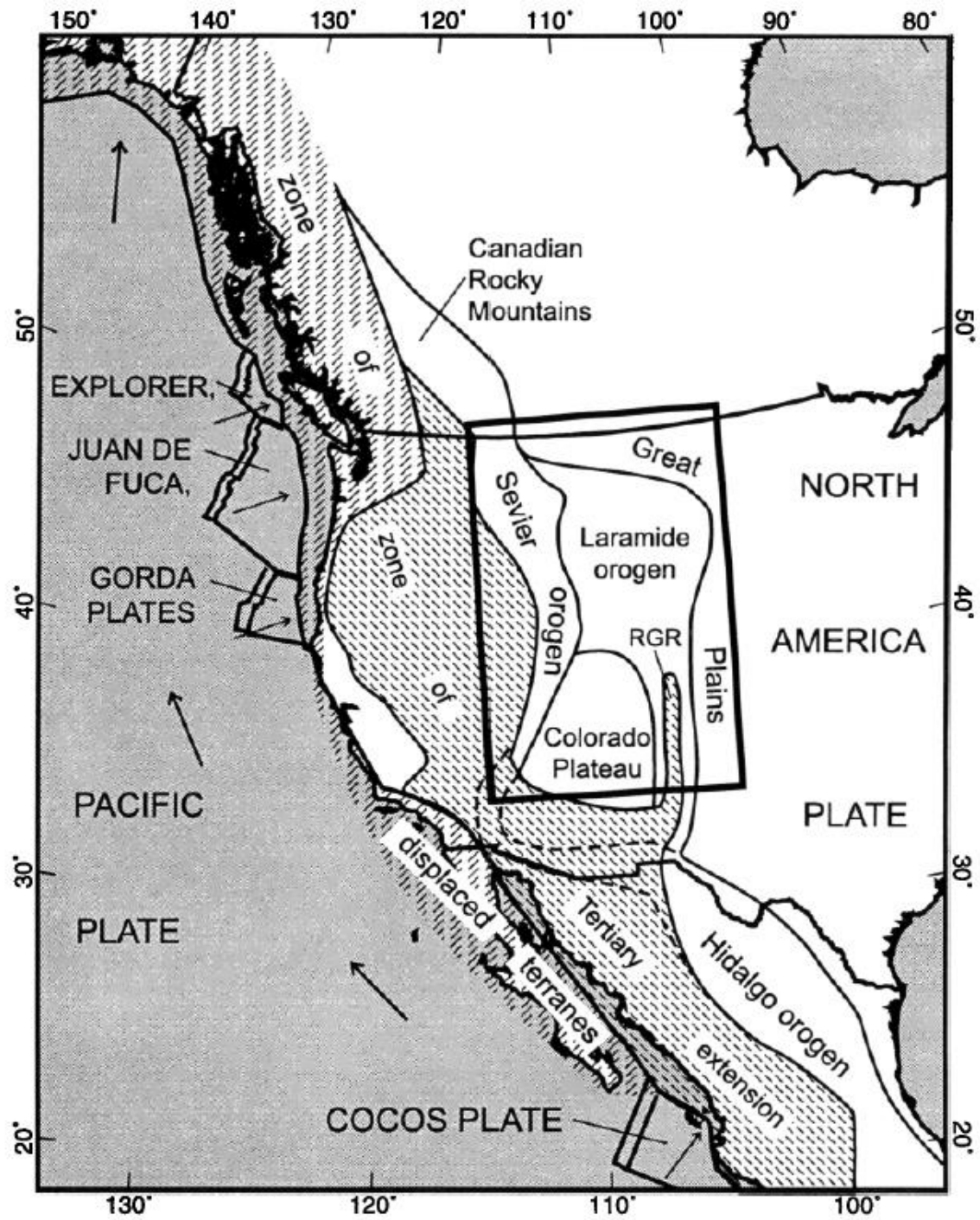
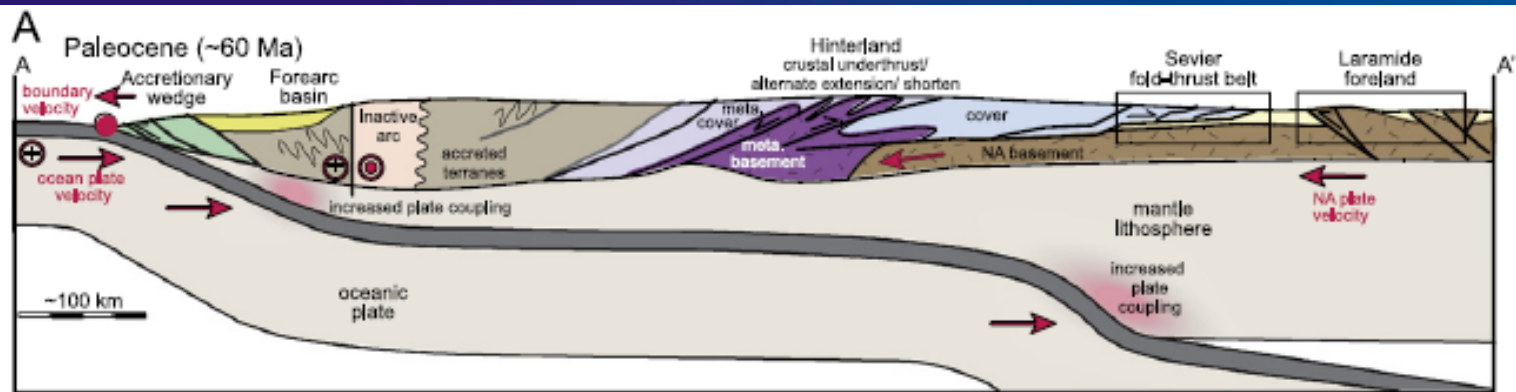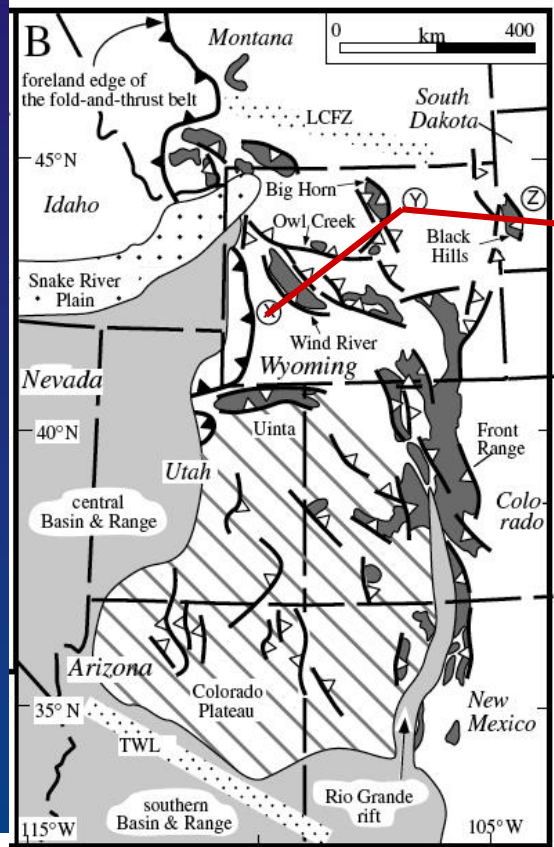# Jurassic – Cretaceous: The Western Interior Basin

(DeCelles, 2004)
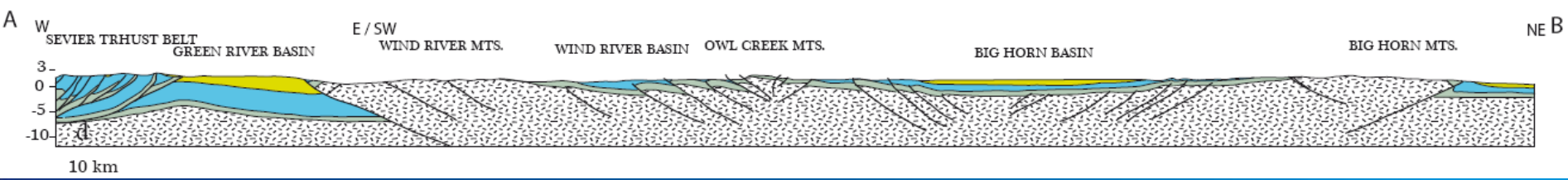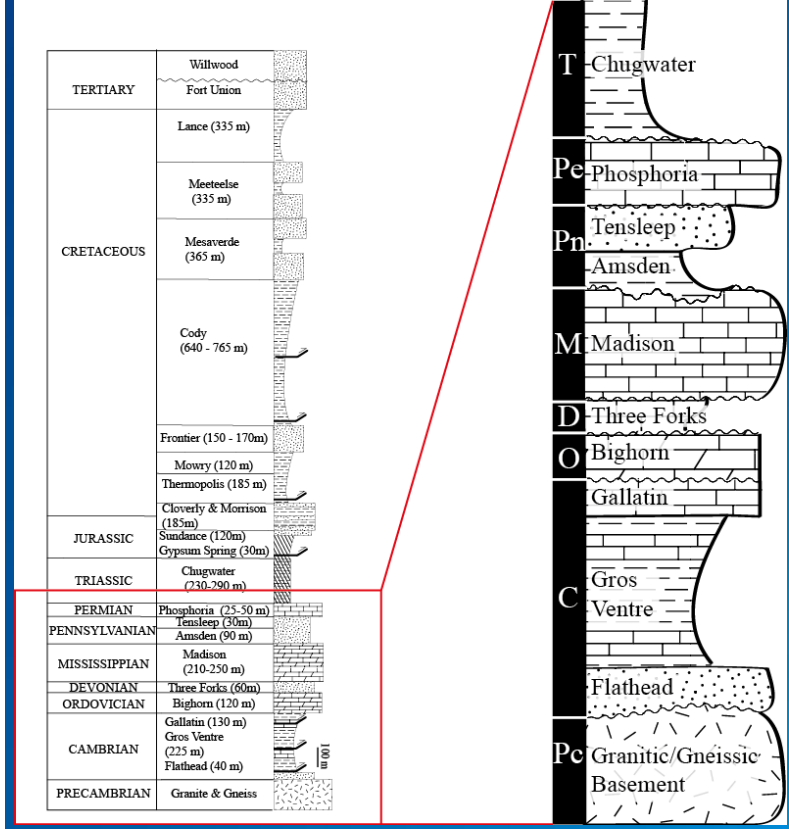
Late Cretaceous – Paleocene: The Bighorn Basin

(DeCelles, 2004)

(Weil and Yonkee, 2012)

B

Montana

foreland edge of
the fold-and-thrust belt

LCFZ

South
Dakota

45°N

Idaho

Big Horn

Owl Creek

Y

Z

Black
Hills

Snake River
Plain

Wind River

Wyoming

Nevada

40°N

Uinta

Front
Range

Utah

central
Basin & Range

Colo-
rado

Arizona

35°N

Colorado
Plateau

New
Mexico

TWL

southern
Basin & Range

Rio Grande
rift

115°W

105°W

0   km   400

(Marshak et al. ,2000)

X   Wind River Mts.   Owl Creek Mts.   Big Horn Mts.   Y Y   Black Hills   Z
GRB   WRB   BHB   PRB

mid-crustal weak zone

A   Moho   30 km

Proterozoic sea level   speculative model of Proterozoic rifts from which the Rocky Mountain evolved

B   Moho   future level of erosion

(Beaudoin et al., Basin Research , 2014)

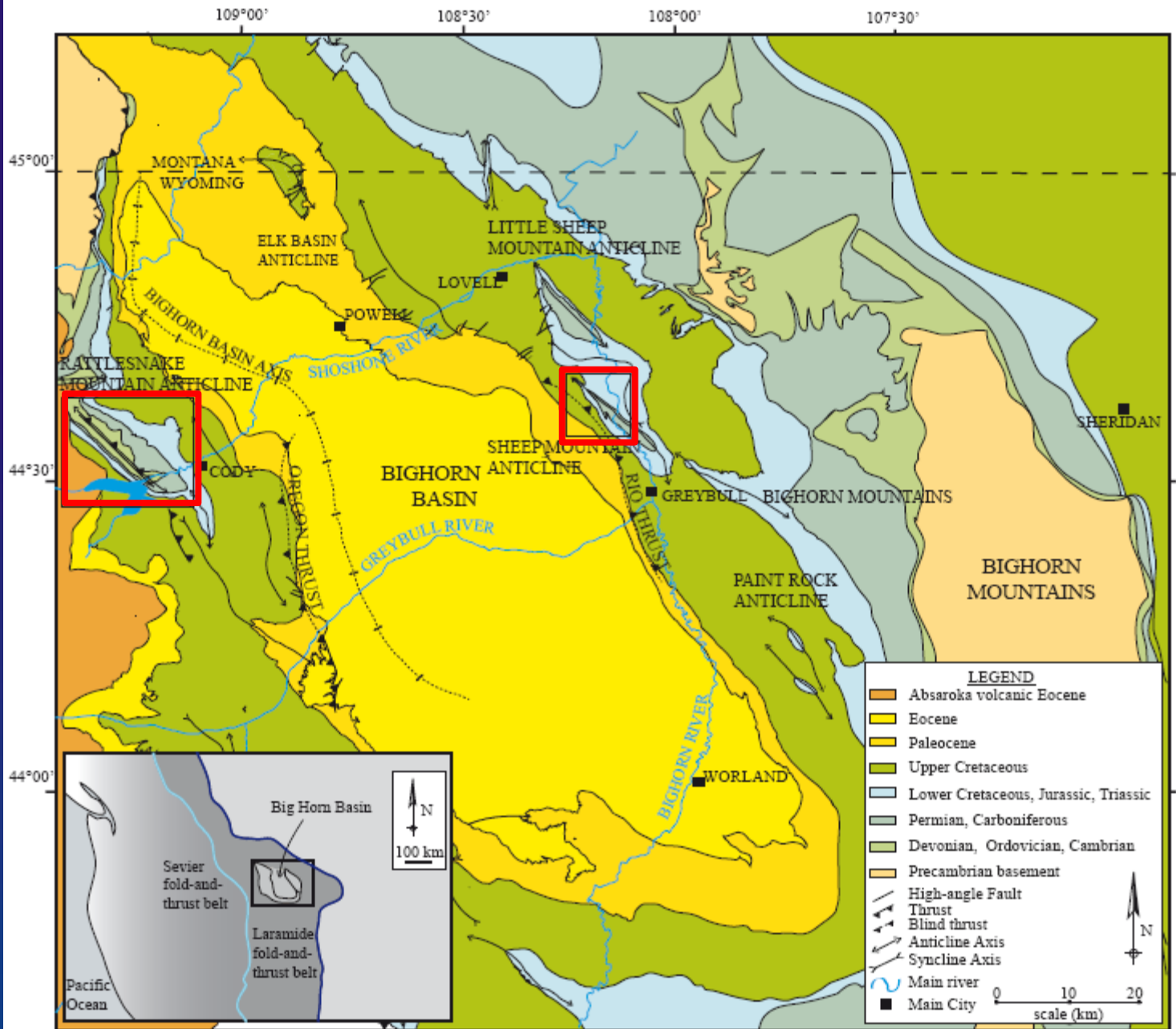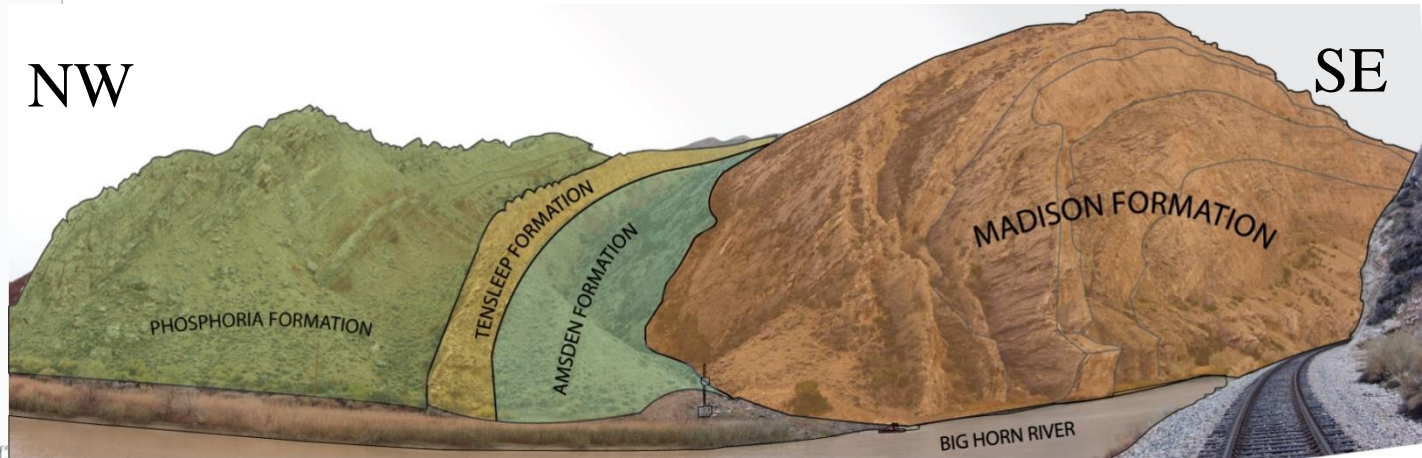# Structural, microstructural and paleo-hydrological evolution of Sheep Mountain and Rattlesnake Mountain anticlines
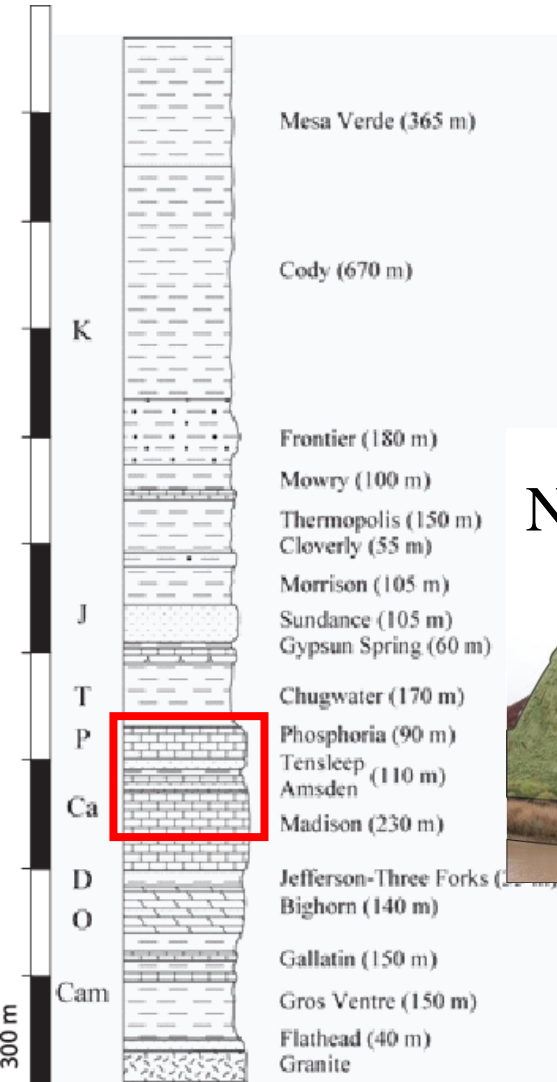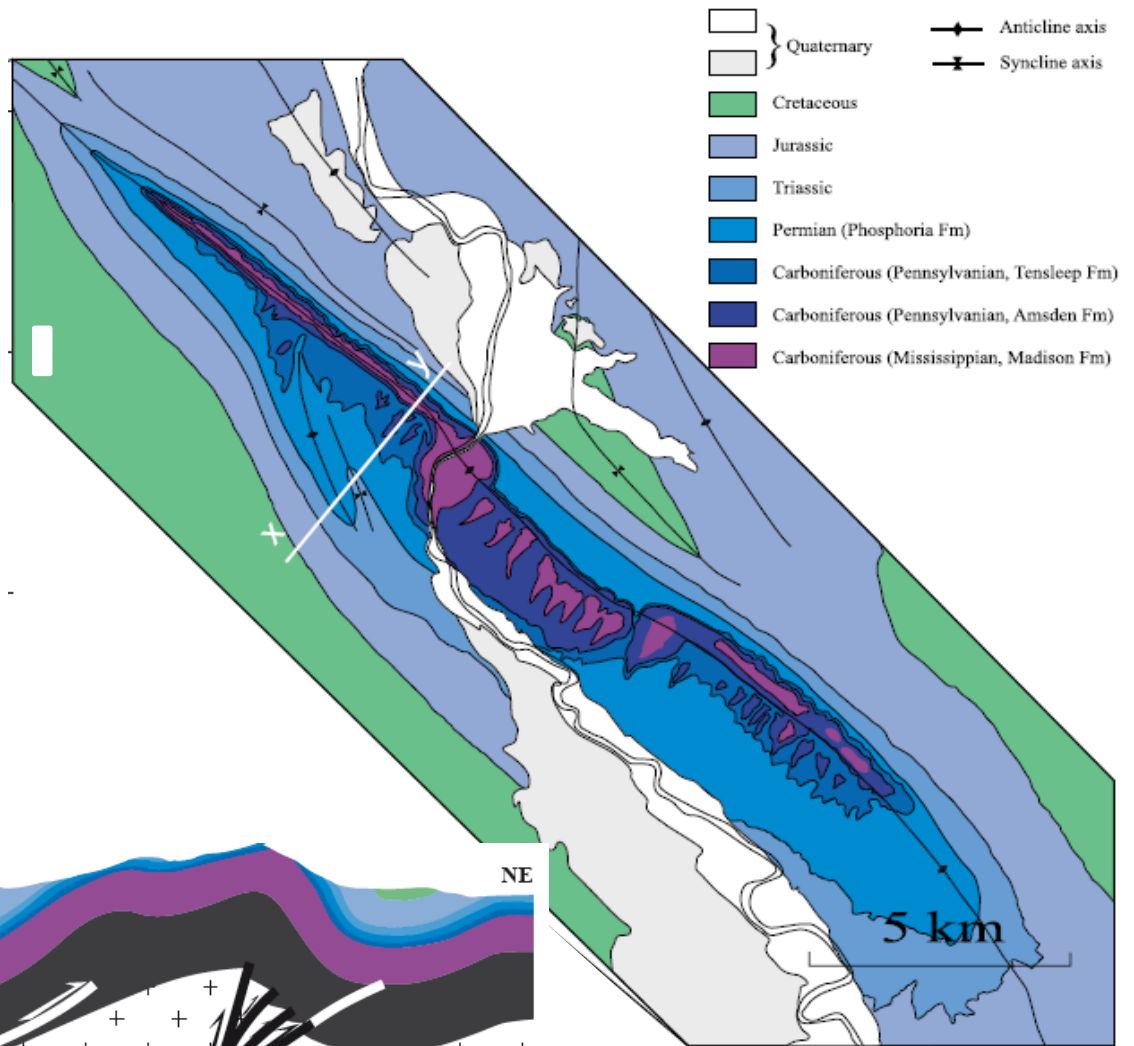
Sheep Mountain anticline
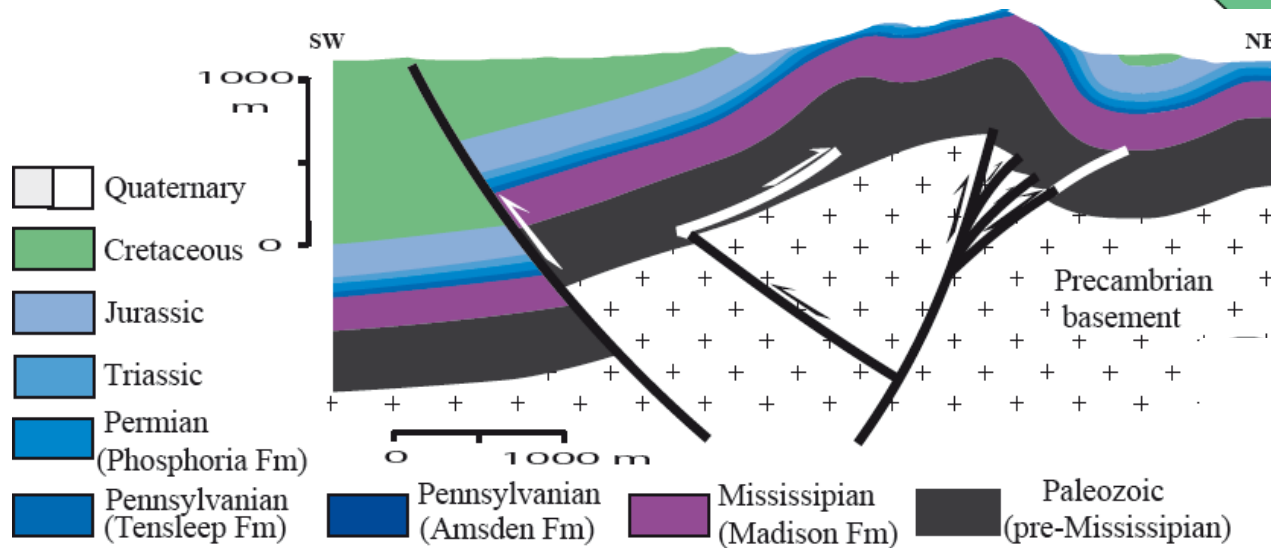
Sheep Mountain anticline

- 300 meters of exposed competent formations (mainly carbonates)
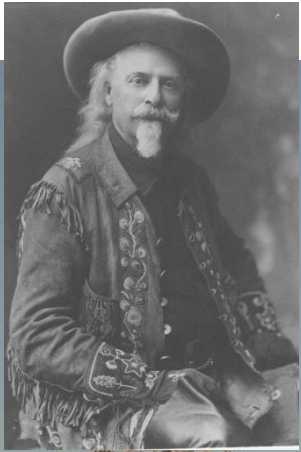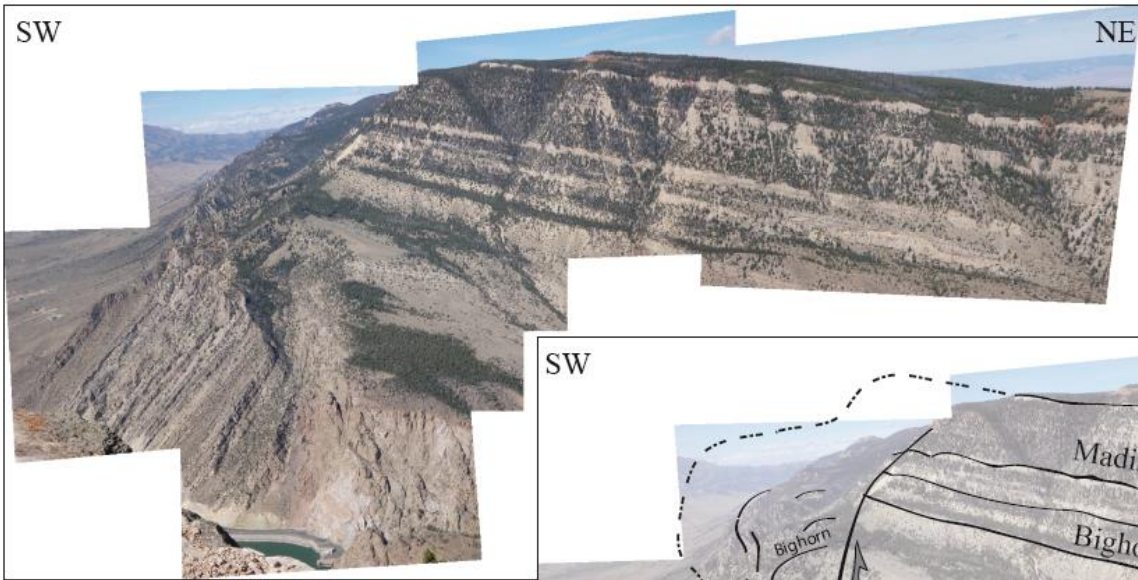- Argillaceous stratigraphic series (3000m in thickness)
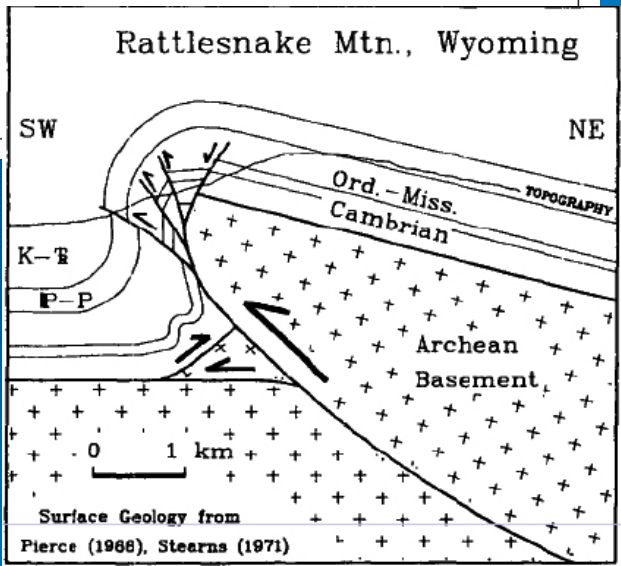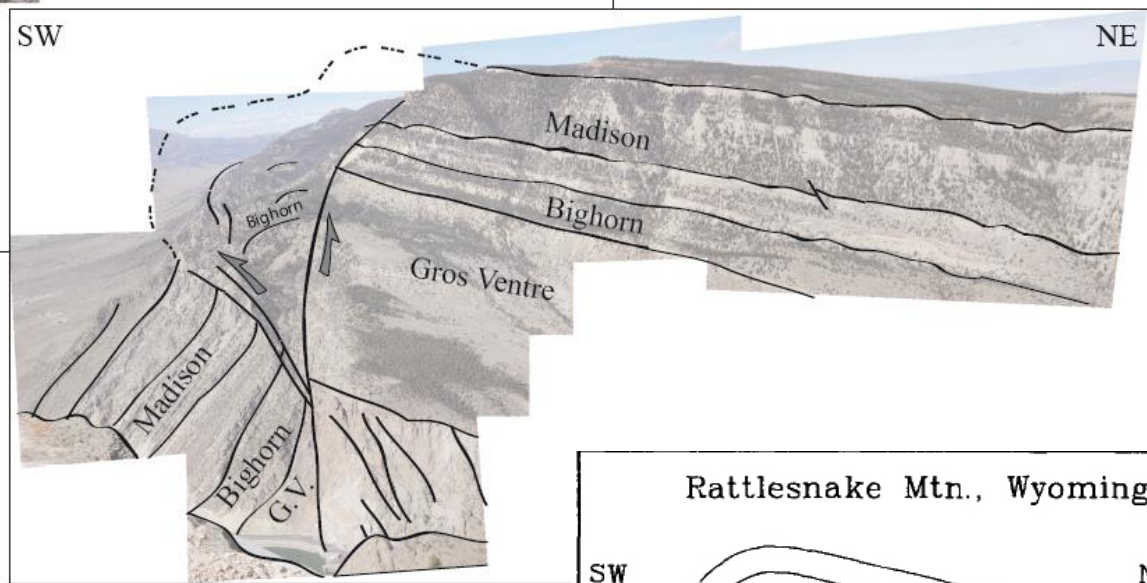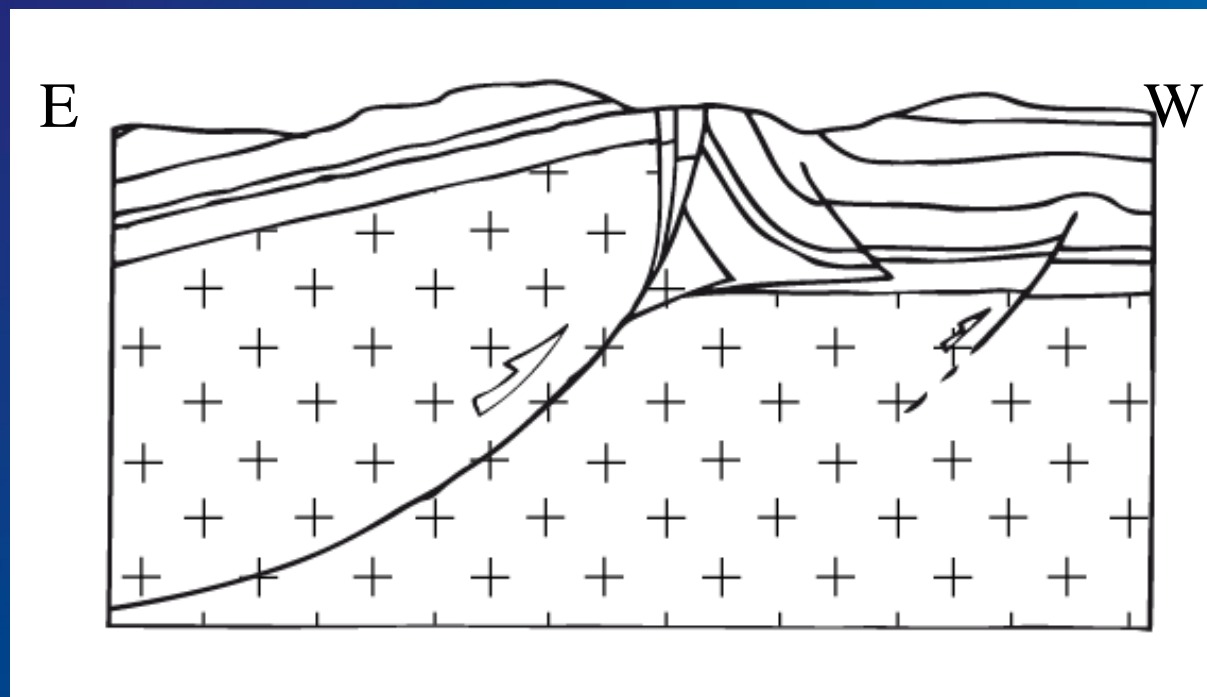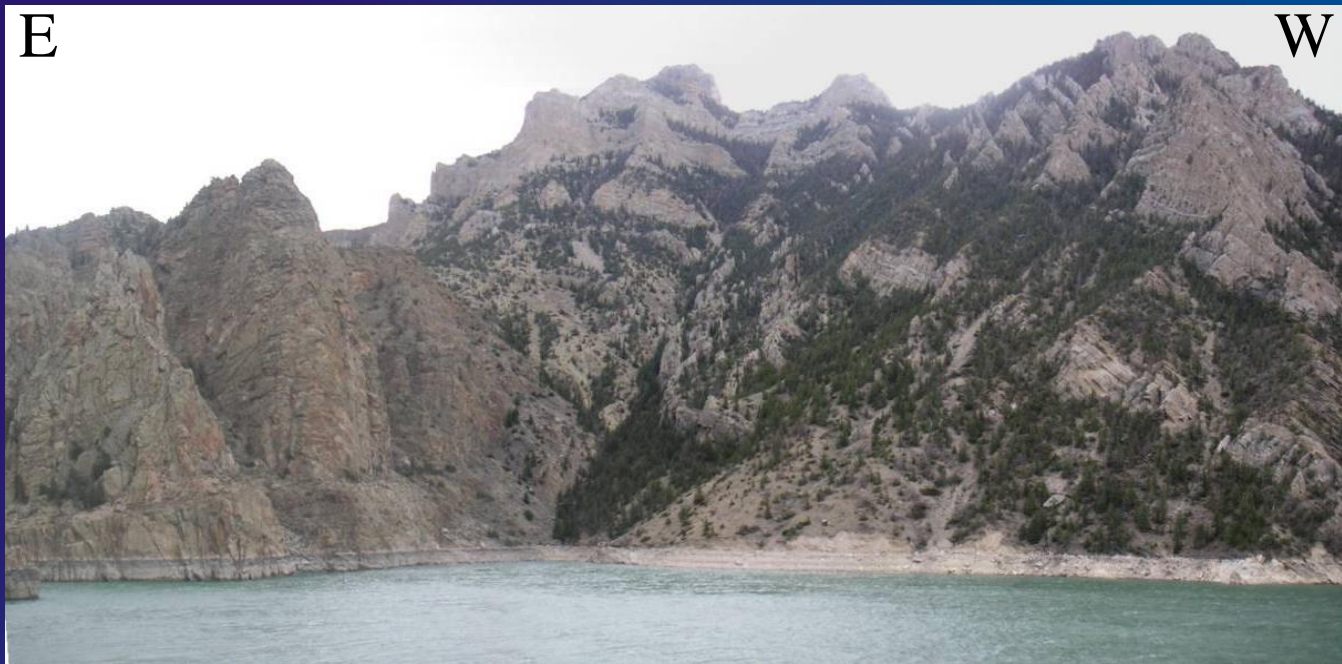
(Amrouch et al. Tectonics, 2010)

Sheep Mountain anticline

Legend (map):
Quaternary
Cretaceous
Jurassic
Triassic
Permian (Phosphoria Fm)
Carboniferous (Pennsylvanian, Tensleep Fm)
Carboniferous (Pennsylvanian, Amsden Fm)
Carboniferous (Mississippian, Madison Fm)
Anticline axis
Syncline axis

5 km

Legend (cross-section):
Quaternary
Cretaceous
Jurassic
Triassic
Permian (Phosphoria Fm)
Pennsylvanian (Tensleep Fm)
Pennsylvanian (Amsden Fm)
Mississippian (Madison Fm)
Paleozoic (pre-Mississipian)

SW
NE
1000 m
0
Precambrian basement
0   1000 m

(Beaudoin et al., Tectonophysics, 2012)

Rattlesnake Mountain anticline

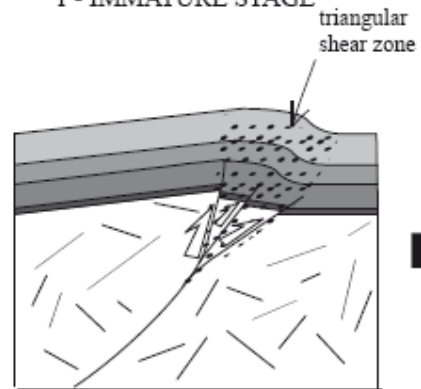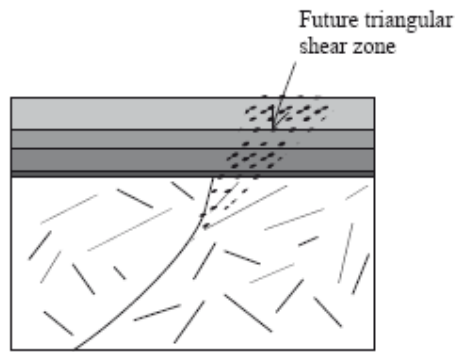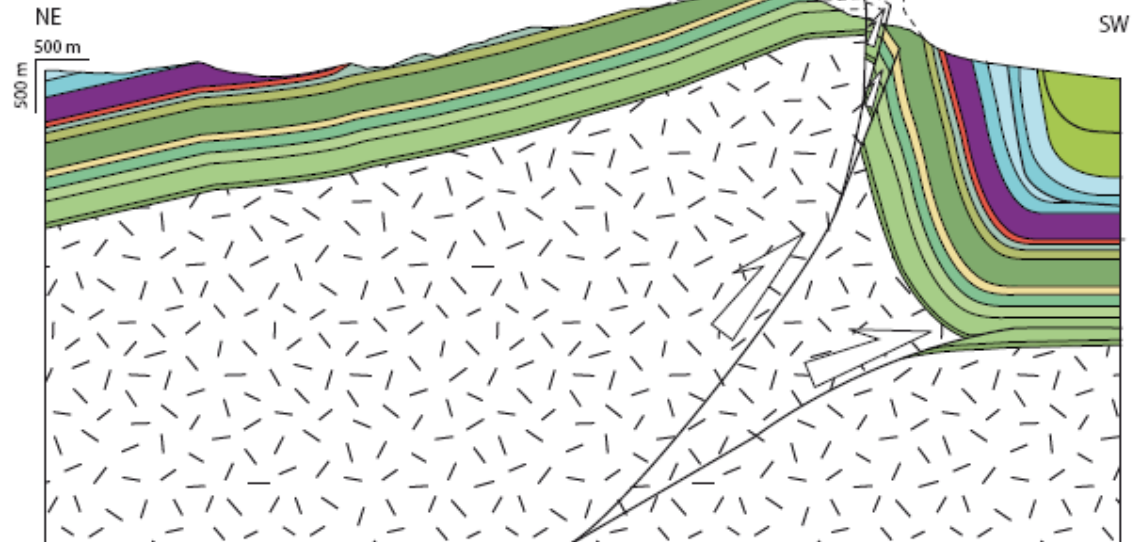(Erslev, 1986)

E W

W

E

a

0- INITIAL STAGE

1 - IMMATURE STAGE

2 - MATURE STAGE

Future triangular shear zone

triangular shear zone

b

SMA (IMMATURE)

SW

NE

500 m

RMA (MATURE)

NE

SW

500 m
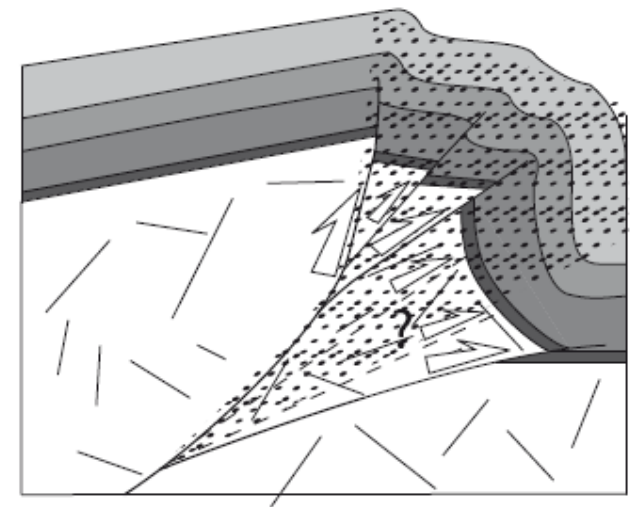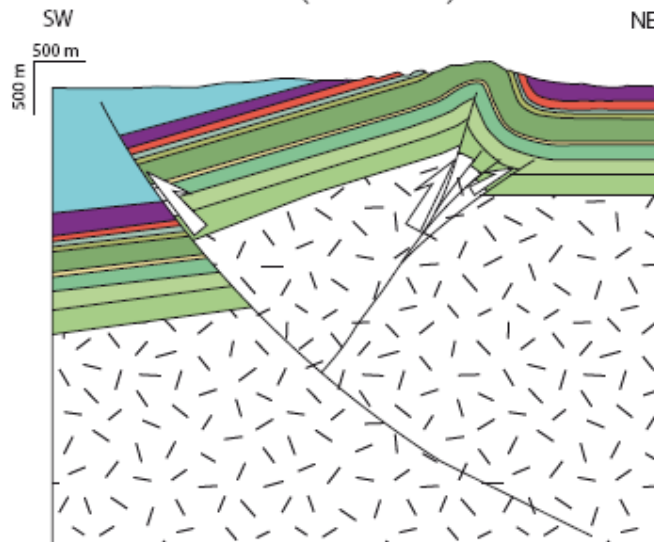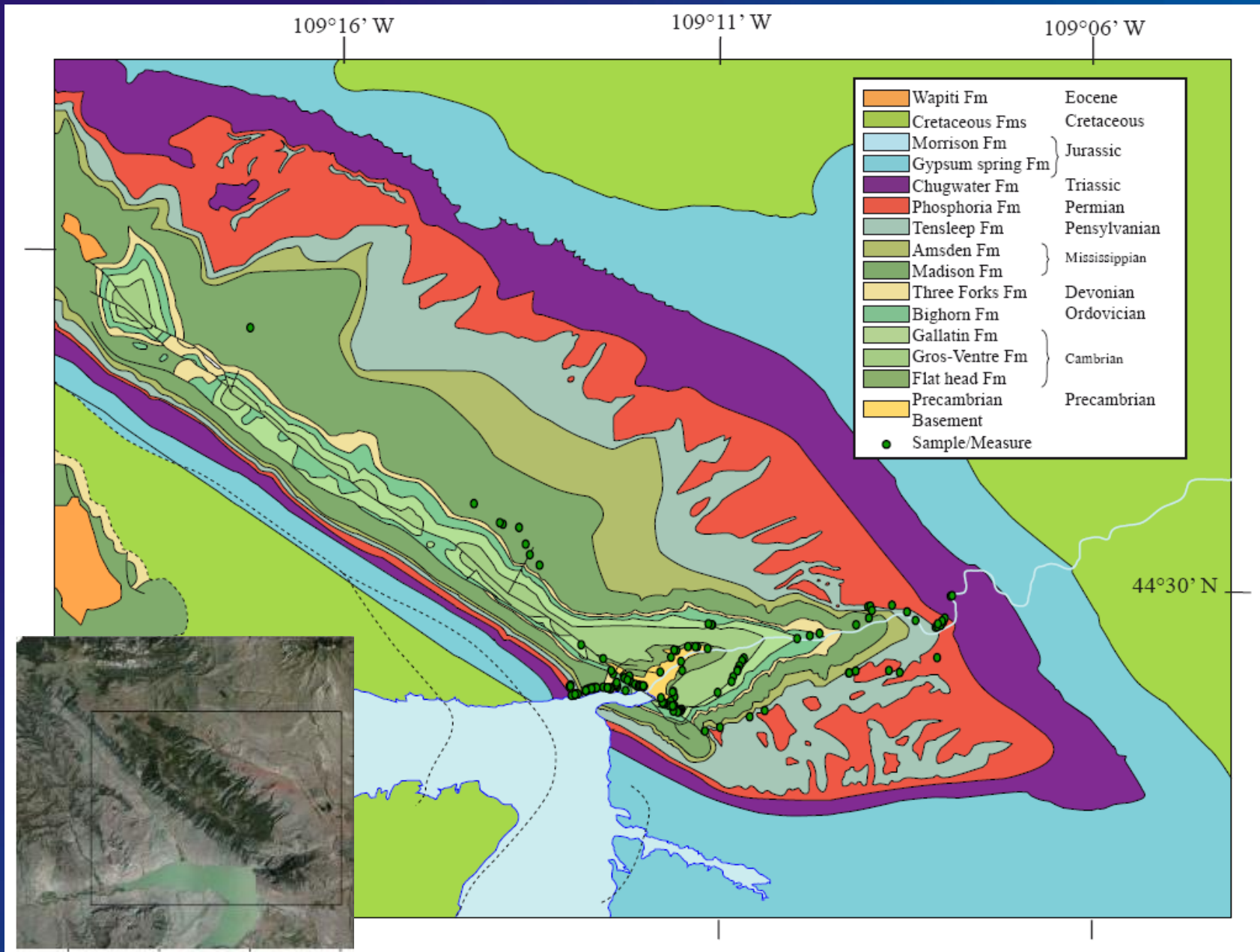
(Beaudoin et al., Tectonophysics, 2012)

ATTENTION

YOU ARE ENTERING GRIZZLY BEAR COUNTRY!
PLEASE TAKE THE NECESSARY PRECAUTIONS.
IF YOU WOULD LIKE TO LEARN MORE ABOUT
THE GRIZZLY BEAR AND YOUR SAFETY, PLEASE
CONTACT THE CODY OFFICES OF THE BLM, U.S.
FOREST SERVICE OR WYOMING GAME AND FISH.

Fracture populations
at Sheep Mountain and Rattlesnake Mountain anticlines

Sheep Mountain anticline

NW
SE
N045°E
N110°E
3 m]

(a)

NW
SE
Set II
Set III
10 cm
(b)

N   N   N
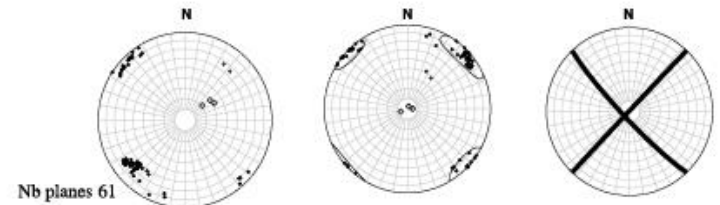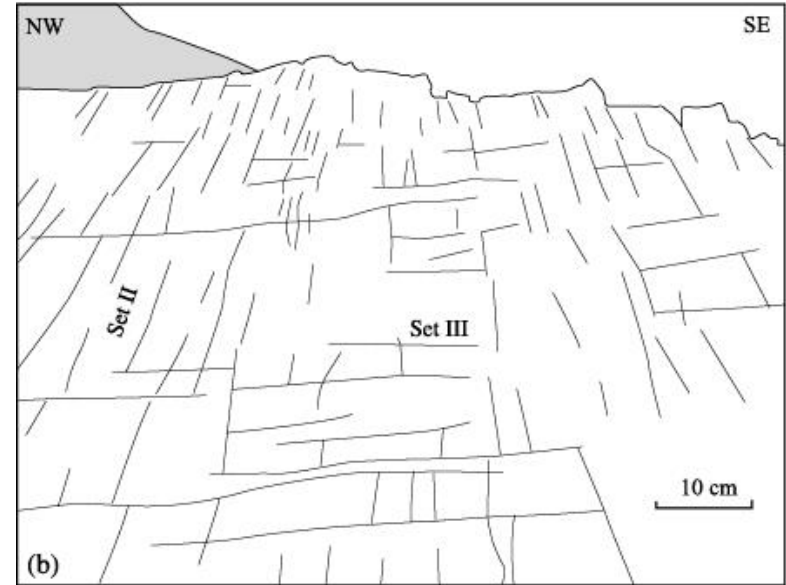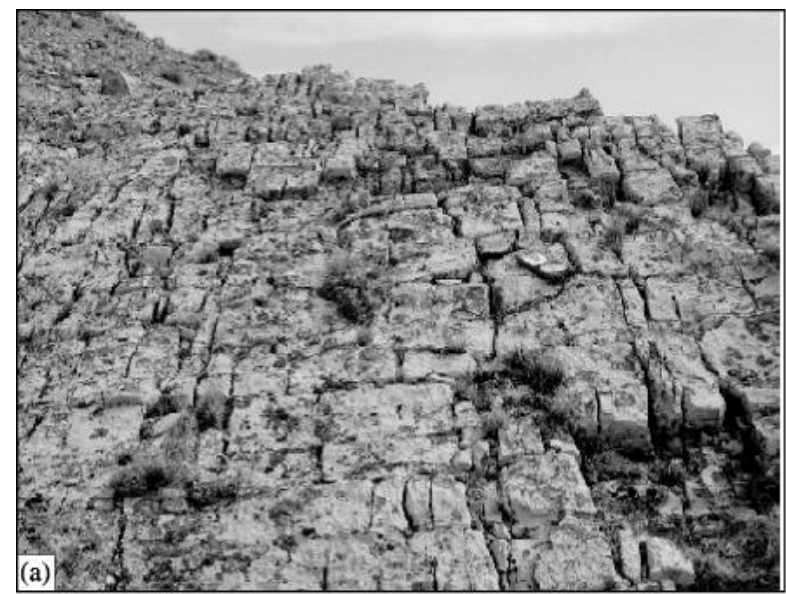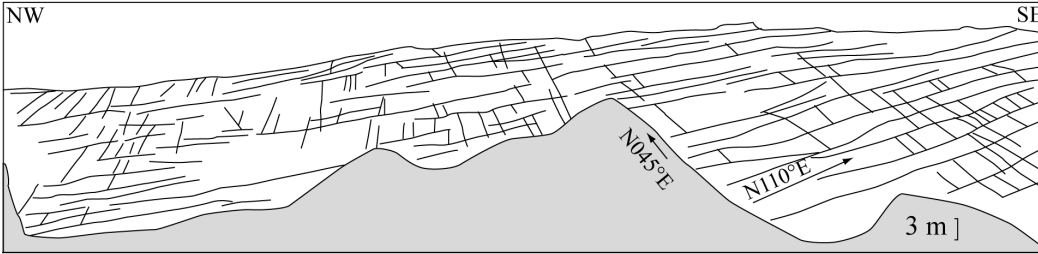
Nb planes 61

(Bellahsen et al., 2006; Amrouch et al., Tectonics, 2010)

Sheep Mountain anticline

(Bellahsen et al, 2006)

Sheep Mountain anticline

(Barbier et al., Tectonophysics, 2012)
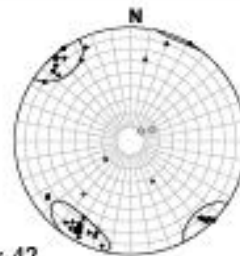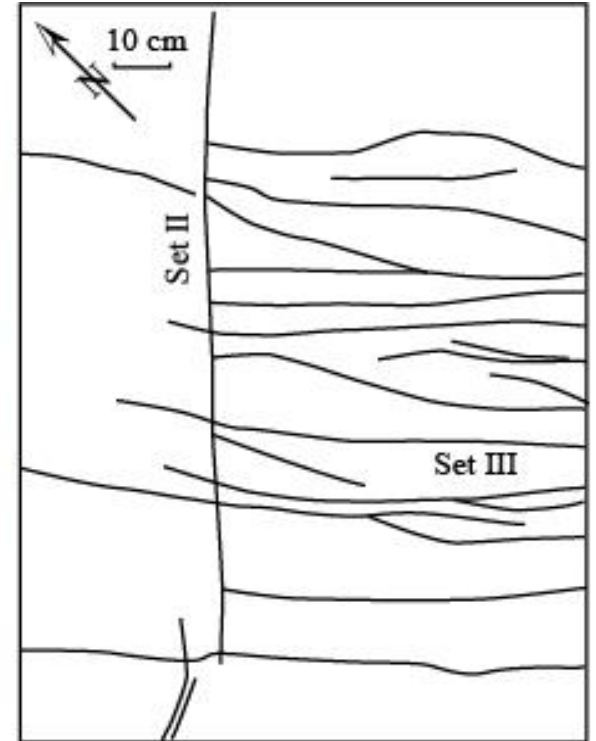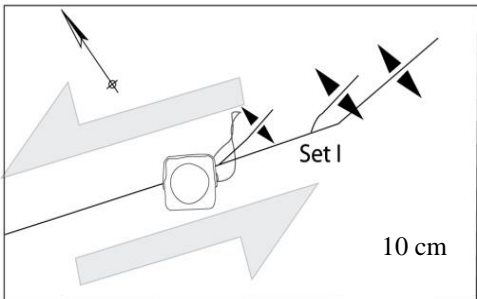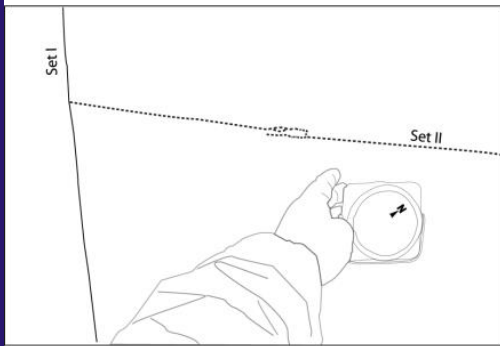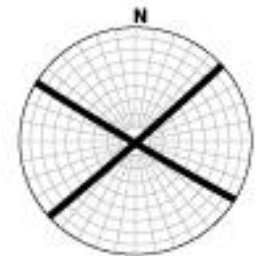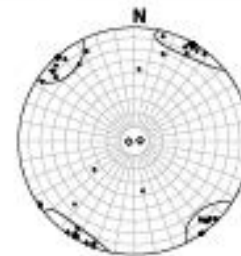
Checking opening mode of joints/veins in thin sections
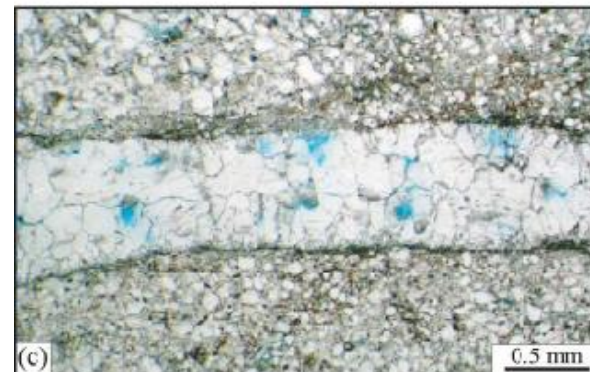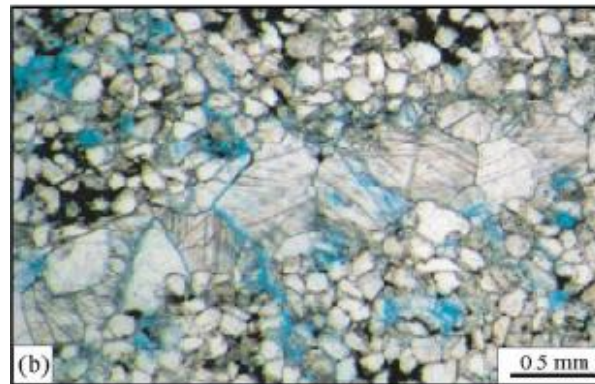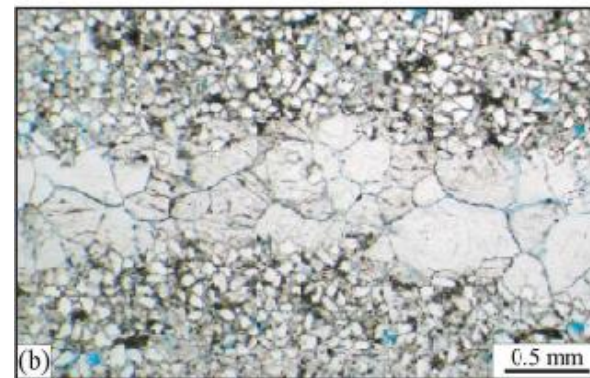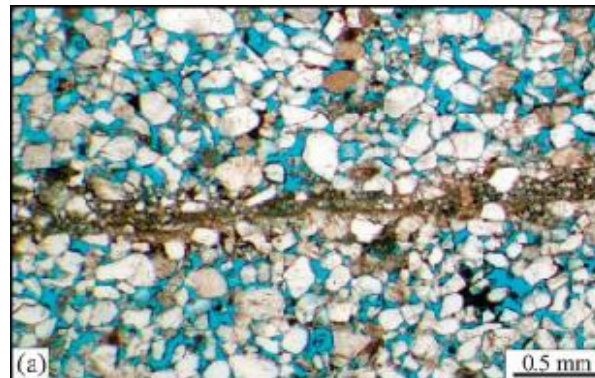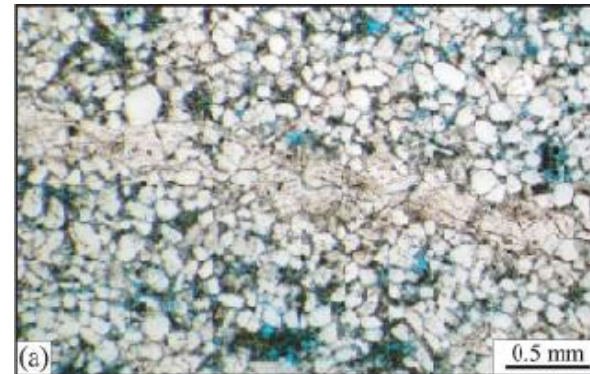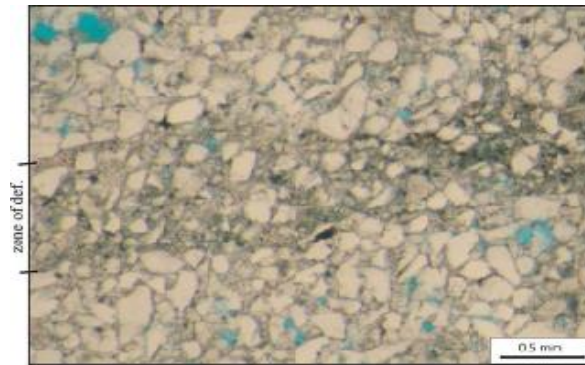
Sheep Mountain anticline
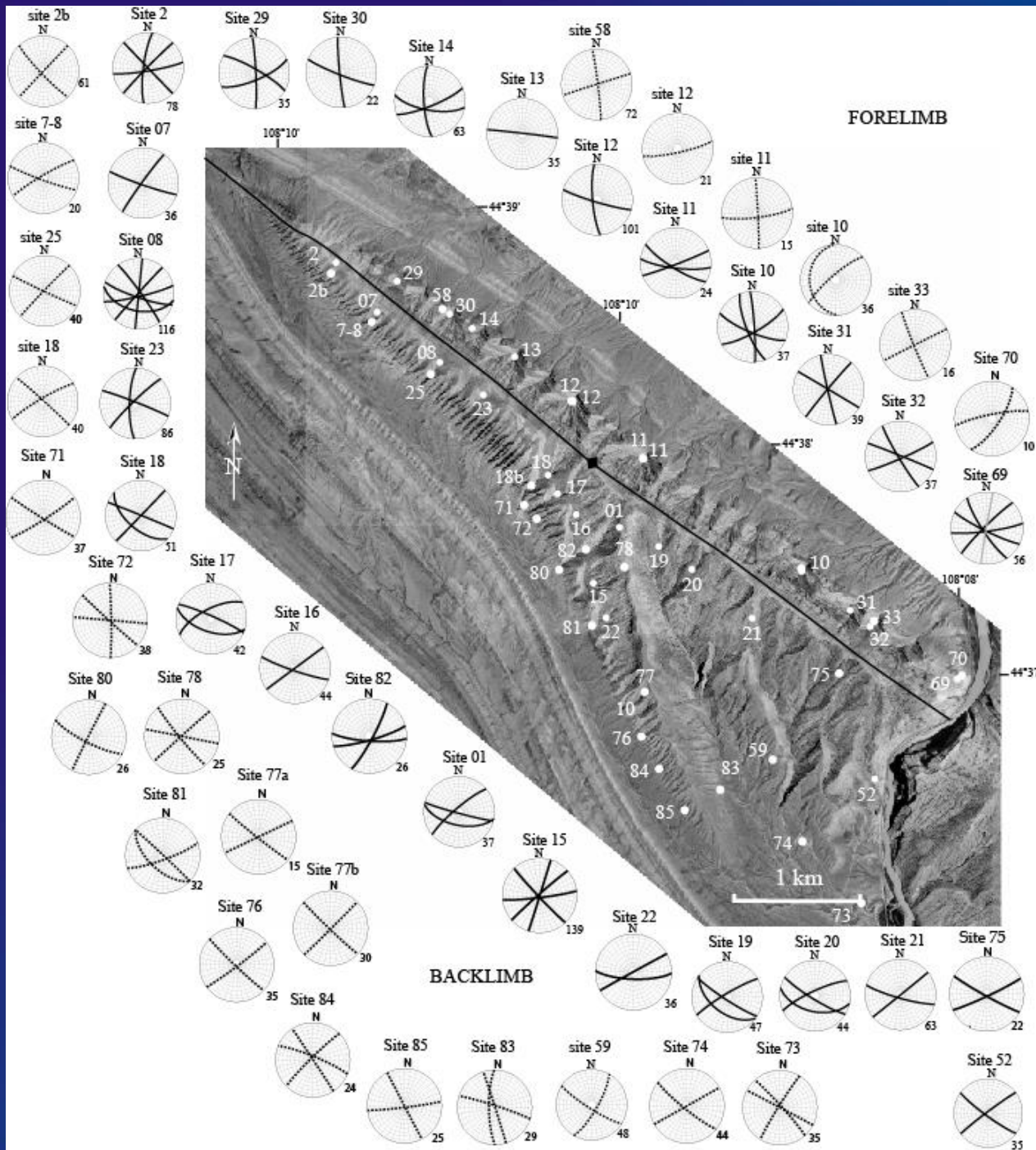
Distribution of joint/vein sets

(Bellahsen et al., 2006;
Fiore, 2007;
Amrouch et al., Tectonics, 2010)
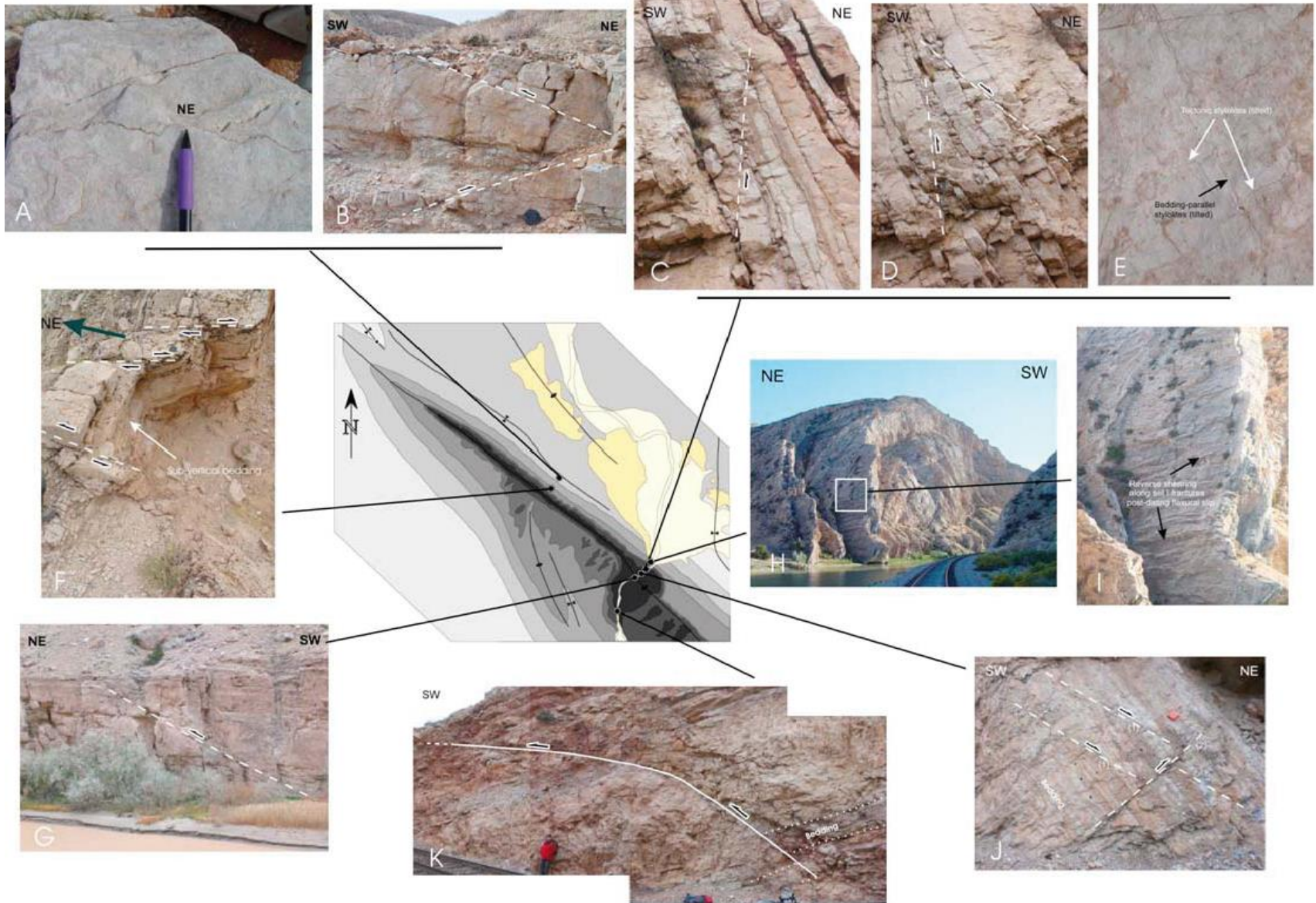
(Amrouch et al., Tectonics, 2010)

Relationships between pressure solution seams and fractures
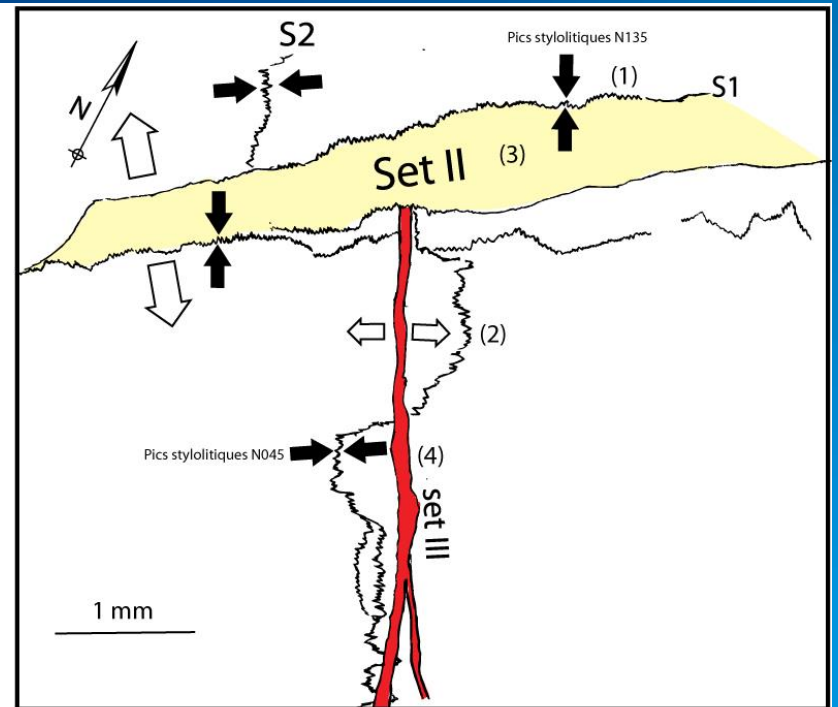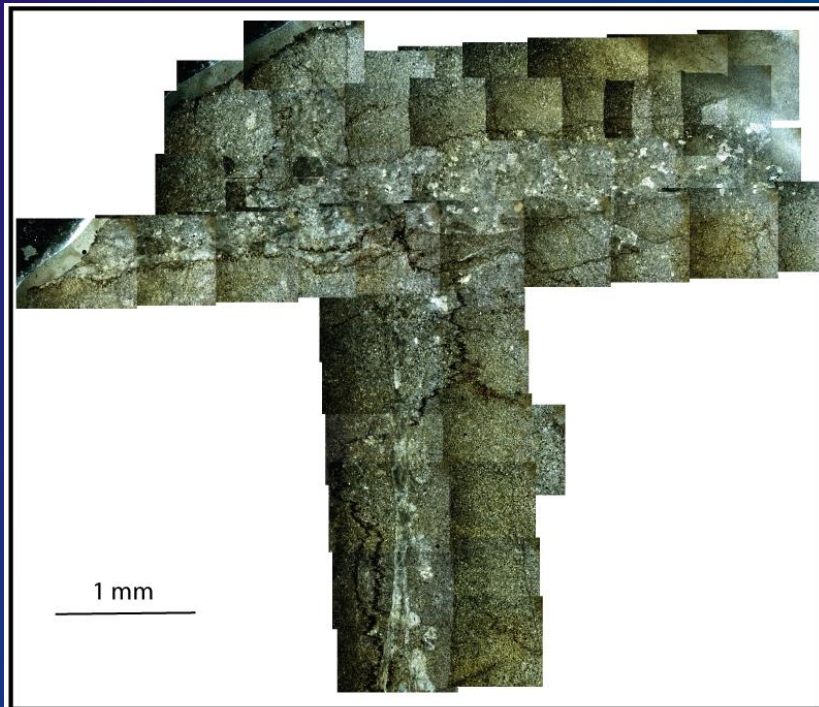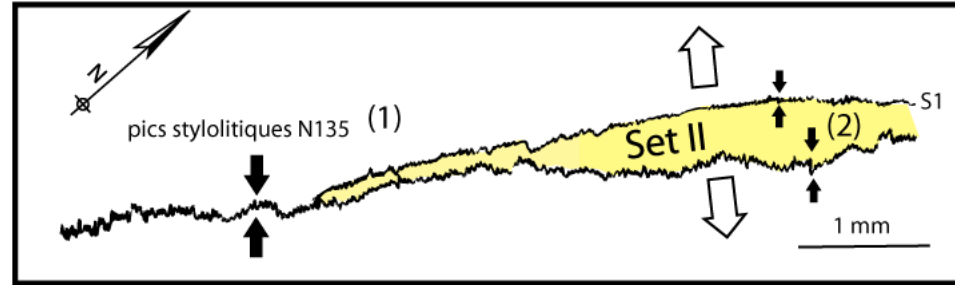
Scenario of fault-fracture development in space and time for Sheep Mountain anticline

(Amrouch et al., GRL, 2011)
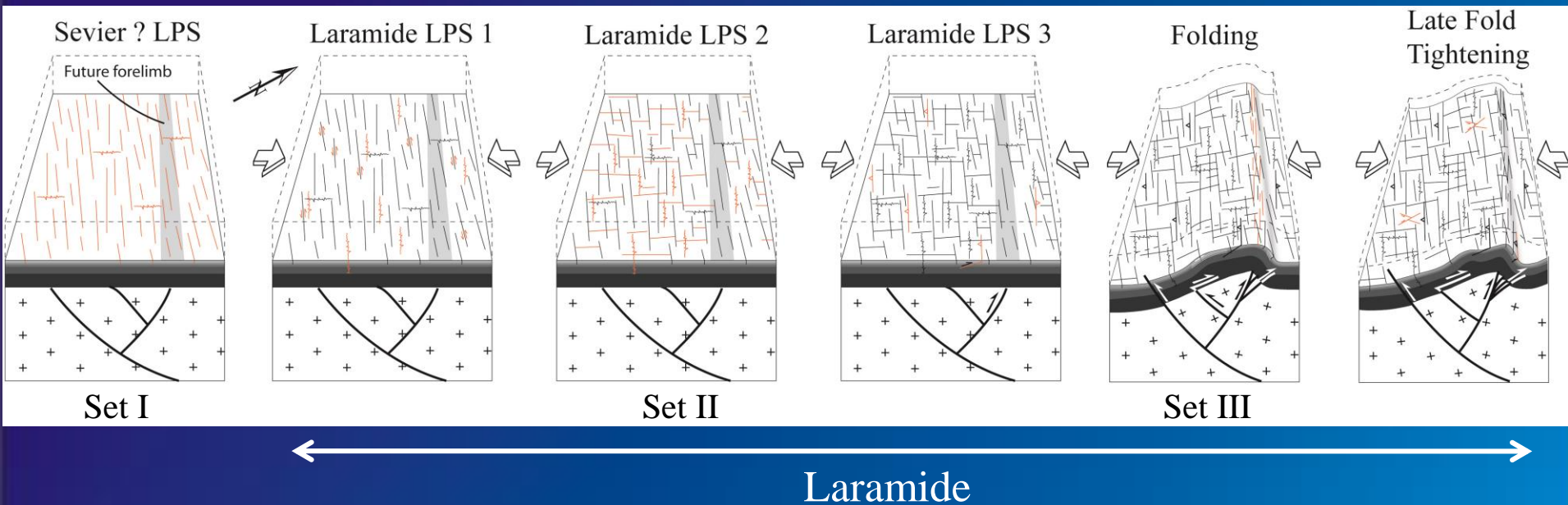
- Mode I opening of pre-Laramide set I fractures
- Shear reactivation of pre-Laramide set I fractures (LPS 1).
- Laramide stylolites with NE-trending peaks and mode I opening of set II fractures (LPS2)
- Reverse faulting parallel to the fold axis (LPS3).
- Mode I opening of syn-folding, outer-rim extension-related set III fractures
- Late stage fold tightening (LSFT) marked by strike-slip faults and reactivation of tilted set I fractures as small reverse faults in the forelimb

Distribution of joint/vein sets

(Beaudoin et al., Tectonophysics, 2012)
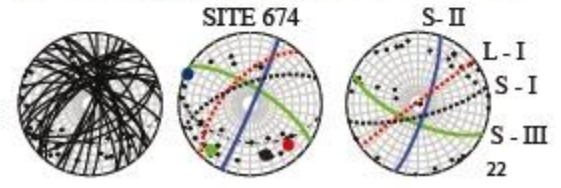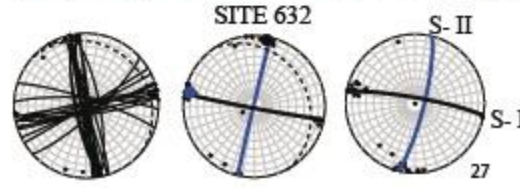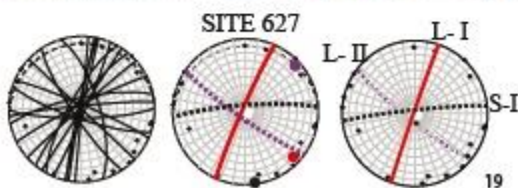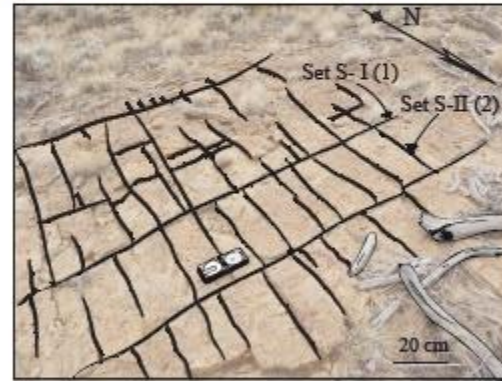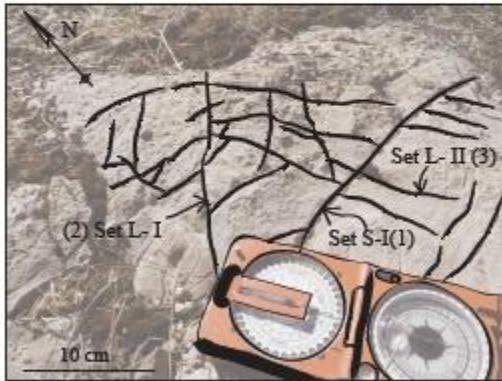
Fracture sequence in the Bighorn Basin

Fracture set	Mean strike of fractures	Related Tectonic events	
Set S-I	090°E to 060°E	Sevier layer-parallel shortening	Pre-Laramide
Set S-II	180°E to 020°E	Formation of the flexural foreland basin	
Set S-III	110°E	Sevier layer-parallel shortening	
Set L-I	045°E	Laramide layer-parallel shortening	Laramide
Set L-II	135°E	Local curvature-related extension	
Set L-III	045°E	Late stage of fold tightening	
Set P-I	180°E to 160°E	Basin and Range extension	Post Laramide

(Beaudoin et al., Tectonophysics, 2012)

Summary on fractures at SMA and RMA

Strong occurrence of early-folding, LPS-related fractures, faults and stylolites.

In addition to fold-related fractures (early-, syn- and late- folding), occurrence of fracture sets having originated before folding and being unrelated to either fold geometry or kinematics (i.e., pre- or post-folding).

Fracture systems observed in folded strata may result from the interplay between kinematic boundary conditions (e.g. far-field collisional stresses, foreland flexural stresses) and local deformational events such as fold growth or movements along major faults.

Pre-folding fractures are commonly reopened or sheared or passively tilted during folding. They can also inhibit development of classical sets of fold-related fractures.

Occurrence of such pre-folding (fold-unrelated) fractures has to be carefully considered in order to build realistic conceptual fold–fracture models.

Fractures show variable vertical persistence (stratabound vs through-going), hence potential variable vertical connectivity and break in stratigraphic compartmentalization.
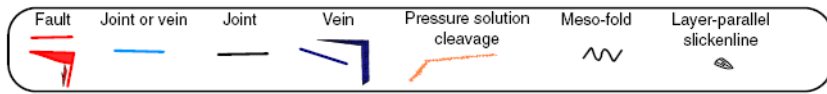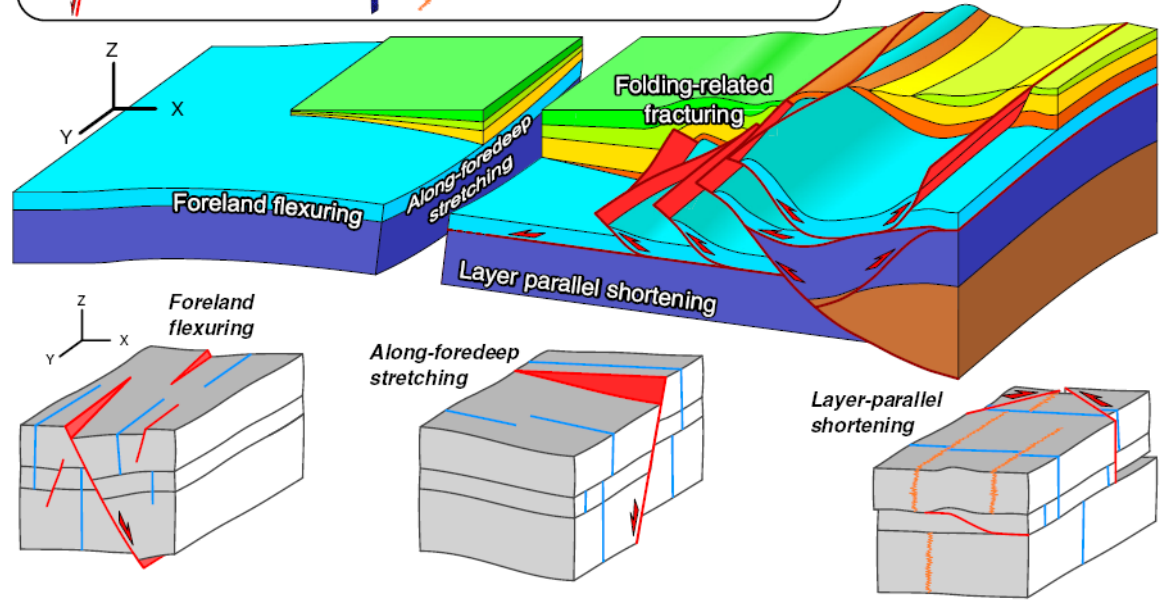
Typical (micro) structural assemblages potentially observed in folded strata
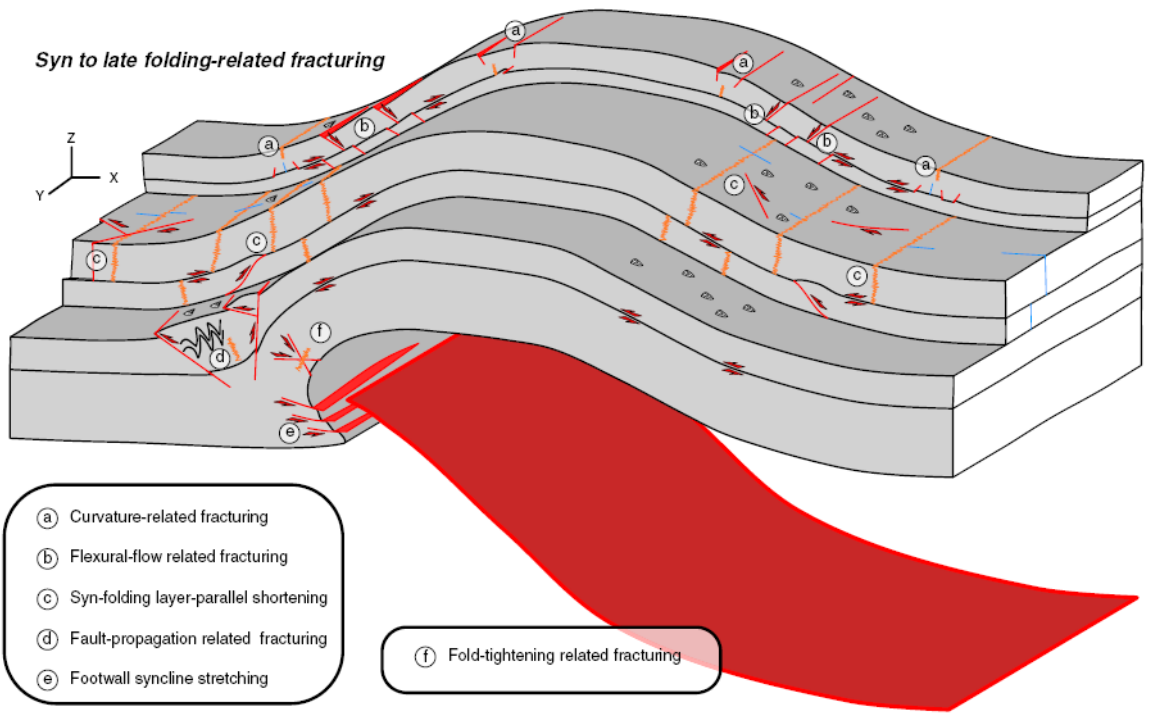
(Tavani et al., ESR, 2015)
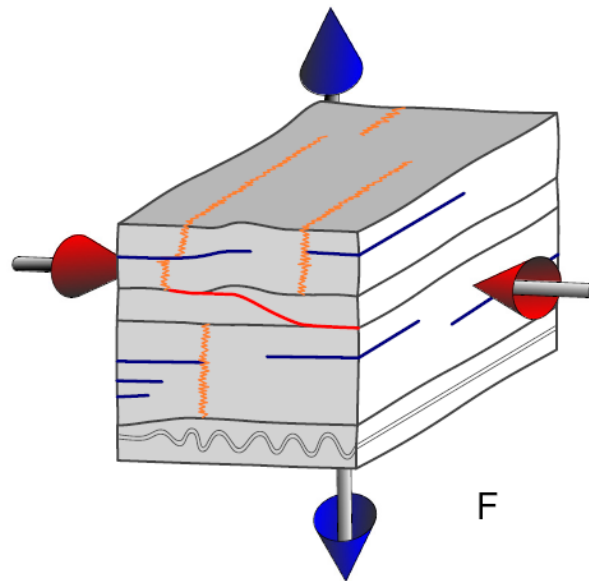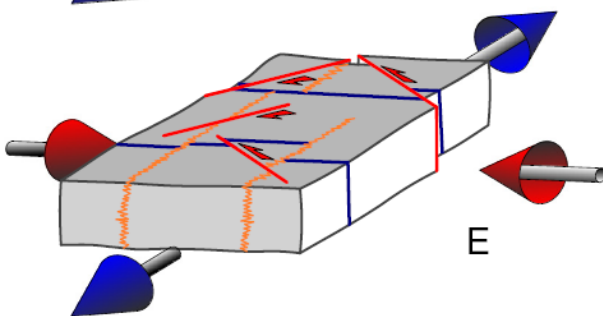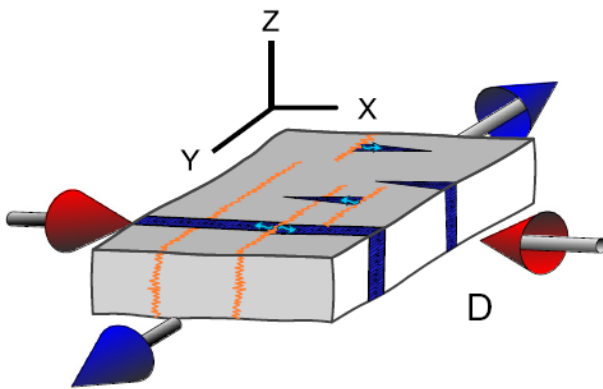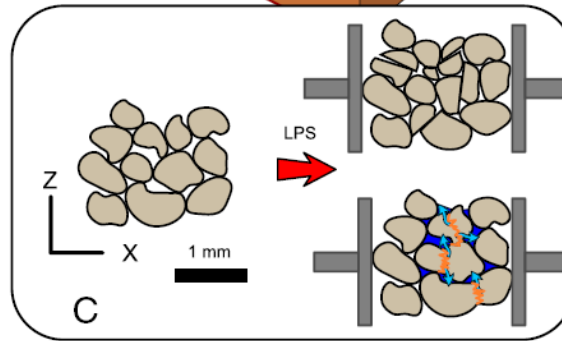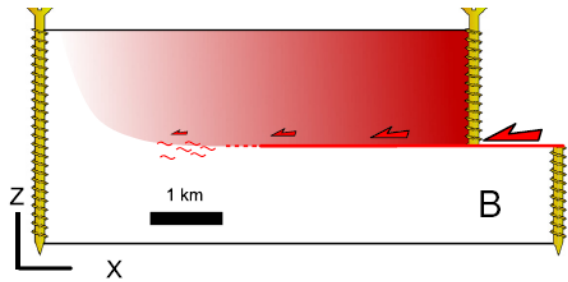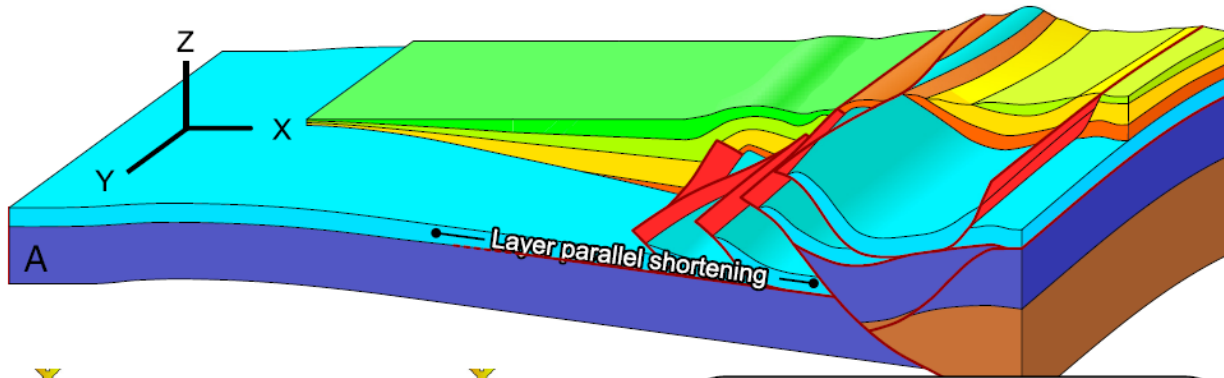
Layer-parallel shortening

(Tavani et al., ESR, 2015)

Physical properties of rocks, proxies of internal strain at Sheep Mountain anticline

Anisotropy of sedimentary rocks

The anisotropic behaviour of sedimentary rocks with respect to a particular physical property (elasticity, magnetic susceptibility, electrical conductivity and permeability) is determined by both matrix properties and pore space distributions.

The matrix of a sedimentary rock can be anisotropic because of preferred mineral orientation, water currents during deposition or pressure solution.

The pore space distribution can be anisotropic because of depositional processes driven by gravity or water currents, or presence of preferentially oriented cracks within or between the minerals.

AMS

The AMS technique provides an accurate image of the petrofabric structure, which reflects the average preferred orientation of tens of thousands of magnetically susceptible minerals in the rock matrix, called the "magnetic fabric".

Measurement of AMS helps characterize penetrative tectonic fabrics in deformed rocks because AMS is sensitive to even slight preferred orientations of magnetic minerals.

K1 □
K2 △
K3 ○

$K1 \geq K2 \geq K3$ representing the maximum, intermediate and minimum axes of susceptibility

Shape factor

Planar

Triaxial

Anisotropy degree

Linear

The magnetic fabric is defined using the orientation of :
- the magnetic foliation, i.e., the plane containing the K1 and K2 axes when $K1 \approx K2 > K3$,
- the magnetic lineation, i.e., the direction of the K1-axis.
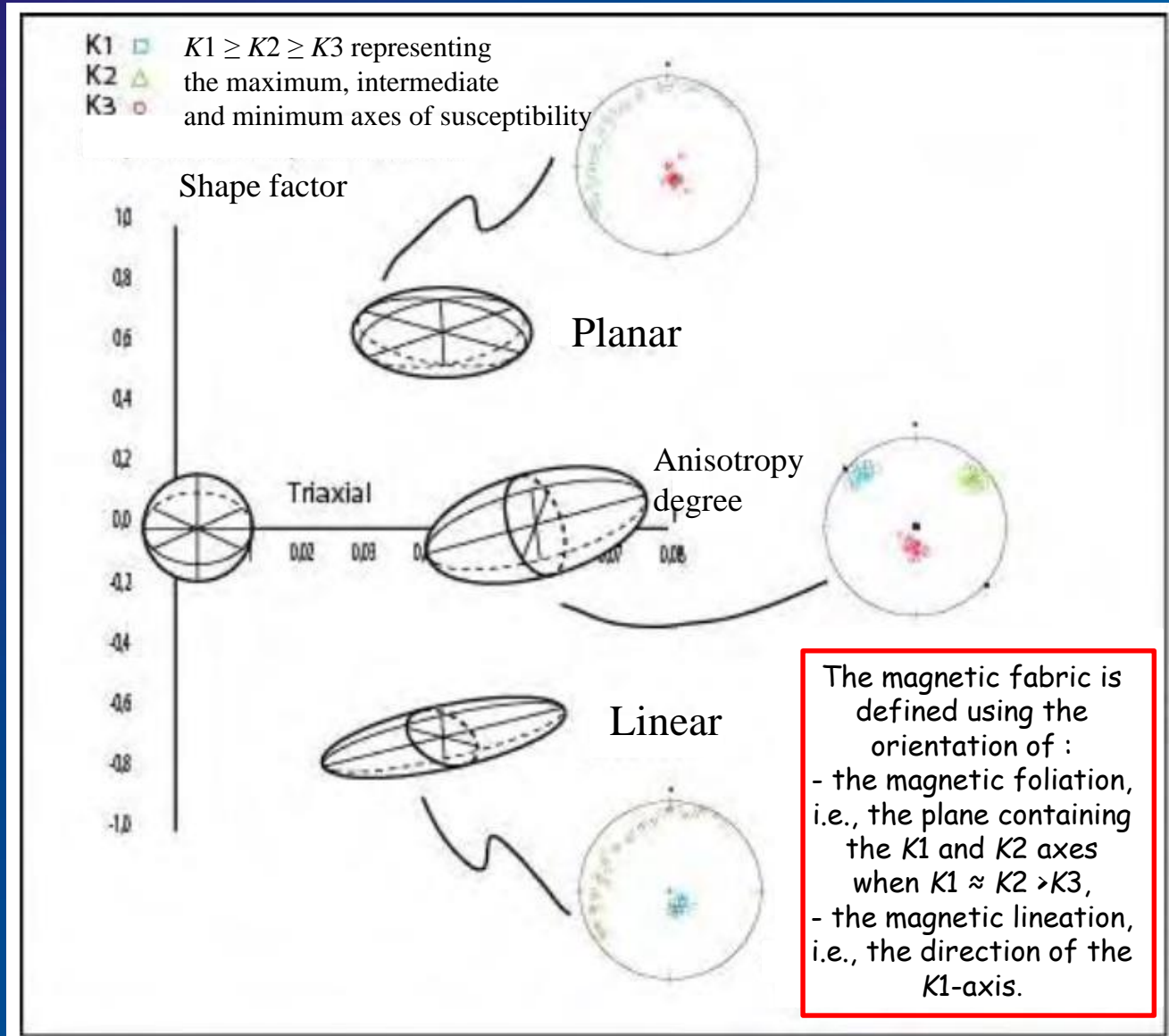
In sedimentary rocks, magnetic susceptibility K_m originates primarily from three distinct sources:
- the dominant diamagnetic minerals (quartz or calcite),
- the paramagnetic minerals (clays and other Fe-bearing silicates)
- diluted ferromagnetic minerals (magnetite, hematite and pyrrhotite), depending on their relative proportion.

Generally, K_m ranges between low negative values and low positive values (from $-10 \times 10{-6}$ SI to $10 \times 10{-6}$ SI). In Fe-bearing silicate rocks K_m covered susceptibilies up to $500-1000 \times 10{-6}$ SI whereas ferromagnetically dominated rocks are generally characterized by values higher than $1000 \times 10{-6}$ SI.

AMS
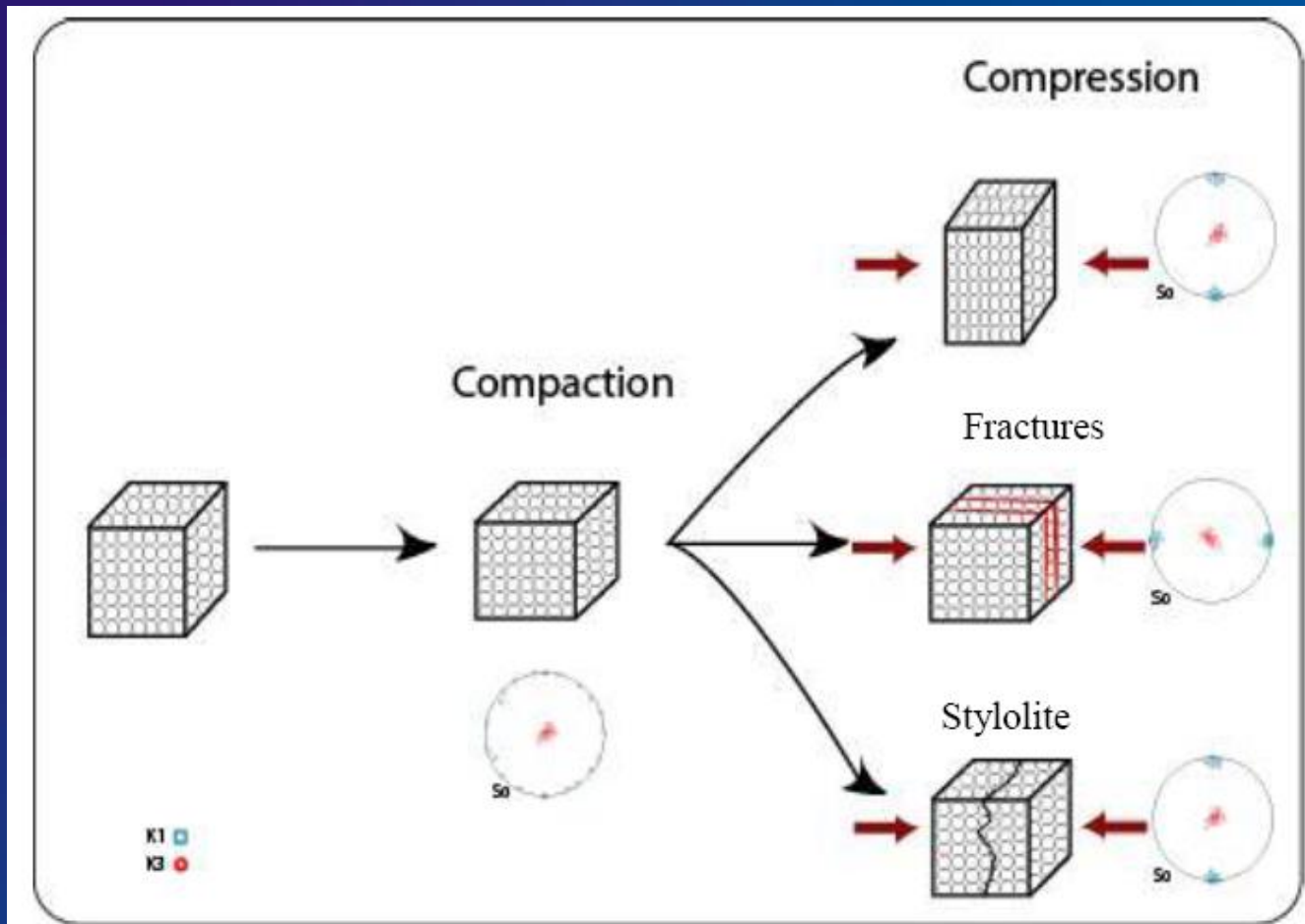
The interpretation of AMS fabrics is strongly dependent on the carrier of the magnetic signal and so requires additional careful microstructural and petrographic characterization.

AMS

Increasing internal strain in pure shear regime
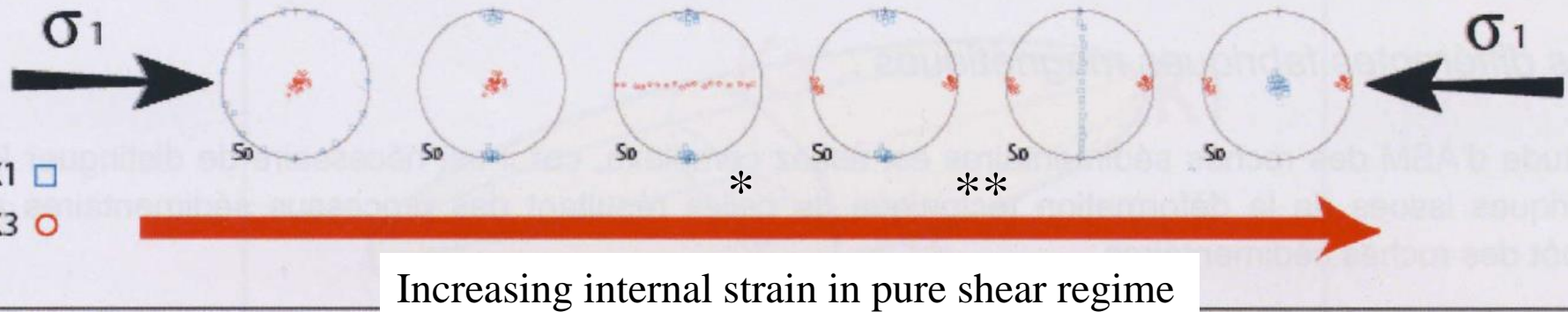
* Intermediate fabric : magnetic lineation K1 still contained within the bedding but clustered at right angle to the shortening direction; K3 leaves the pole to bedding and exhibits a girdle distribution around K1.

** Tectonic fabric with K3 parallel to the shortening direction. K1 is either parallel to the intersection between the bedding and the incipient cleavage or exhibits a girdle distribution around K3

(Frizon de Lamotte et al., 1992)

While the correlation between the orientations of principal AMS axes and principal strain axes tends to be very consistent, the correlation between the magnitudes of principal AMS axes and corresponding principal strain axes is not.

AMS (sandstones)

Sheep Mountain anticline
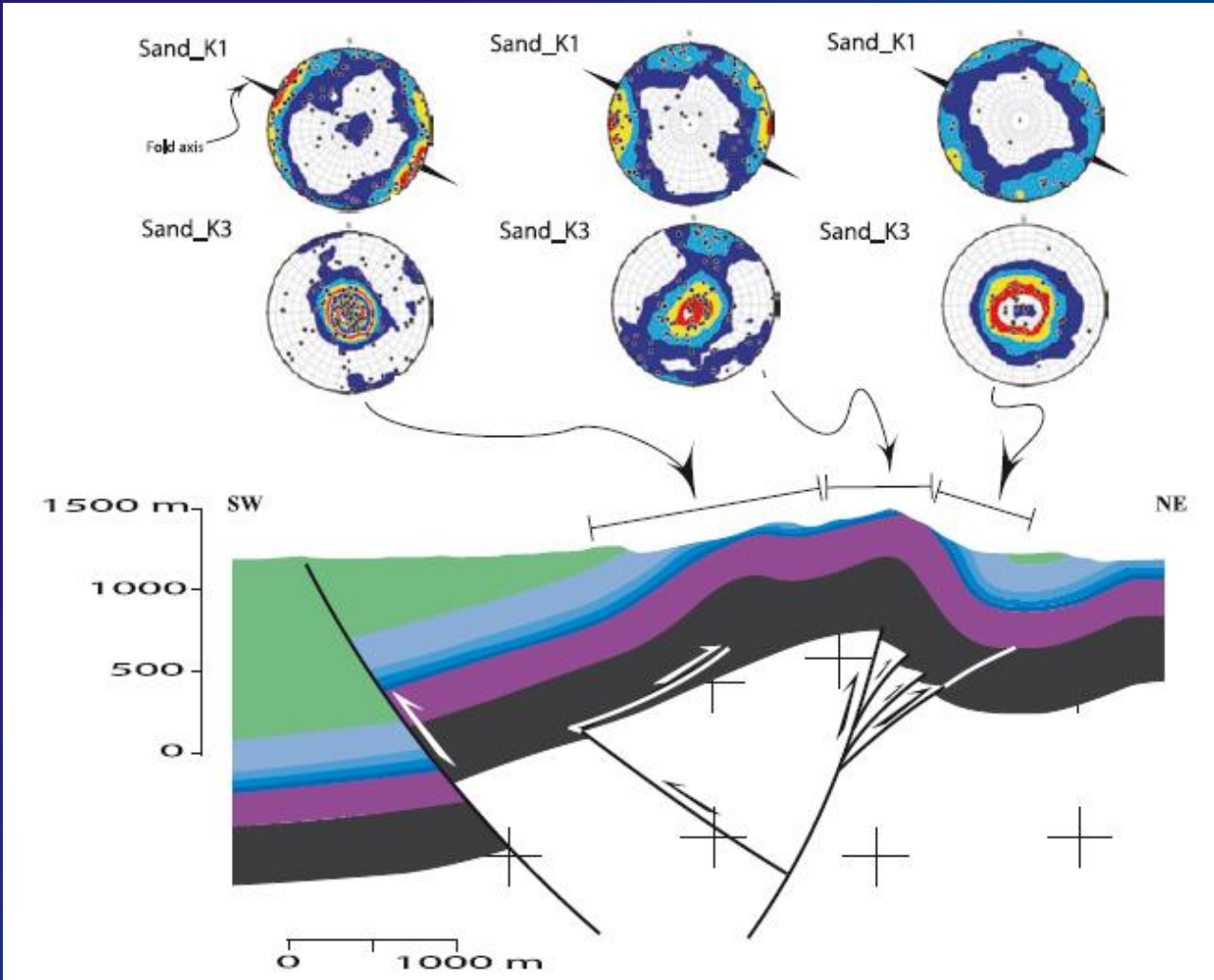
Forelimb : planar oblate fabrics with K1 scattered in the plane of bedding, K3 normal to it.
→ Sedimentary fabric.

Backlimb : similar fabric but with clustering of K1 close to the direction of fold axis in the plane of bedding. Fabric mixing both shortening direction and pole of bedding
→Slight tectonic fabric (early-folding LPS).

Hinge : linear fabric with a girdle distribution of K3;
→ competition between intermediate and true tectonic fabrics. Inferred shortening direction, normal to the magnetic lineation and parallel to the K3 girdle.

(Amrouch et al., GJI, 2010)

AMS (carbonates)

Sheep Mountain anticline
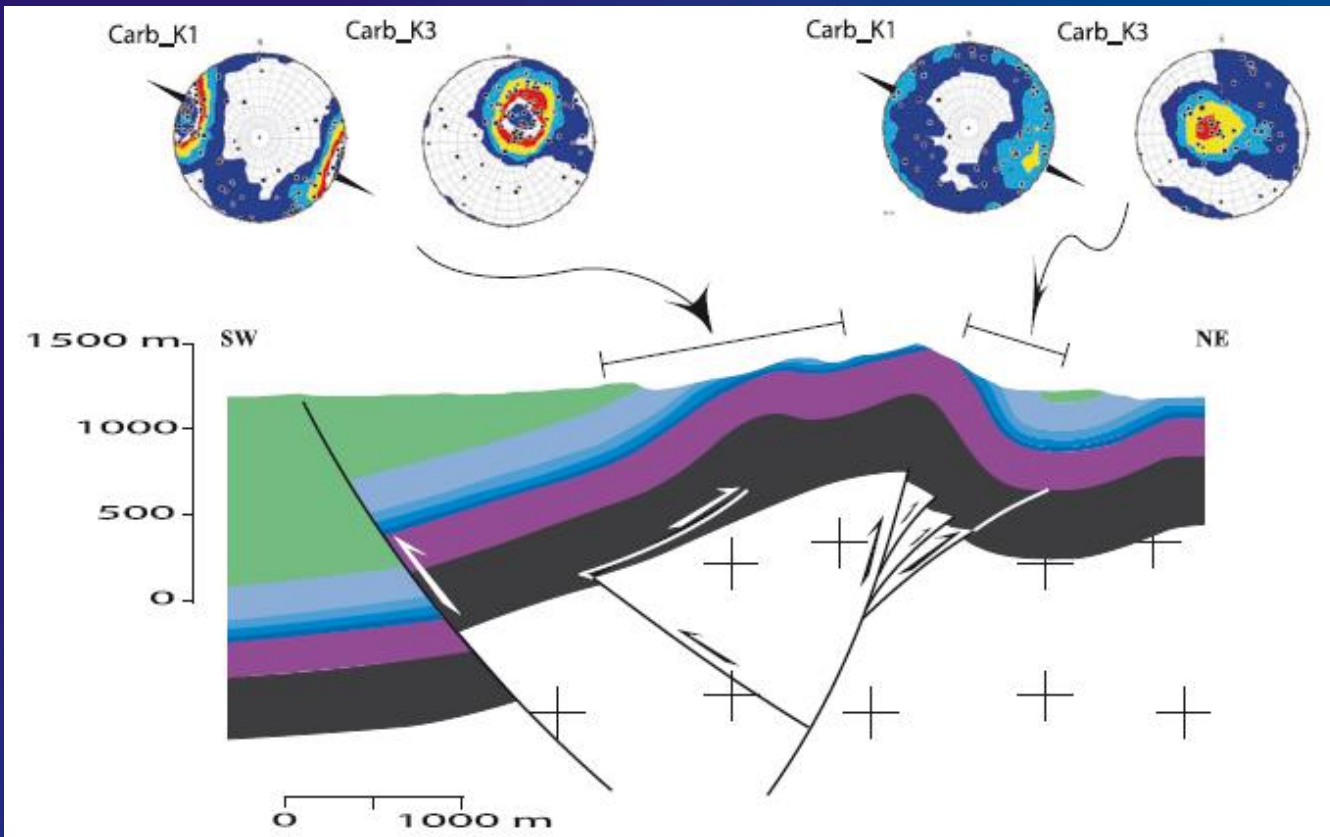
<u>Forelimb</u> : K1 scattered in the plane of bedding with a weak maximum close to the fold axis trend.
K3 clustered either along the pole of bedding or perpendicular to K1.
→combination of relict sedimentary fabrics with intermediate and tectonic fabrics locally.
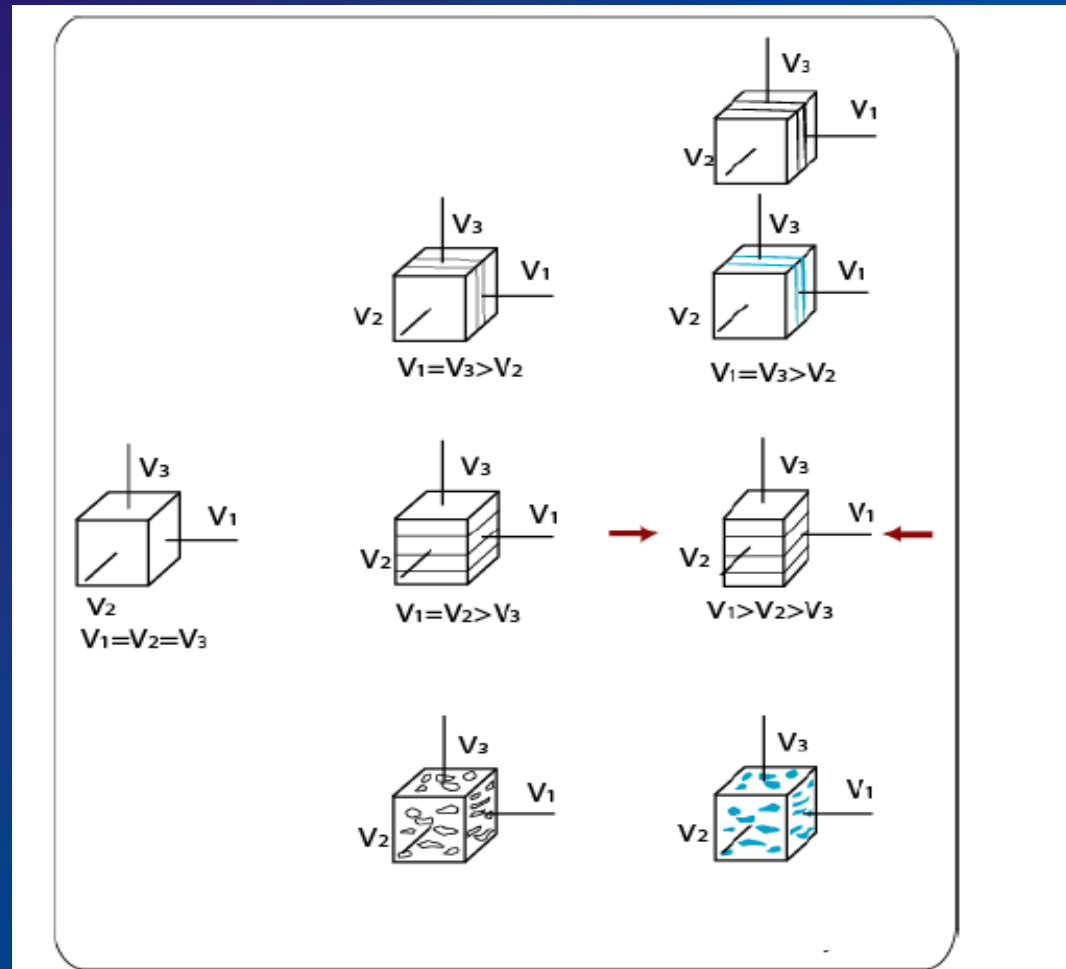
<u>Backlimb</u> : well defined cluster of K3, which significantly deviates from the pole of bedding, and very well clustered K1 axes ~N120°, close to the fold axis (~ sandstones).
→ fabric associated to the regional shortening direction.
Obliquity of the magnetic foliation with respect to bedding plane
→ bed-parallel shearing instead of standard LPS

(Amrouch et al., GJI, 2010)

APWV

At laboratory conditions (no confining pressure), APWV is mainly controlled by microstructures (at μm scale) leading to a reduction of the inter- or intragranular cohesion.
Such microstructures can be the pore network, the microfractures and/or the contacts between grains.

(Amrouch et al., GJI, 2010)
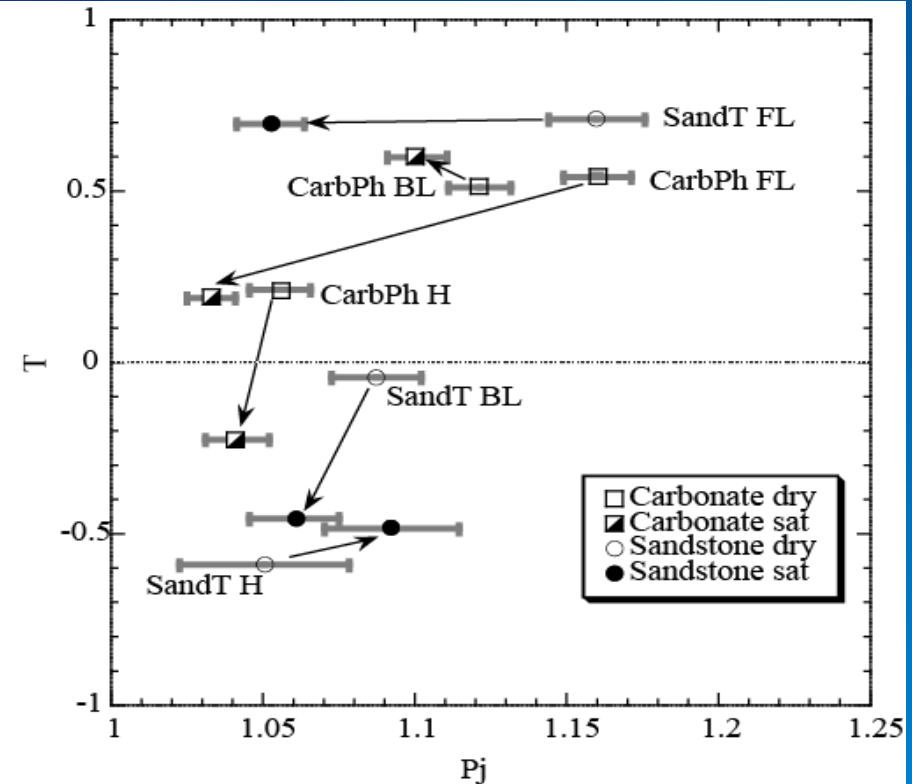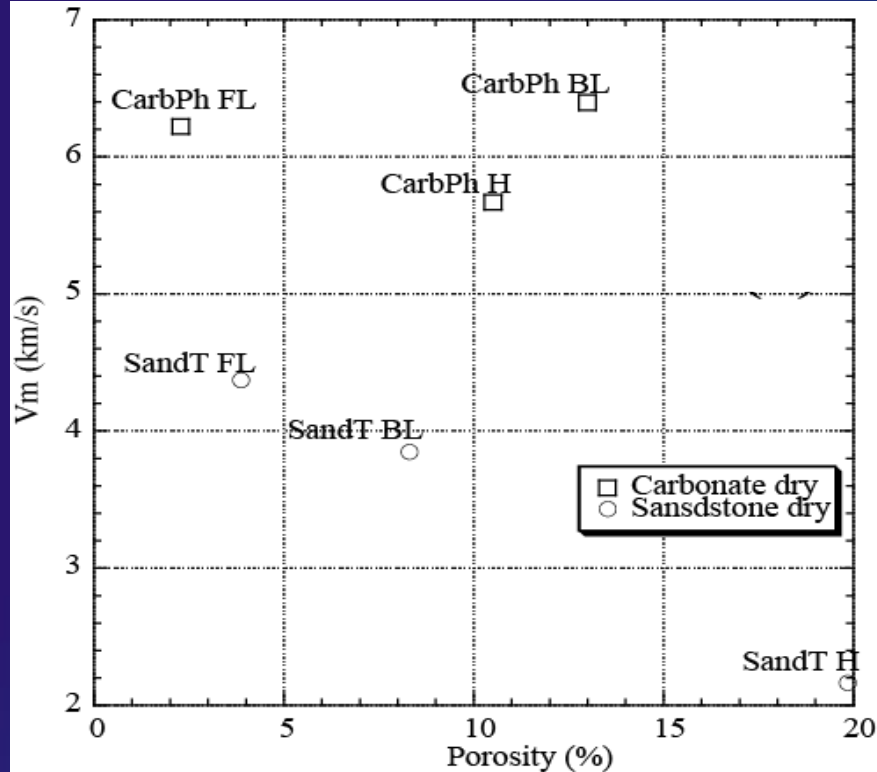
T is the shape parameter, *Pj* the Jelinek anisotropy parameter (Jelinek 1981).

Velocity measurements performed on dry and saturated samples.
Velocities range between the velocities of the mineral
grains (higher in calcite than in quartz) and those of the mineral–pore fluid filled (air or water)
assemblage.

A rock made of an anisotropic matrix and an isotropic pore space is characterized
by velocity and anisotropy increase when it is saturated with incompressible material
(water) → degree of anisotropy of the matrix

Sheep Mountain anticline

APWV

(Amrouch et al., GJI, 2010)
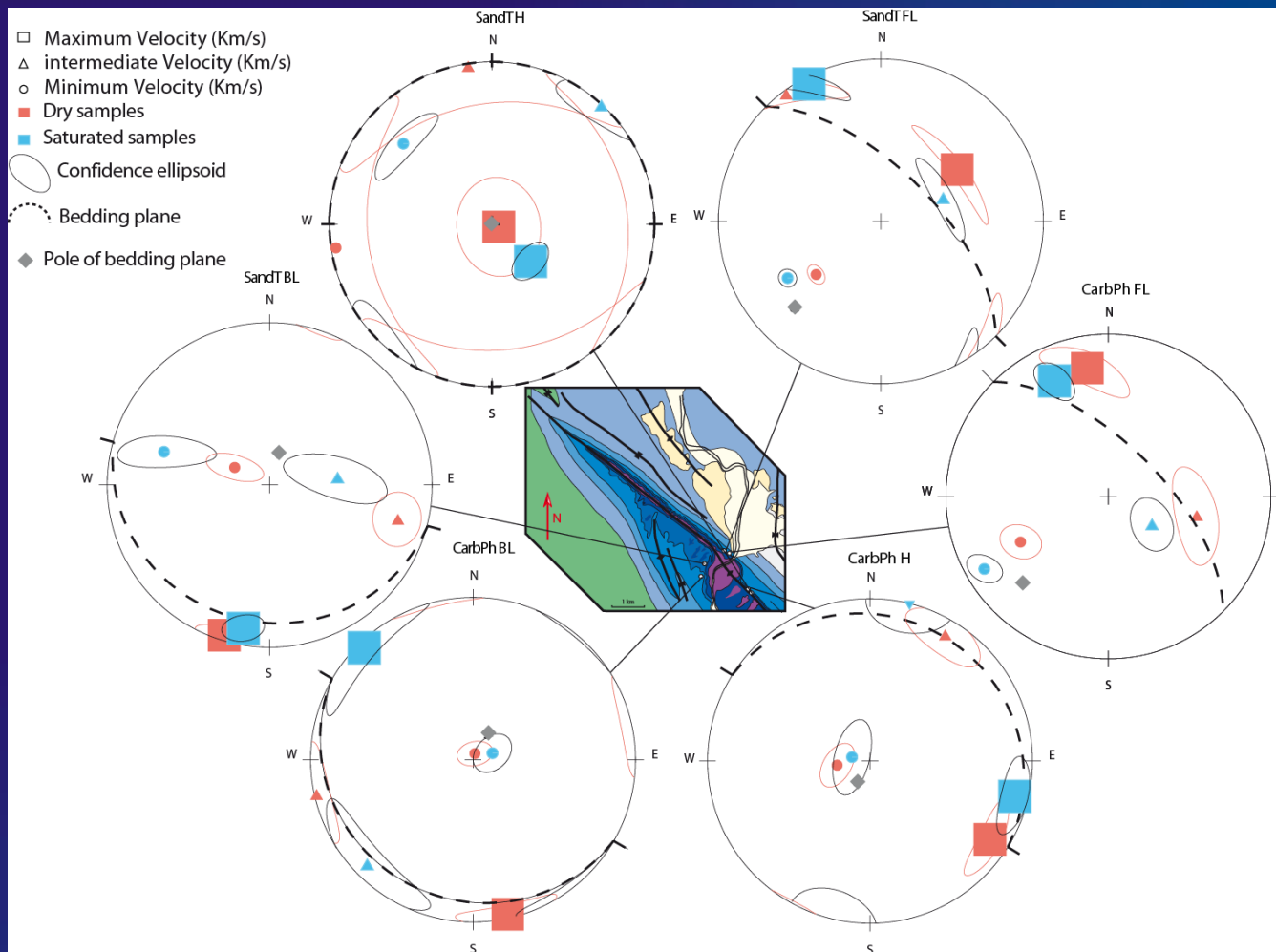
Forelimb : Deformation preferentially revealed by porosity, oriented with its long axis parallel to the fold axis. Anisotropy dominated by anisotropic pore network within an almost isotropic matrix.

Backlimb : Grain-supported APWV fabrics → the matrix is more anisotropic in the backlimb than in the forelimb. The direction of anisotropy is roughly related to the plane of bedding indicating that APWV fabrics could be linked to early-folding LPS.
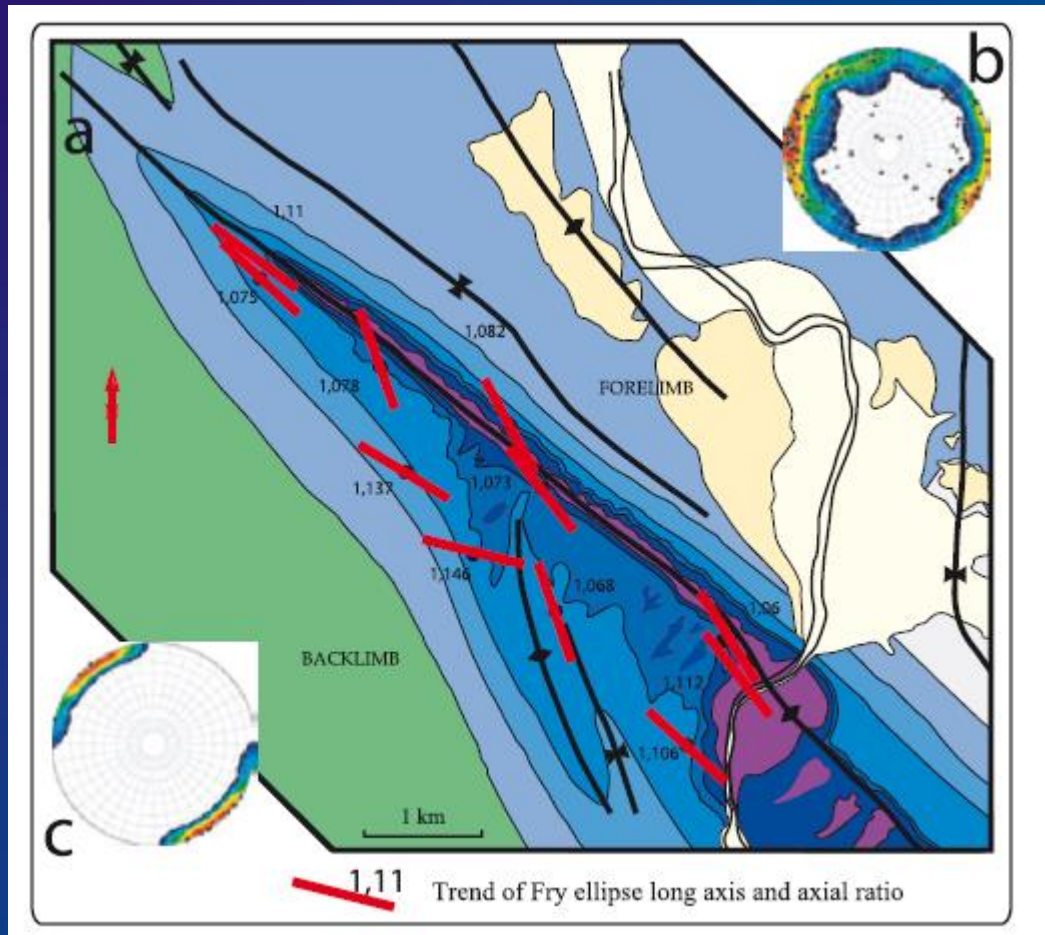
Strain axes in sandstones deduced from Fry method

(Amrouch et al., GJI, 2010)
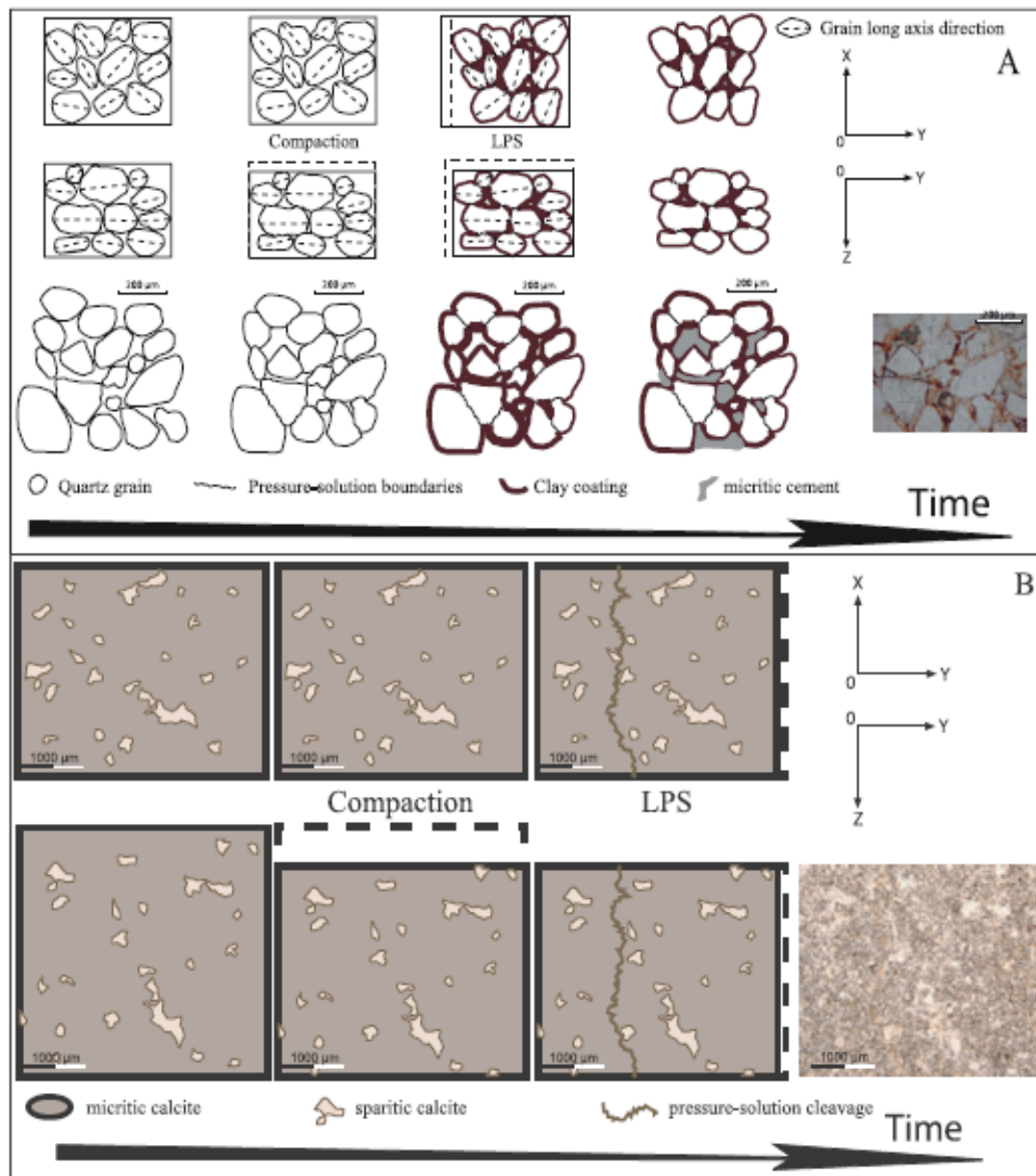
Sketches of different stages of formation/deformation of a sedimentary rock until a final state illustrated by the microphotographs of polished thin sections observed in natural light. (a) Sandstones (Amsden); (b) Carbonates (Phosphoria). *XY* plane is the bedding plane (*X*: Strike; *Y*: dip), *YZ* is the plane perpendicular to the bedding plane.

(Amrouch et al., GJI, 2010)

Paleo-stress/strain orientations
and magnitudes of differential stresses revealed by calcite twin analysis
at Sheep Mountain and Rattlesnake Mountain anticlines

B 27

KAL 4

SMA 1

B 12
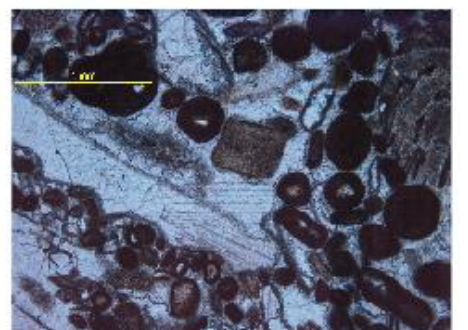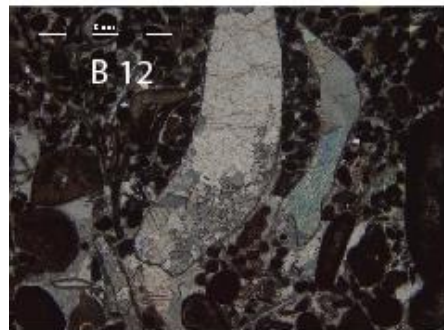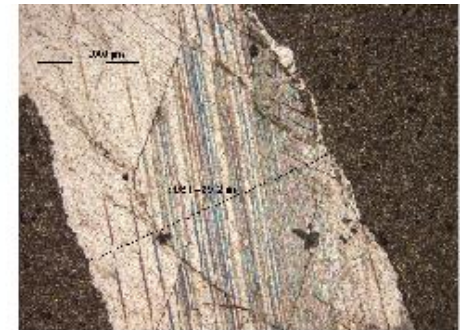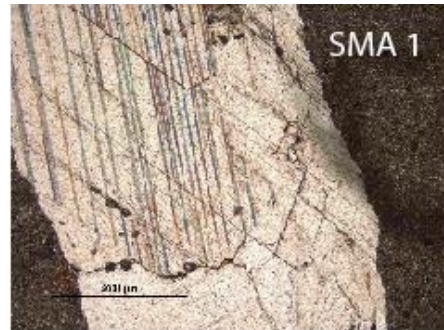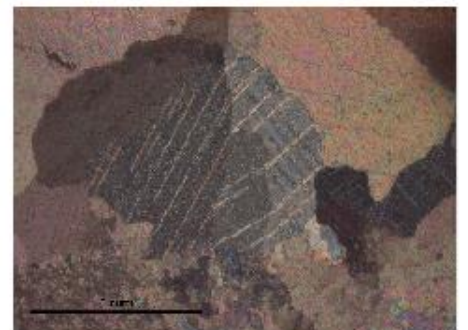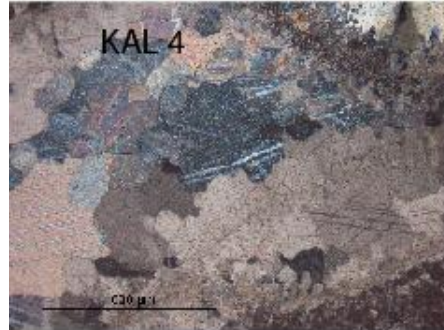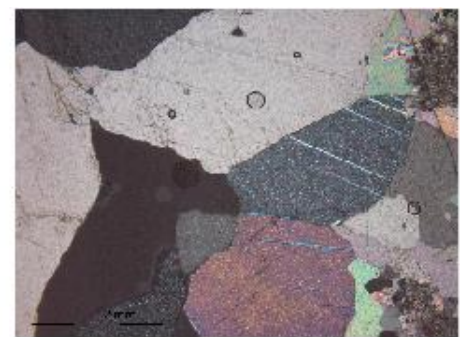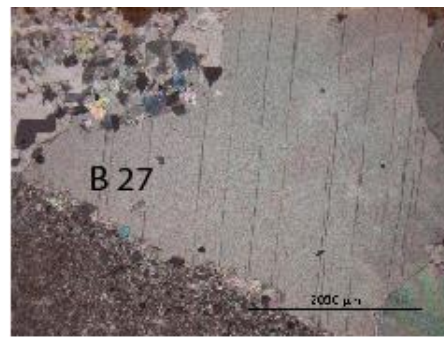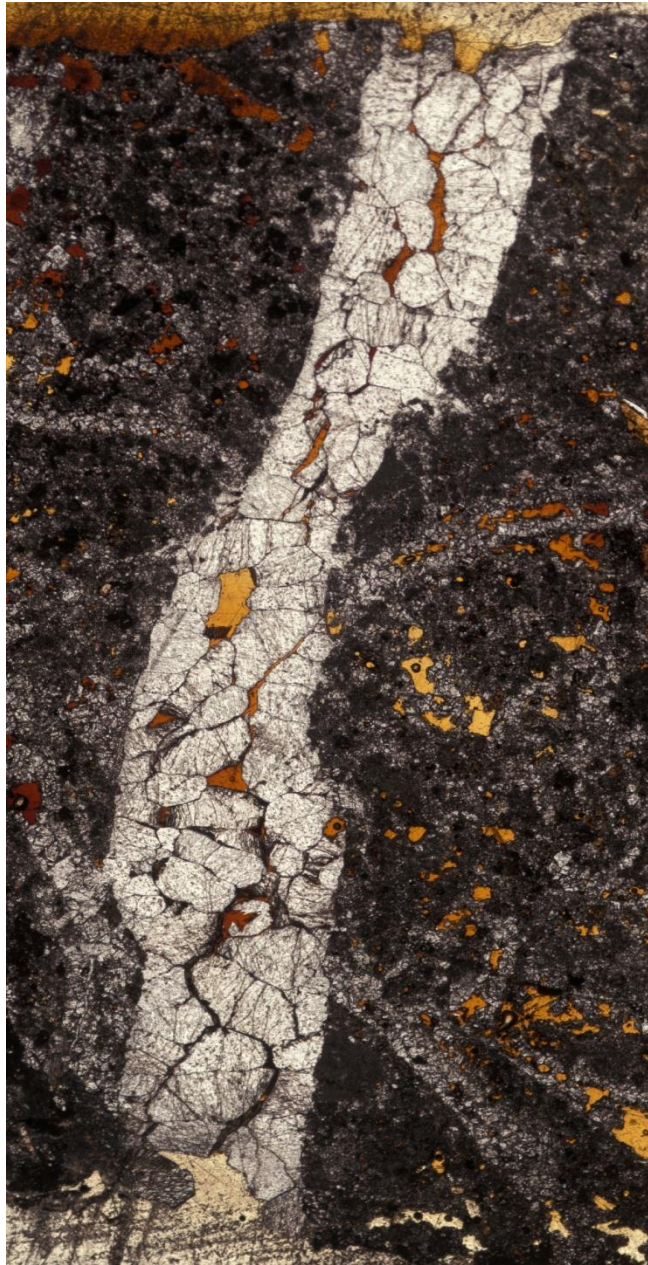
Twinning ~ simple shearing in a particular sense and direction along e-planes {01-12}

Twin lamella

Host crystal

Twinning sense

Twin lamella

Twin plane

Twinning direction

$-(\sigma_1-\sigma_3)/2 \leq \tau_s = (\vec{\sigma} \cdot \vec{s}) \leq (\sigma_1-\sigma_3)/2$

$$\begin{bmatrix} \sigma_1 \\ \sigma_2 \\ \sigma_3 \\ \Phi \end{bmatrix} \quad \Phi = \frac{(\sigma_2-\sigma_3)}{(\sigma_1-\sigma_3)}$$

The inversion process is very similar to that used for fault slip data :
twin gliding along the twinning direction within the twin plane is geometrically comparable to slip along a slickenside lineation within a fault plane.

But the inversion process takes into account both twinned planes (resolved shear stress > CRSS)
AND
untwinned planes
(resolved shear stress < CRSS),
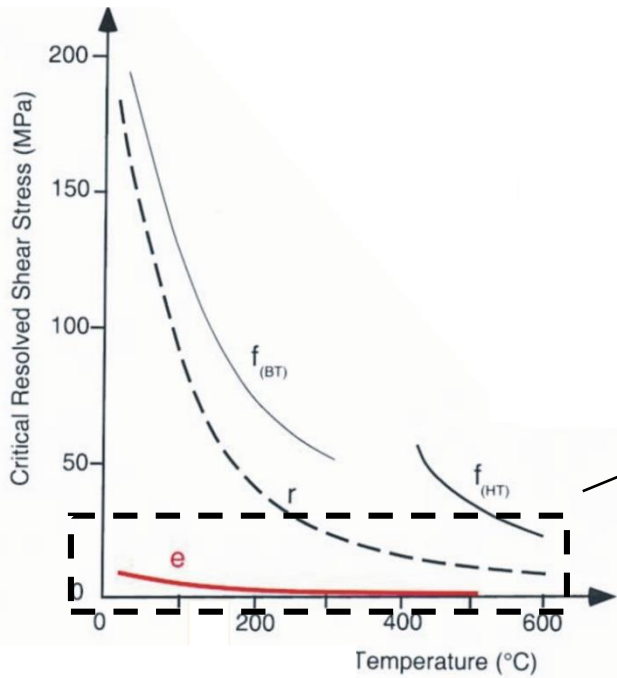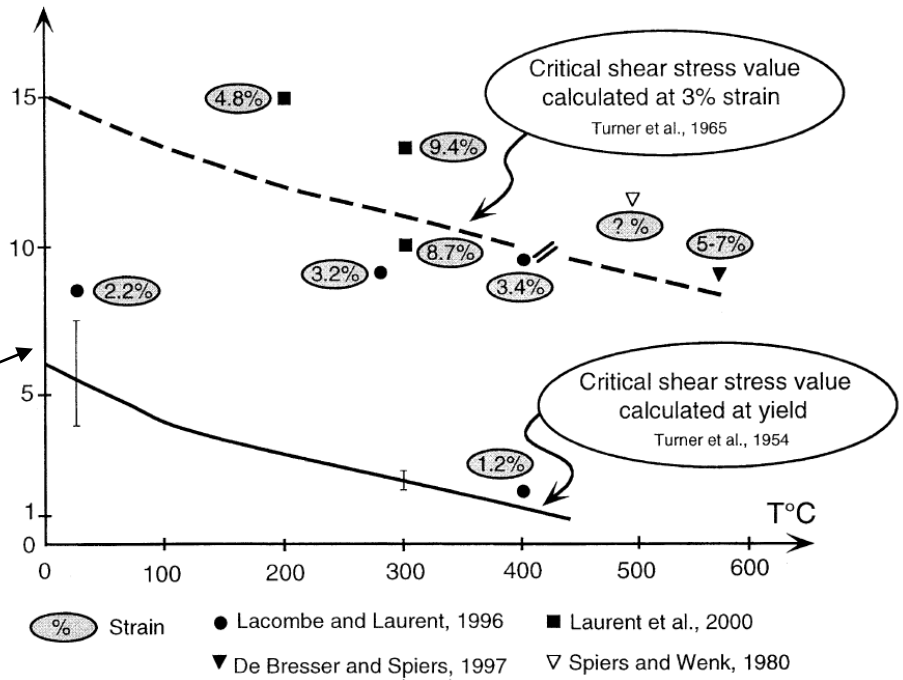
The Critical Resolved Shear Stress for twinning is ~ independent on T°C but depends on grain size and internal strain (hardening)

(Lacombe, 2001, 2010)

Inversion of calcite twin data

➡ **Reduced stress tensor : 4 parameters**

Orientation of principal stresses and stress ellipsoid shape ratio

$$\Phi = \frac{(\sigma_2 - \sigma_3)}{(\sigma_1 - \sigma_3)}$$
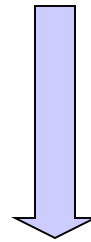
'constant' CRSS
for a set of calcite grains
of homogeneous size

**Deviatoric stress tensor
5 parameters**

Orientation of principal stresses and differential stress magnitudes

$$(\sigma_1 - \sigma_3) \qquad (\sigma_2 - \sigma_3)$$

« Groshong » (1974, 1984) technique : determination of the strain tensor
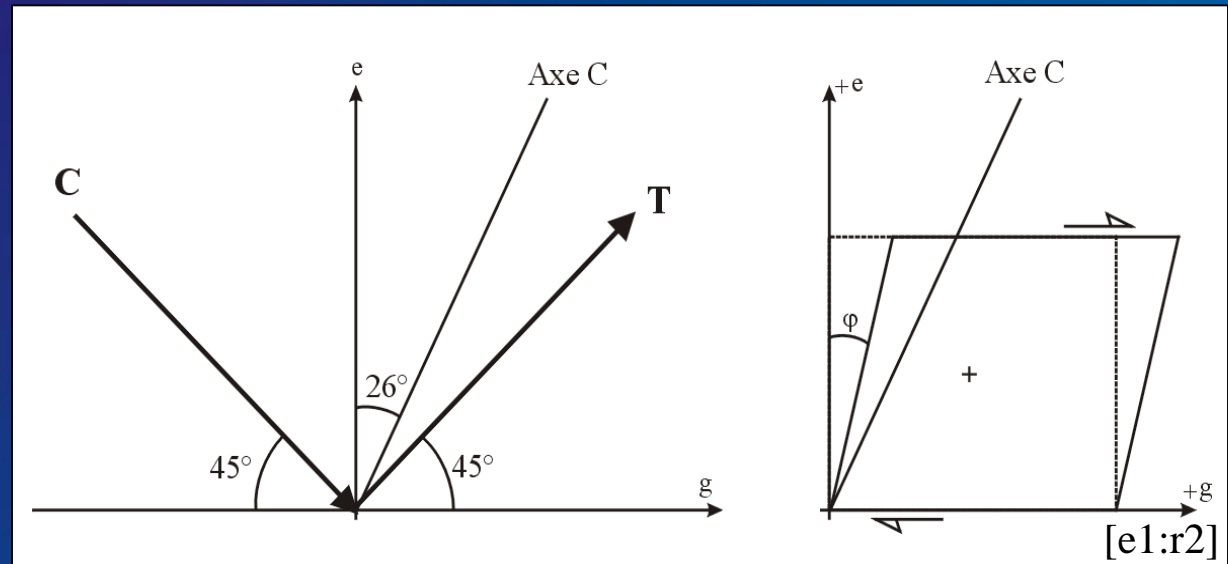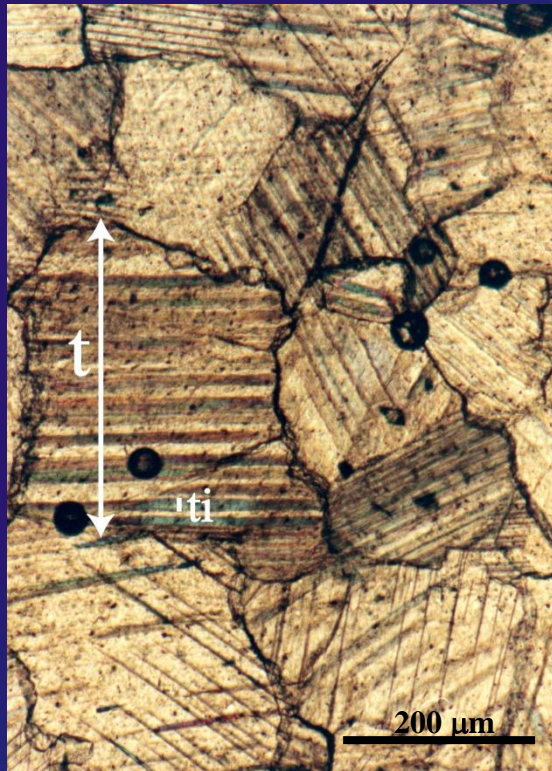

$$\Gamma eg = \frac{1}{2} \cdot \tan\varphi = \frac{0.347}{t} \cdot \sum_{i=1}^{n} ti$$

Deformation
by shearing
for a twin set

$\Gamma eg = (lelg - neng)\, \varepsilon x + (memg - neng)\, \varepsilon y + (lemg + melg)\, \Gamma xy + (meng + nemg)\, \Gamma yz + (nelg + leng)\, \Gamma zx,$

with εx, εy, Γyz, Γxy and Γzx being the components of the strain tensor in (x,y,z) and le, me, ne and lg, mg, ng the direction cosines of e and g in (x,y,z). $\varepsilon z = -(\varepsilon x + \varepsilon y)$ assuming $\Delta V = 0$

Pre-folding stage:
Paleostress /strain orientations related to Sevier LPS.
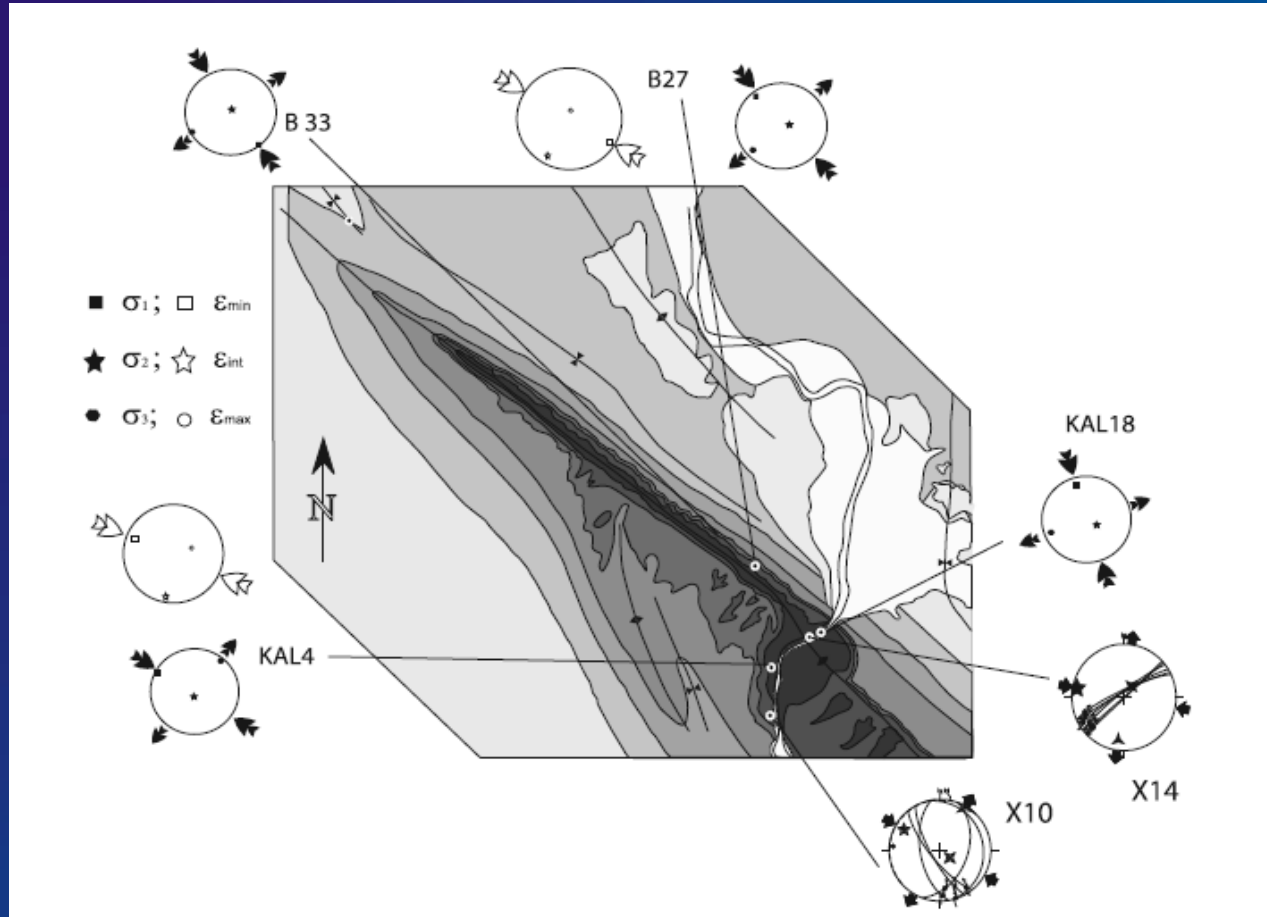
The oldest fracture set (I) strikes 110° to 130° and is interpreted as a regional fracture set that predates the Laramide orogeny (Sevier ?). This set formed in a strike-slip stress regime under a NW-SE horizontal compression

Early-folding stage:
Paleostress /strain orientations related to Laramide LPS.
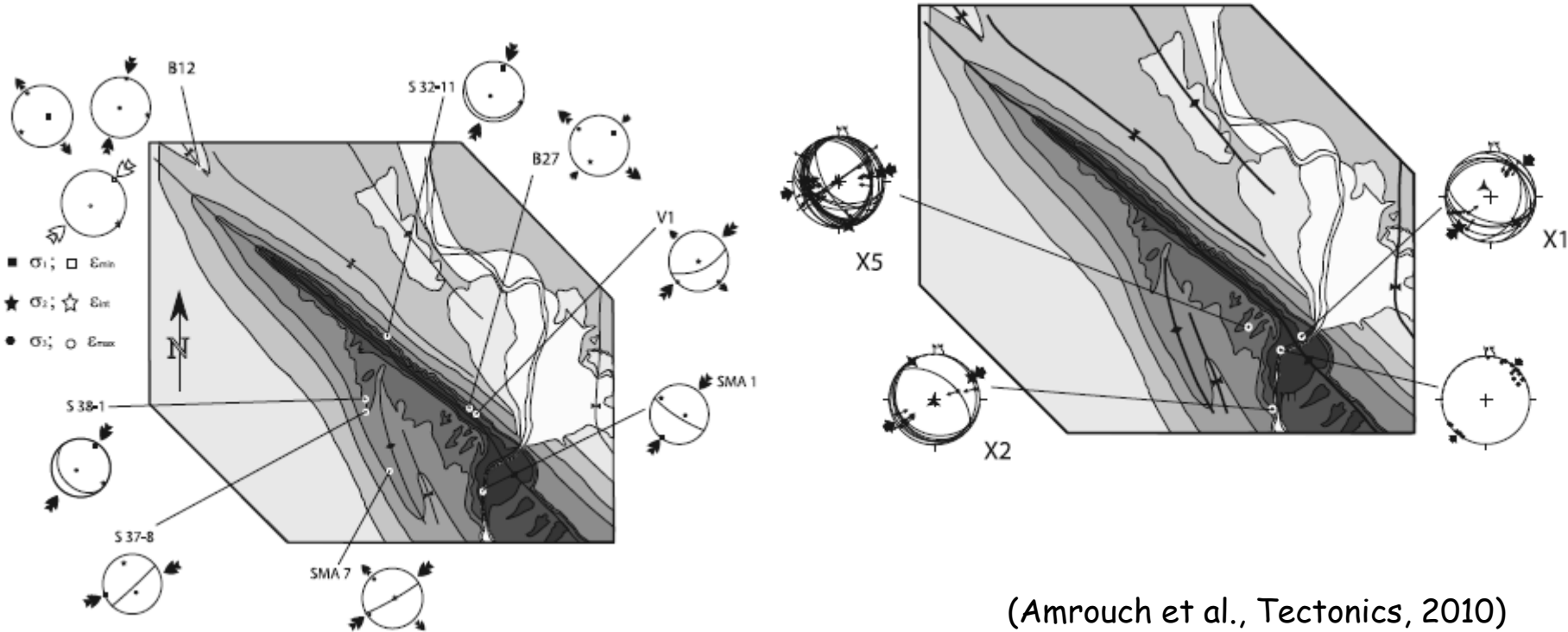
(Amrouch et al., Tectonics, 2010)

Set II joints striking ~045° and associated stylolites are related to the Laramide Layer-Parallel Shortening (LPS). The compression was oriented NE to ENE either in a strike-slip or in a compressional regime.

Late-folding stage: paleostress / strain orientations related to Laramide late stage fold tightening (LSFT).

(Amrouch et al., Tectonics, 2010)
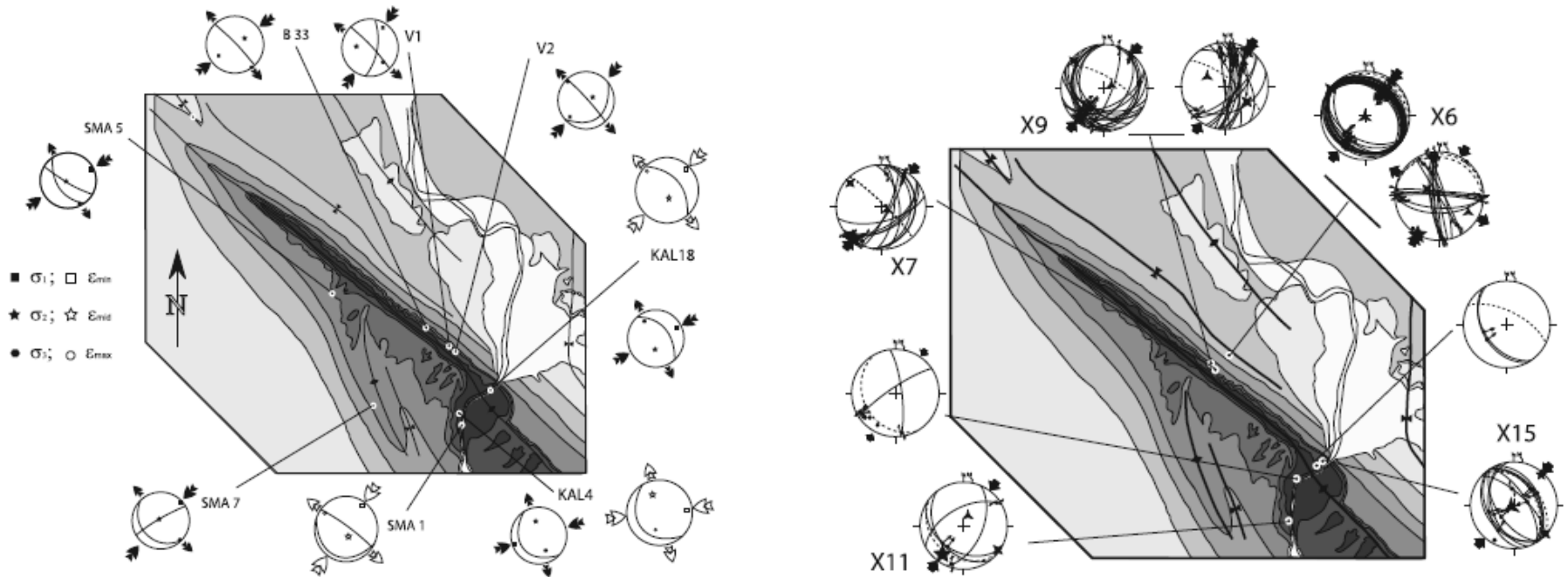
Faults and calcite twins reveal a late fold tightening stage, associated with a strike-slip stress regime and a compression axis also oriented NE.

Paleostress orientations and regimes
in space and time in the Bighorn Basin

Fracture set	Mean strike of fractures	Paleostress from fractures	Paleostress from striated microfaults	Paleostress from calcite twins	Related Tectonic events	
Set S-I	090°E to 060°E				Sevier layer-parallel shortening	Pre-Laramide
Set S-II	180°E to 020°E				Formation of the flexural foreland basin	
Set S-III	110°E				Sevier layer-parallel shortening	
Set L-I	045°E				Laramide layer-parallel shortening	Laramide
Set L-II	135°E				Local curvature-related extension	
Set L-III	045°E				Late stage fold tightening	
Set P-I	180°E to 160°E				Basin and Range extension	Post Laramide

(Beaudoin et al., Tectonophysics, 2012)

Summary

Mesoscopic fracture networks and anisotropy of rock physical properties reveal a similar Laramide NE-SW shortening direction.

Both techniques are complementary and help unravel the tectonic rock damage at different scales, as well as the fracture-related porosity properties.

The type of deformation (fracture formation vs. matrix damage) recorded in the rock depends on the matrix rheological properties, which result from various processes such as fluid flow, degree of cementation of the matrix or diagenesis.

Anisotropy of rock physical properties, differential stresses and fracture distribution outline the strong contrast between forelimb and backlimb, likely related to the way the fold developed asymmetrically above the basement thrust. <u>Structural observations made at the microscopic scale in part of a fold may therefore be relevant to the fold scale</u>.

Micro-mechanisms appear to be more efficient before and at the onset of folding (LPS) and during late stage fold tightening, whereas macro-mechanisms (development of extensional fractures at the hinge or bedding-parallel slip) seem to prevail during folding *ss*. ('partitioning' through time),

Early-folding and late-folding paleo-differential stress magnitudes from calcite twinning paleopiezometry
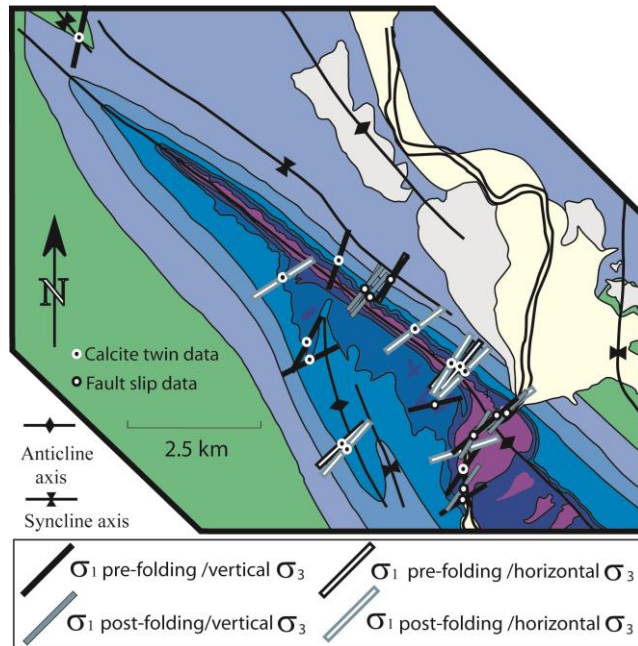
Sheep Mountain anticline
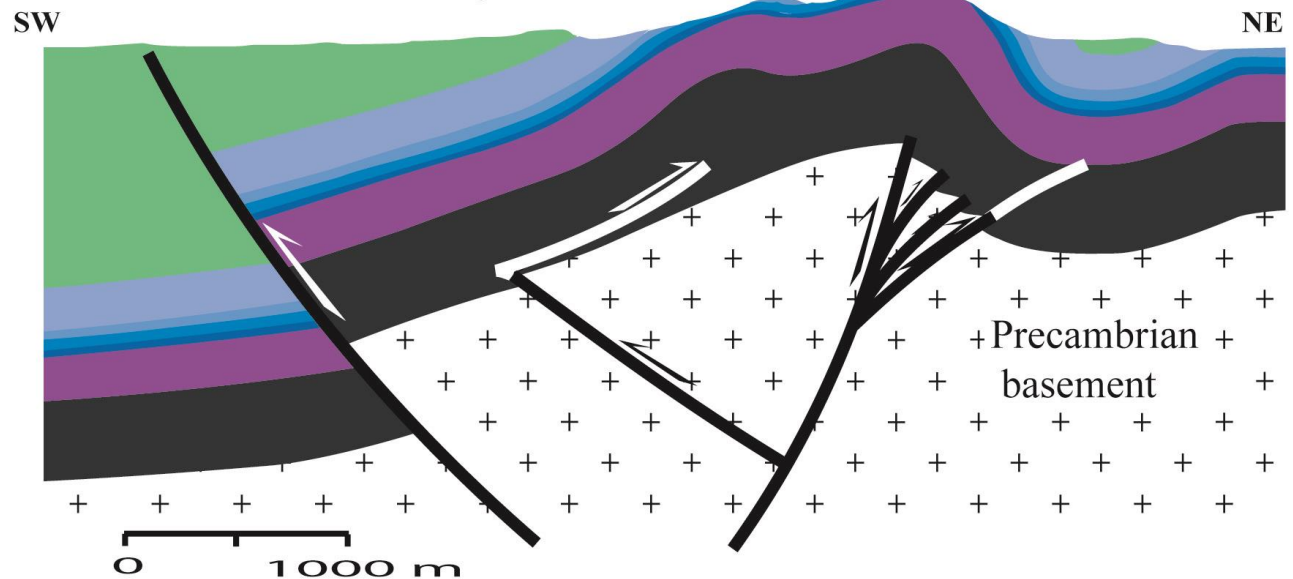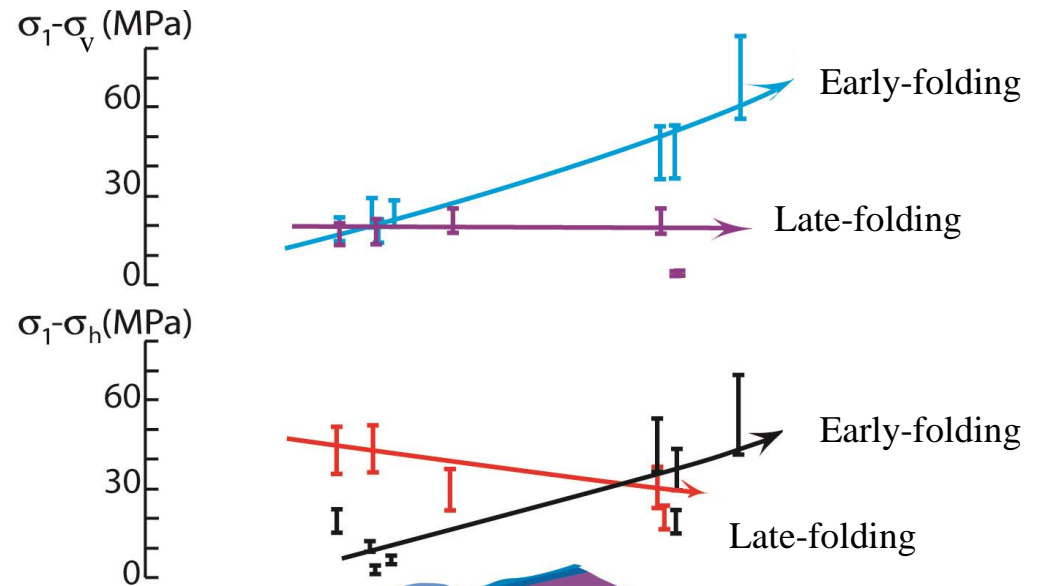
(Amrouch et al., Tectonics, 2010)

Stress perturbations in the sedimentary cover at the tip of the underlying basement fault starting to move during Laramide stress build-up

Minimum principal stress

contrainte (Pa)

6.10^7
-14.10^7
-34.10^7
-54.10^7
-75.10^7

3000m

b)

$\sigma1-\sigma3$ (Pa)
10^8

10^7

3000m

a)

vertical observation grid

thrust fault

c)

— $\sigma1$
– – – $\sigma2$
······· $\sigma3$
–·–·– $\sigma1-\sigma2$
—— $\sigma1-\sigma3$

$1.5.10^8$

10^8

5.10^7

0

0   5000   10000   15000   20000   25000   30000
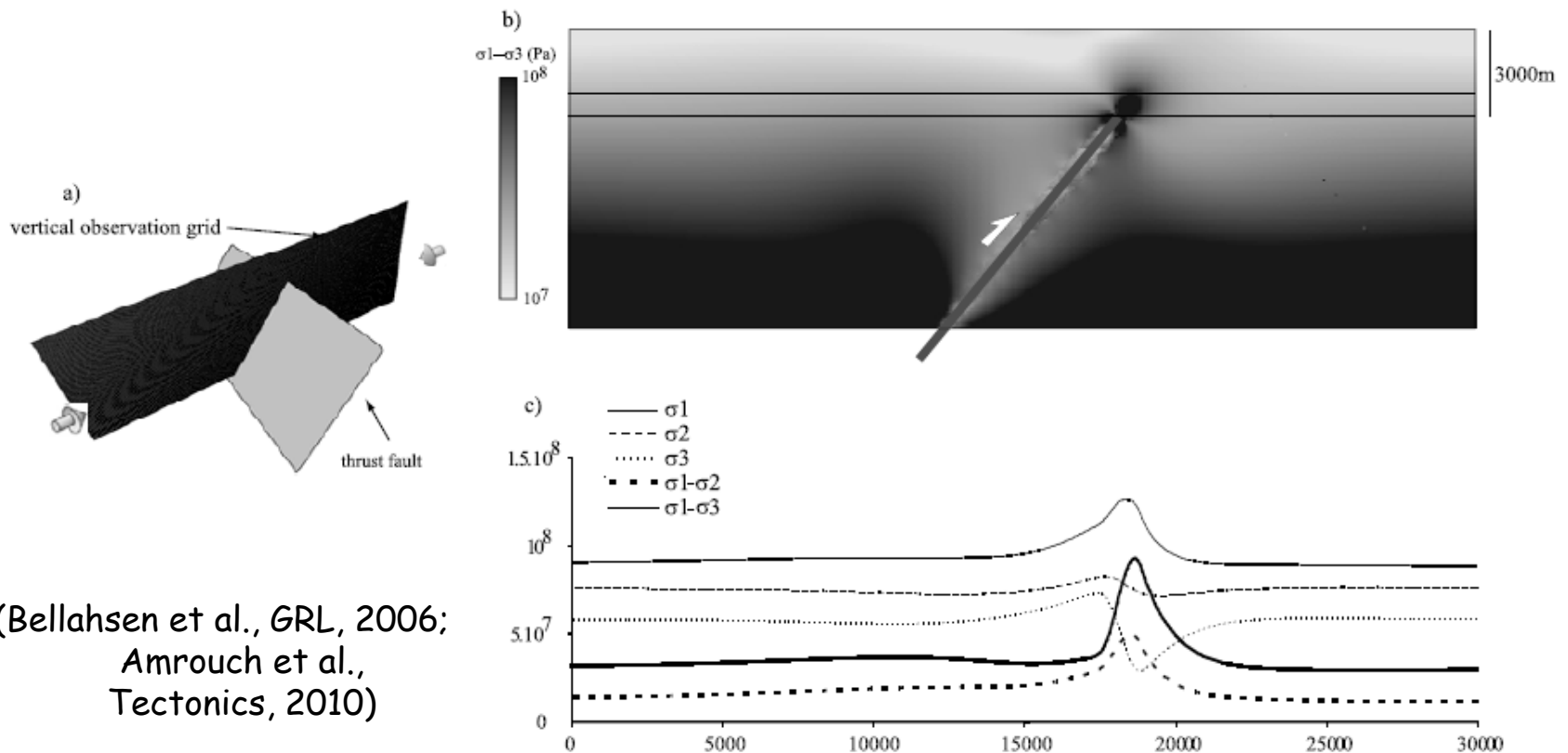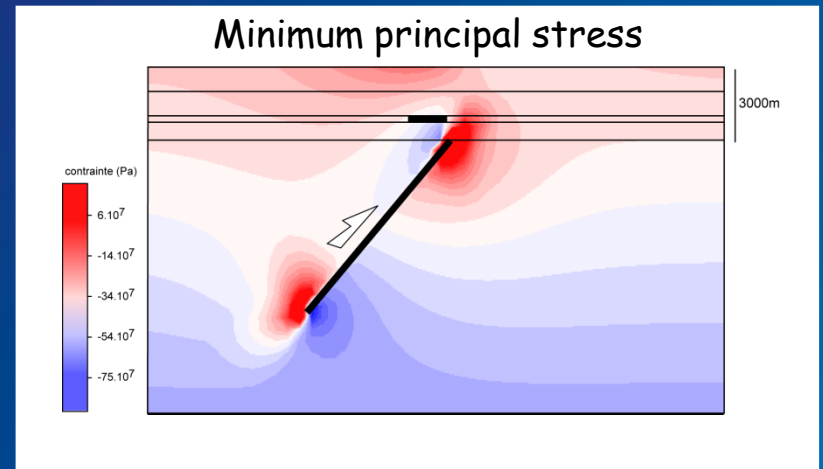
(Bellahsen et al., GRL, 2006; Amrouch et al., Tectonics, 2010)

Conclusion on the mechanical behaviour of folded strata at SMA:

* Early folding stage - LPS :

Forelimb : stress perturbations, that partly inhibited development of fractures.
In turn, limited fracture development + weak internal deformation (AMS and APWV)
→ poor stress relaxation → differential stress increase.

Backlimb : no stress perturbation + stress relaxation by widespread development of fractures and by internal strata deformation (AMS) → much lower differential stresses

* Syn- to late-folding stage – LSFT :

Forelimb : drop of differential stresses while limited internal deformation (poorly evolved AMS fabrics and low anisotropy of the matrix revealed by APWV)
→ strata were tilted during folding without any additional significant internal deformation, LSFT being mainly accommodated by newly formed microfaults and reactivation of earlier fractures → stress relaxation

Backlimb : Strata sustained most of LSFT without developing much fractures,
→ increase of differential stresses and development of more evolved AMS fabrics

Early-folding and late-folding Laramide paleo-differential stress magnitudes from calcite twinning paleopiezometry

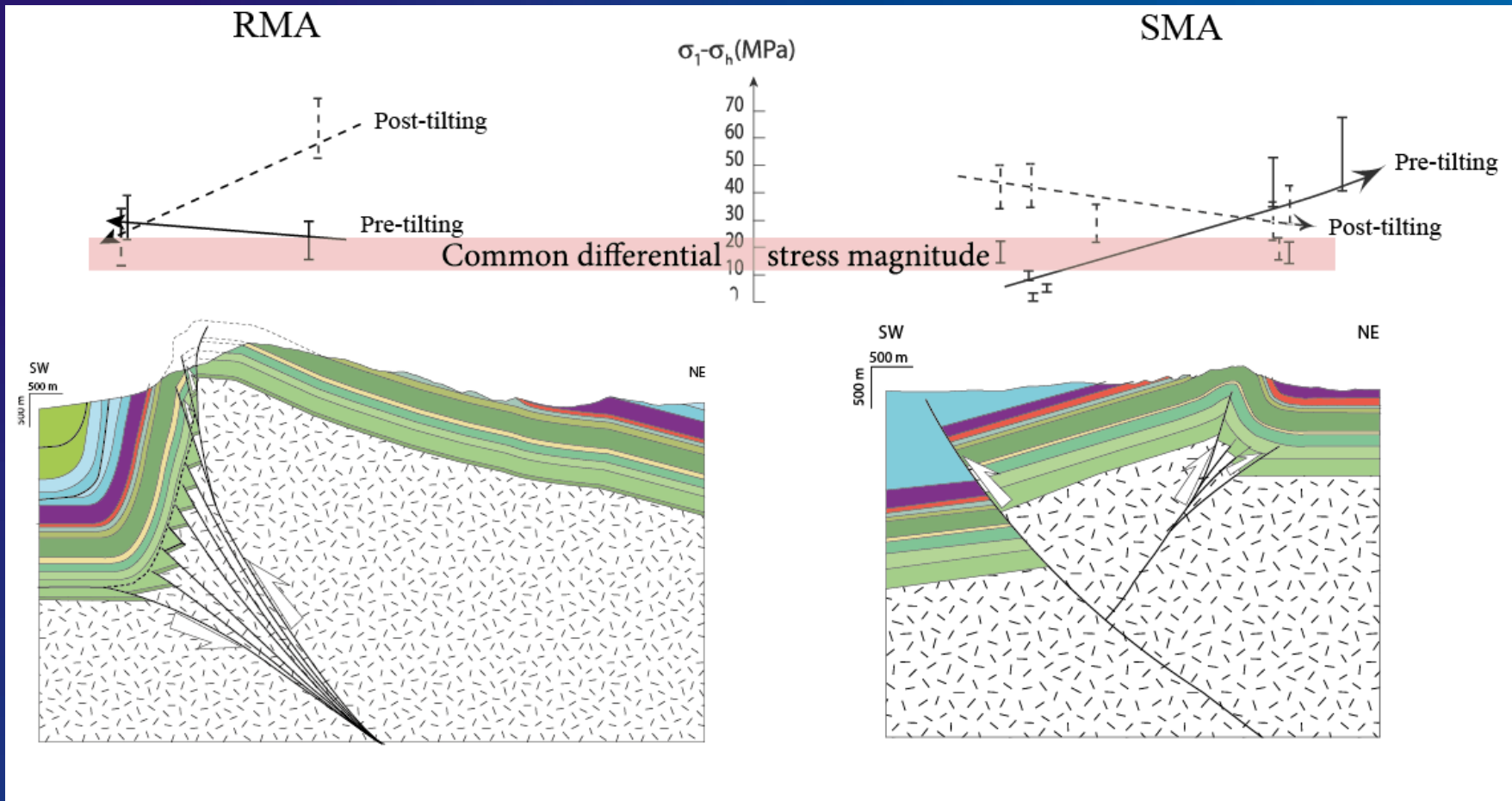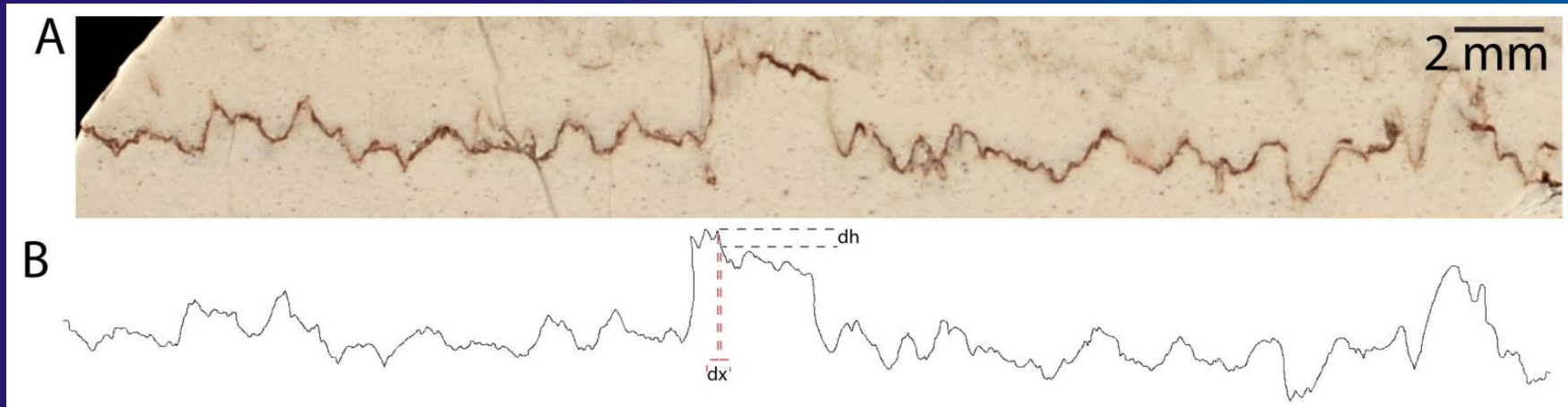(normalization of RMA to same depth than SMA for comparison)

(Beaudoin et al., Tectonophysics, 2012)

Vitesse de dissolution à l'interface (Rolland et al., 2012) :

$$v_d = Ts - \frac{l}{L_c} I_e + \eta$$

Ts : Tension de surface prenant en compte les effets induits par la courbure de la surface.

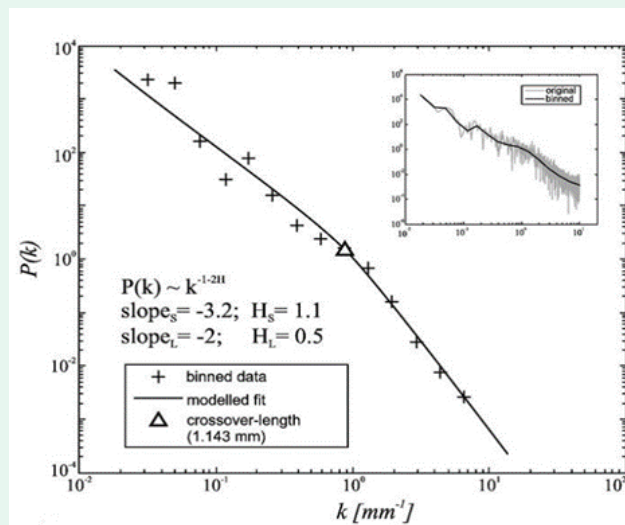I_e : Interactions élastiques décrivant la déformation de la surface.

η : désordre présent dans la roche (hétérogénéités) et dont les variables sont indépendantes du temps.

$$L_c = \frac{\gamma E}{\sigma_s \beta P}$$

E Module d'Young, γ énergie de surface et σ_s contrainte différentielle, P Pression moyenne, β constante dépendant des paramètres élastiques de la roche
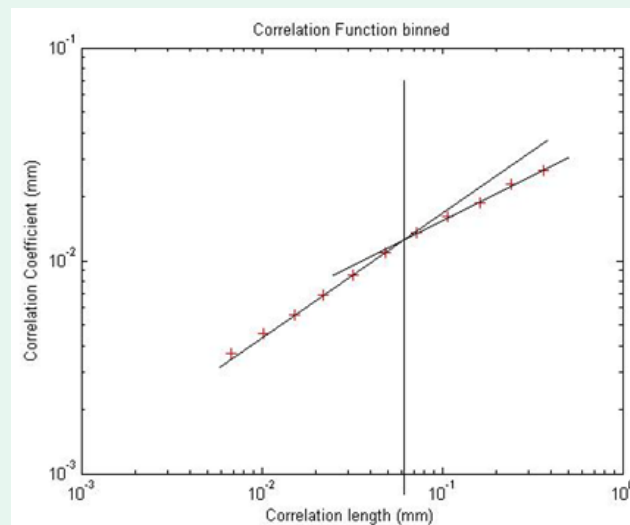
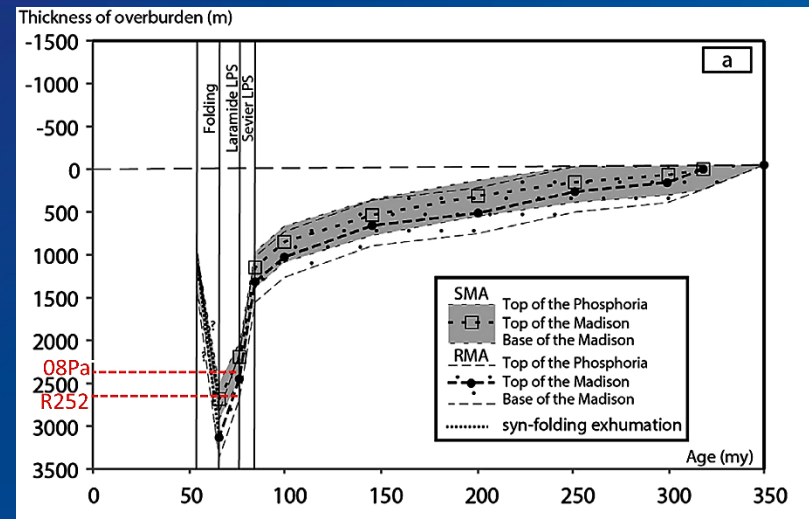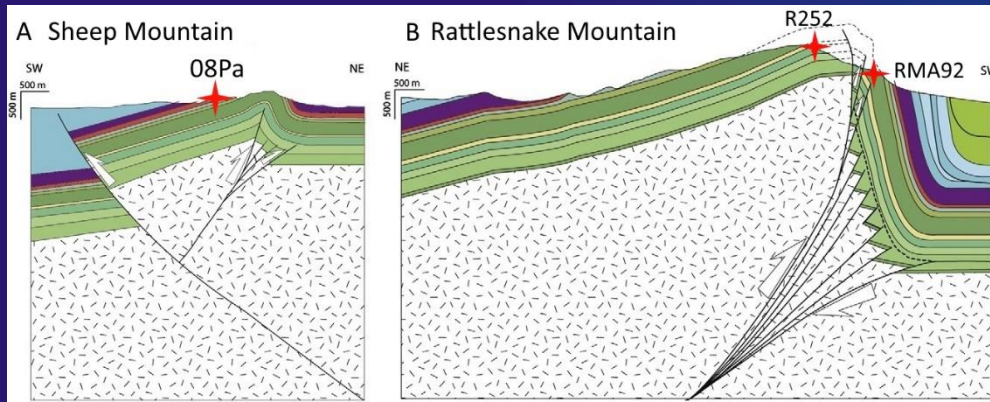| Transformée de Fourier	Fonction de corrélation
$F_i = \sum\limits_{j} \kappa(|x_i - x_j| - l)v_{i,j} + f_p$	$C(\Delta x) = [|(L(x) - L(x + \Delta x))^2|]^{\frac{1}{2}}$

- **2 régimes de développement :** petite et grande échelle en fonction des énergies de surface et élastique
- Principe : retrouver la <u>longueur de coupure</u> entre les 2 régimes de croissance
  - Sédimentaires: 1 Lc → contraintes horizontales isotropes
  - Tectoniques: 3 (Lv + Lh + Lc) → contraintes horizontales anisotropes
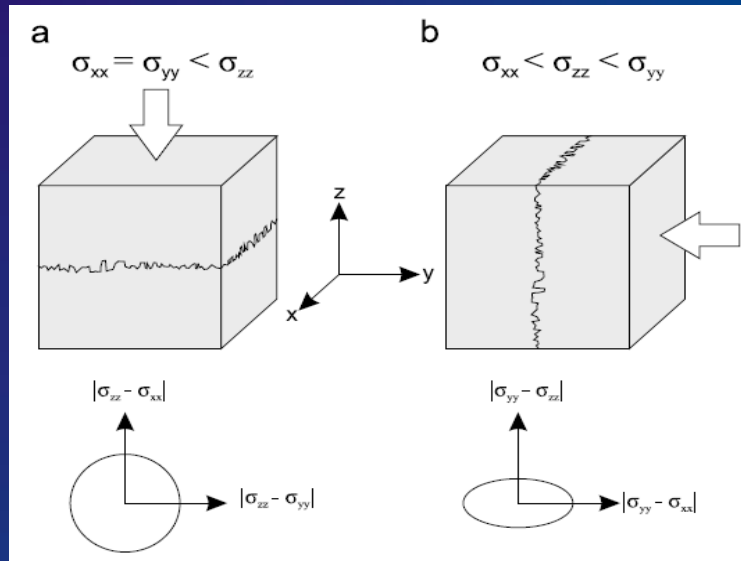
D'après Ebner et al. (2010)
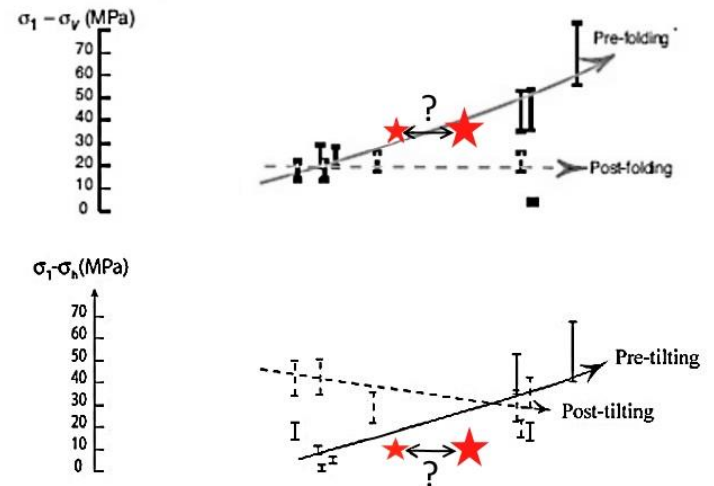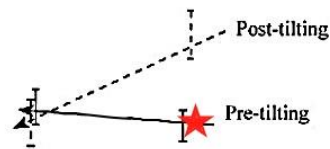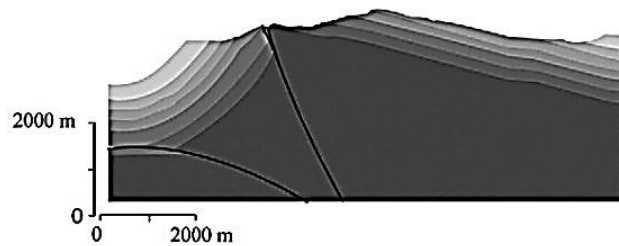
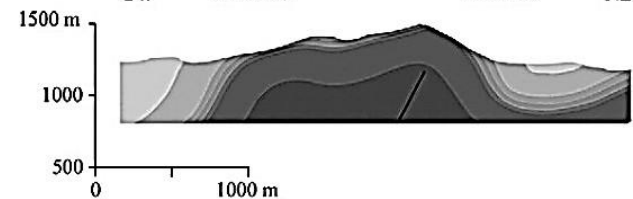| Stylolites sédimentaires	Stylolites tectoniques
$$\sigma_z^2 = \frac{\gamma E}{\alpha \beta L_c}$$	$$\sigma_y = f(\frac{L_v}{L_h}; \sigma_z) \pm \sqrt{\Delta(\frac{L_V}{L_h}, \sigma_z, \frac{a}{L_h})}$$
$$\sigma_x = \sigma_y = \frac{\nu}{1-\nu} \sigma_z$$	$$\sigma_x = \sigma_y - \frac{L_V}{L_h} \sigma_y - \frac{L_V}{L_h} \sigma_z$$

A Sheep Mountain   08Pa   NE   NE B Rattlesnake Mountain   R252   SW

RMA92

Thickness of overburden (m)

-1500
-1000
-500
0
500
1000
1500
2000
2500
3000
3500

Folding
Laramide LPS
Sevier LPS

08Pa
R252

SMA
Top of the Phosphoria
Top of the Madison
Base of the Madison
RMA
Top of the Phosphoria
Top of the Madison
Base of the Madison
syn-folding exhumation

Age (my)

0   50   100   150   200   250   300   350

★ Contraintes différentielles calculées
à partir de la rugosité des stylolites

$\sigma_1 - \sigma_v$ (MPa)

70
60
50
40
30
20
10
0

?

Pre-folding

Post-folding

$\sigma_1 - \sigma_h$ (MPa)

70
60
50
40
30
20
10
0

Post-tilting

Pre-tilting

Pre-tilting

Post-tilting

?

a SW   Forelimb   Backlimb   NE

2000 m

0
0   2000 m

b   SW   Backlimb   Forelimb   NE

1500 m

1000

500

0   1000 m

(Master 1 David, 2015)

Summary

Laramide differential stresses remained at a sub-constant level of about 20±10 MPa, the formation of widespread LPS-related structures preventing stress increase in the sedimentary layers.

Variations from these values are related
either to perturbations at the tip of underlying basement thrusts
(forelimb of SMA during LPS) and/or to stress increase
where strata remain weakly internally deformed.
(backlimb of both folds, during LSFT).

Laramide differential stresses were not attenuated between RMA and SMA, in contrast to the eastward attenuation of Sevier stresses.

→ This likely reflects the <u>influence of the structural style</u> :
stress magnitudes are seemingly mainly controlled by
local (basement) structures during thick-skinned tectonics rather than
by the distance to the orogenic front as in thin-skinned tectonics.

Paleo-hydrology
at Sheep Mountain and Rattlesnake Mountain anticlines

Veins : an access to fossil fluids

Calcite veins :

O, C stable isotopes

Microthermometry of fluid inclusions

Sr ratios

Fluid temperature

Fluid origin and pathways

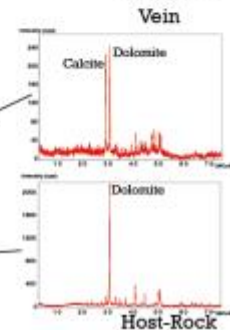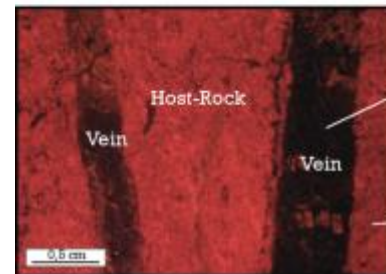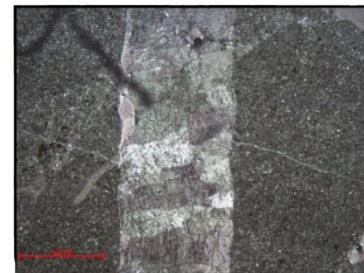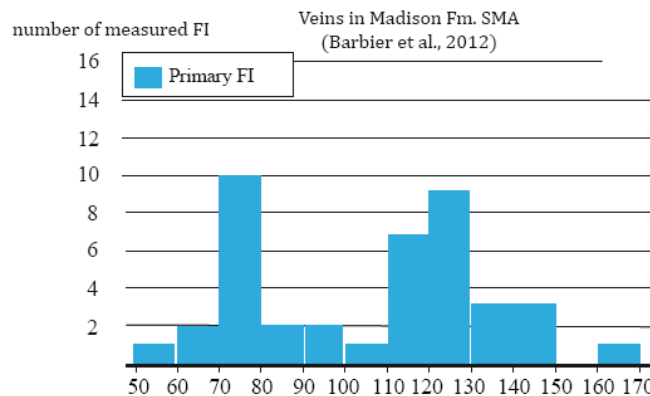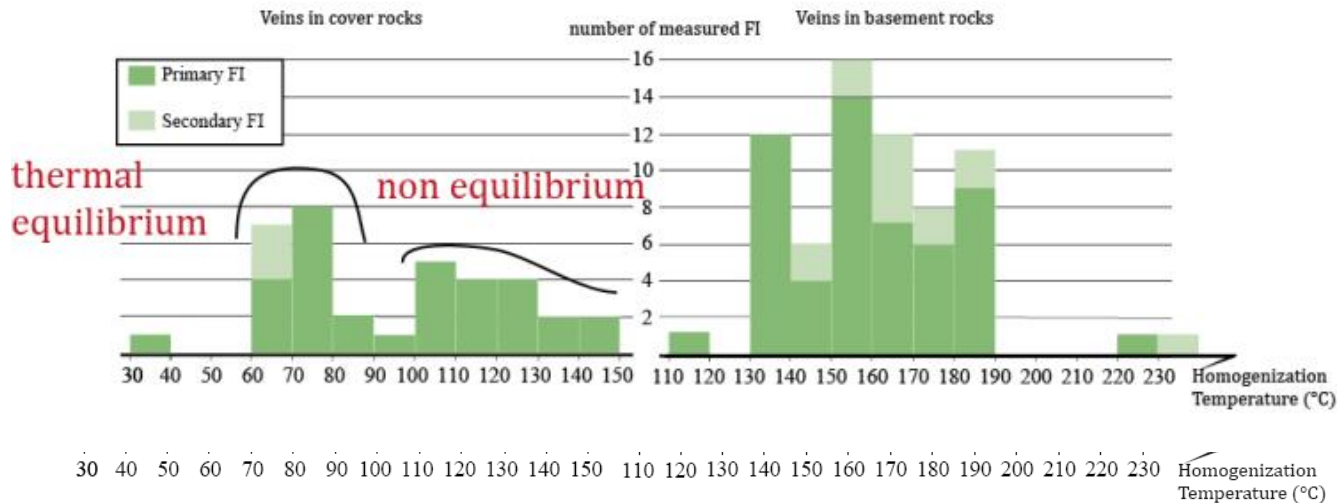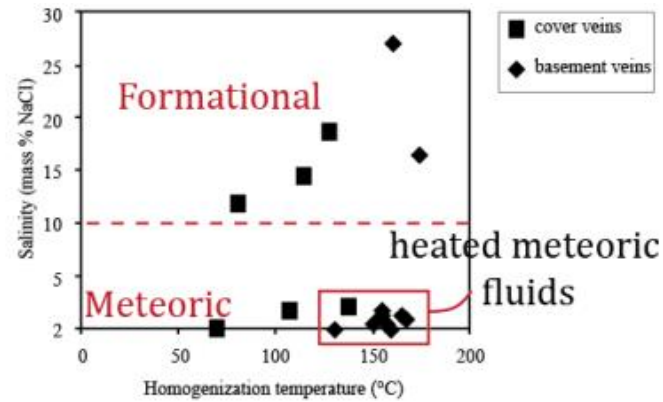5 mm
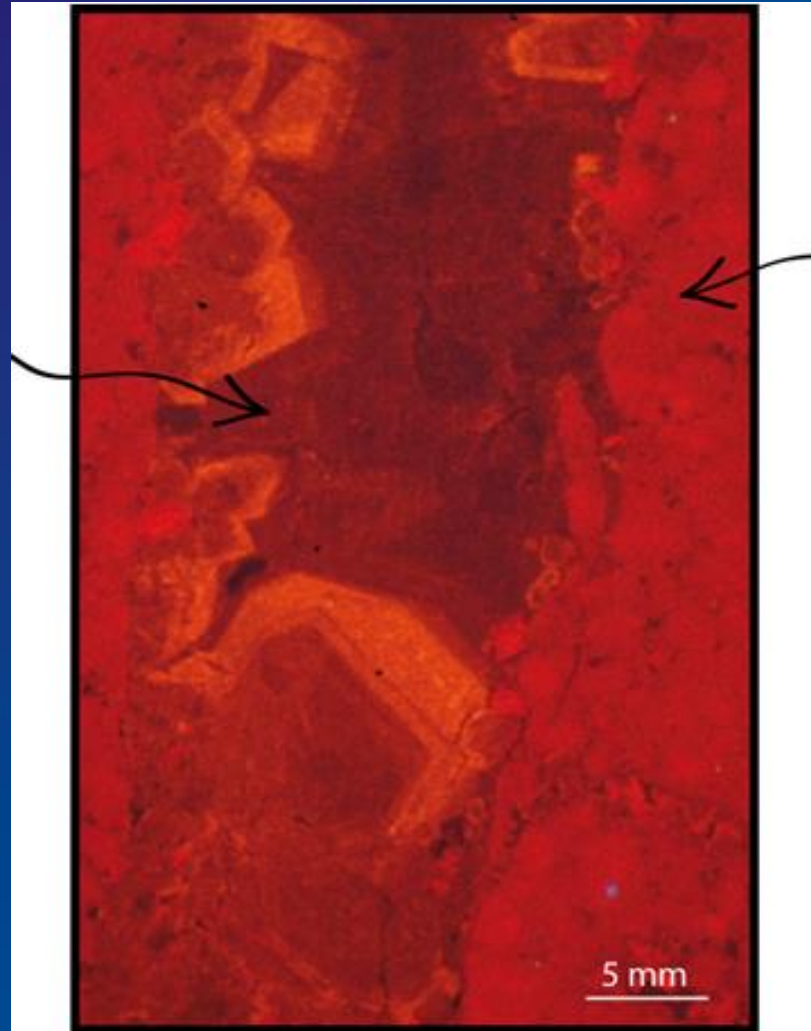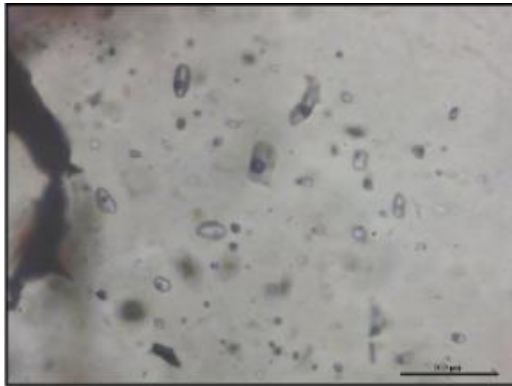
Host rocks :

O, C stable isotopes

Sr ratios

Fluid-Rock Interactions

Textures and vein fillings
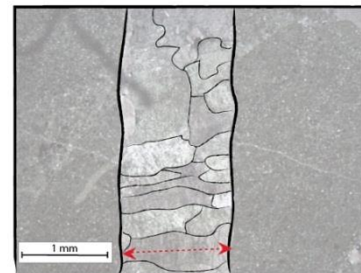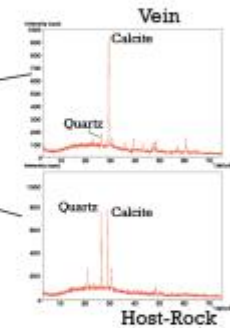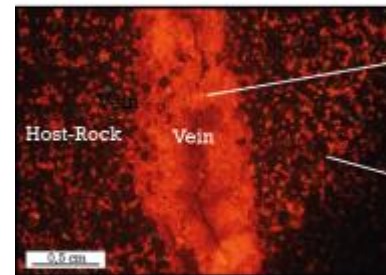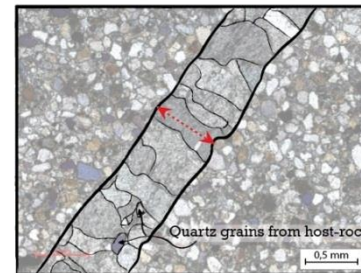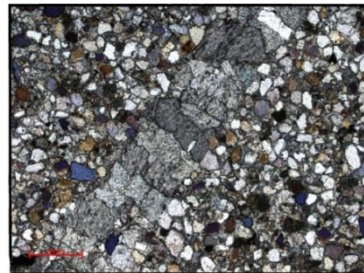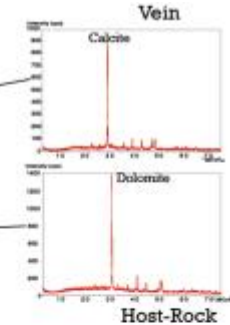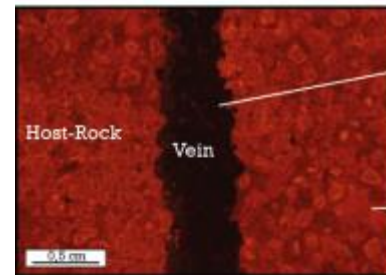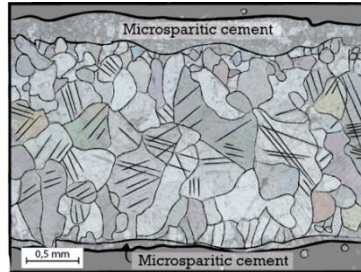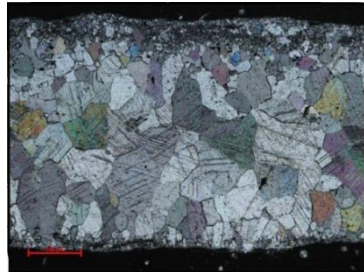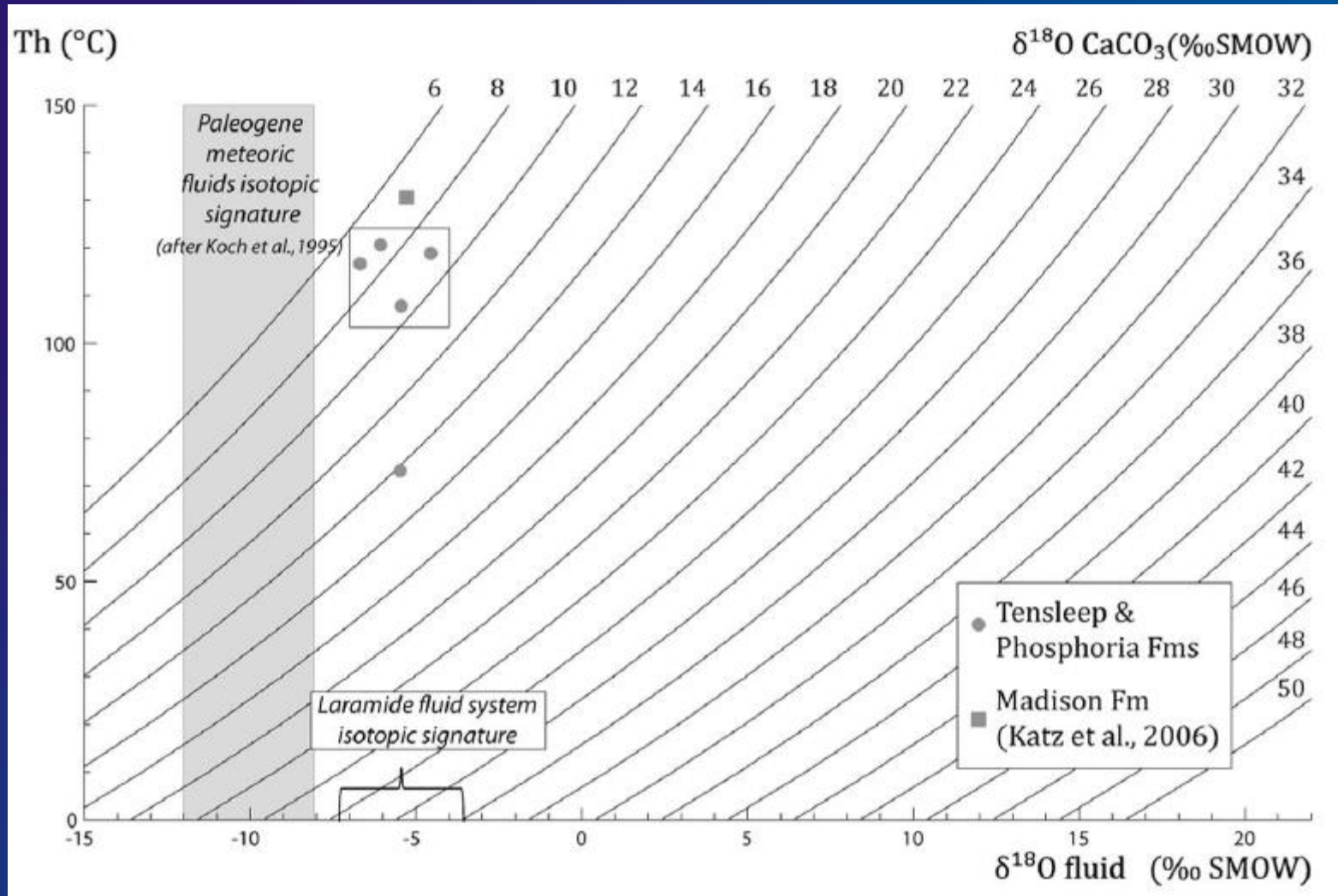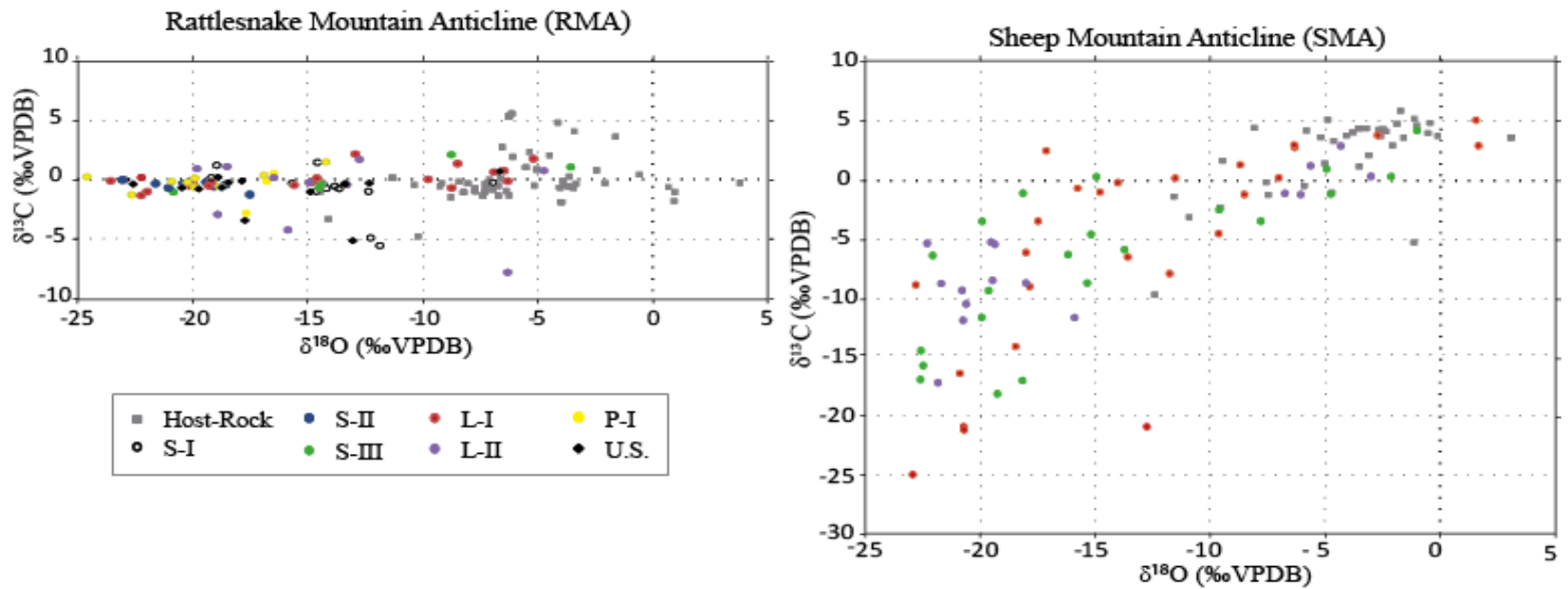
Microthermometry
and Raman
spectrometry
of fluid inclusions

Homogeneization temperatures vs $\delta^{18}O$

(Beaudoin et al, G3, 2011)
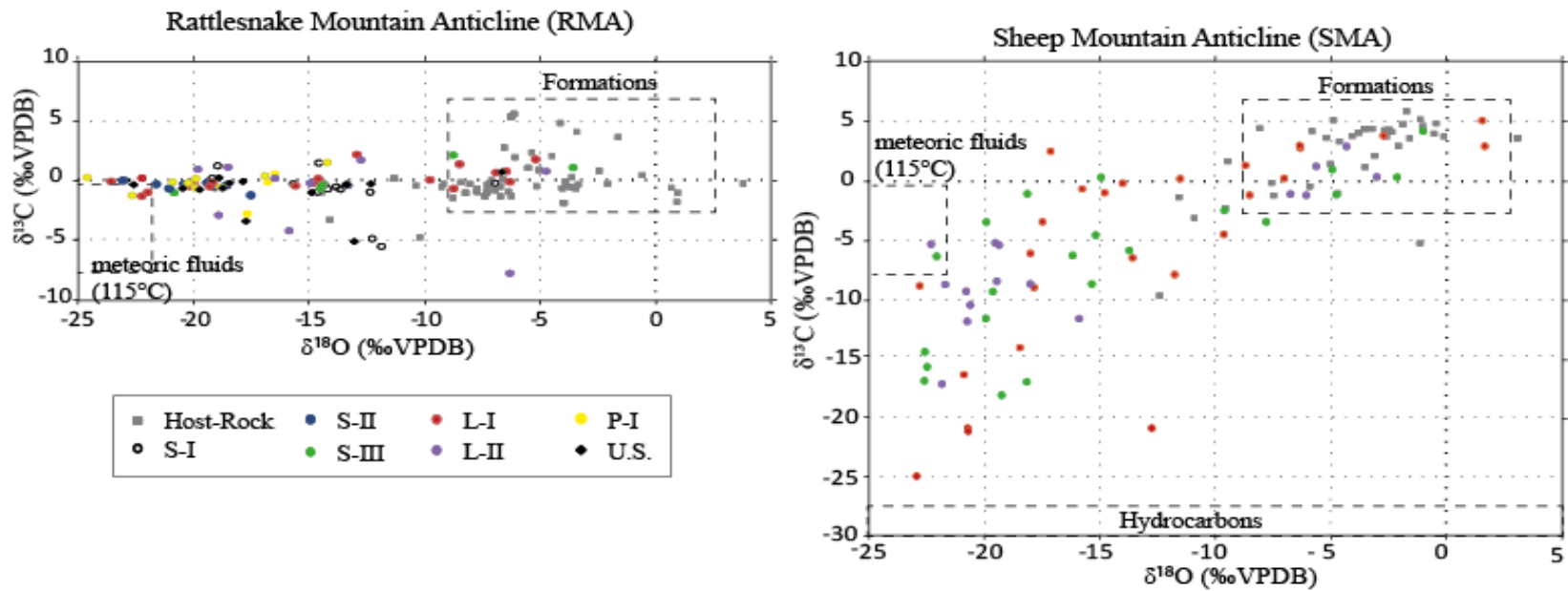
O, C stable isotopic signatures of fluids at SMA and RMA

O, C stable isotopic signatures of fluids at SMA and RMA

Defining the fluid system

Three types of precipitating fluids:

- Total isotopic and thermal equilibrium with host-rock
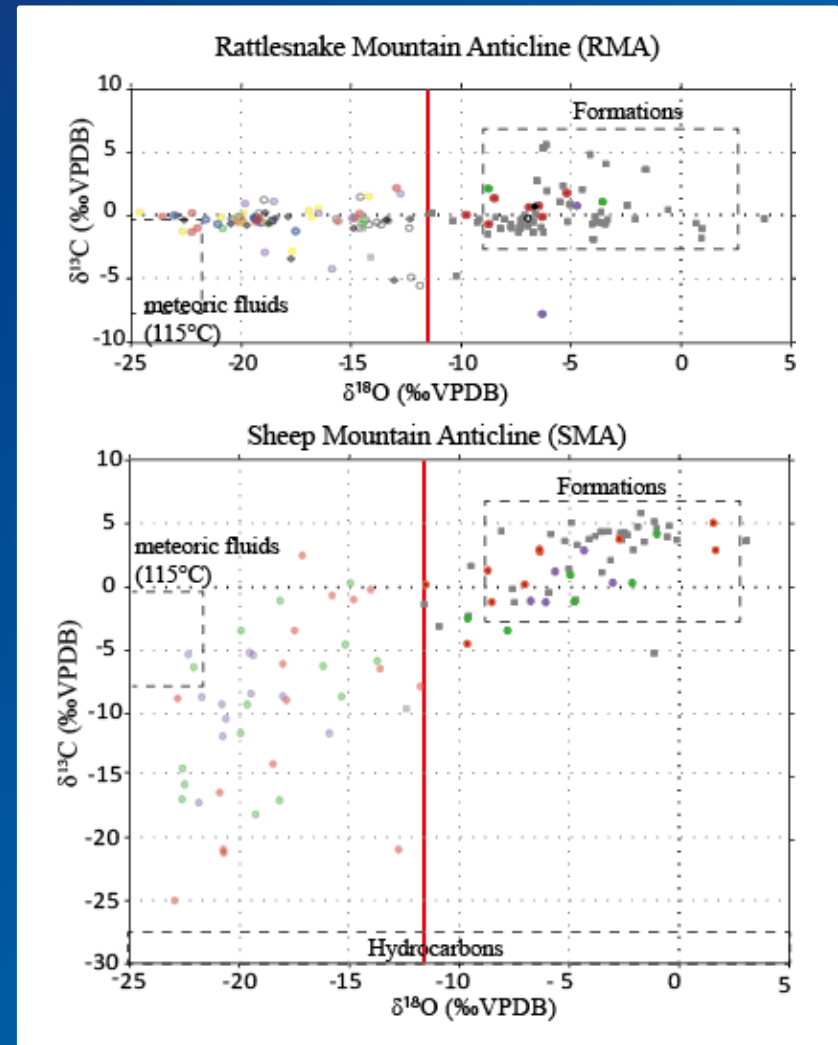
Defining the fluid system

* Total isotopic and thermal equilibrium with host-rock

* $\delta^{18}O$ depletion but thermal equilibrium with host-rock
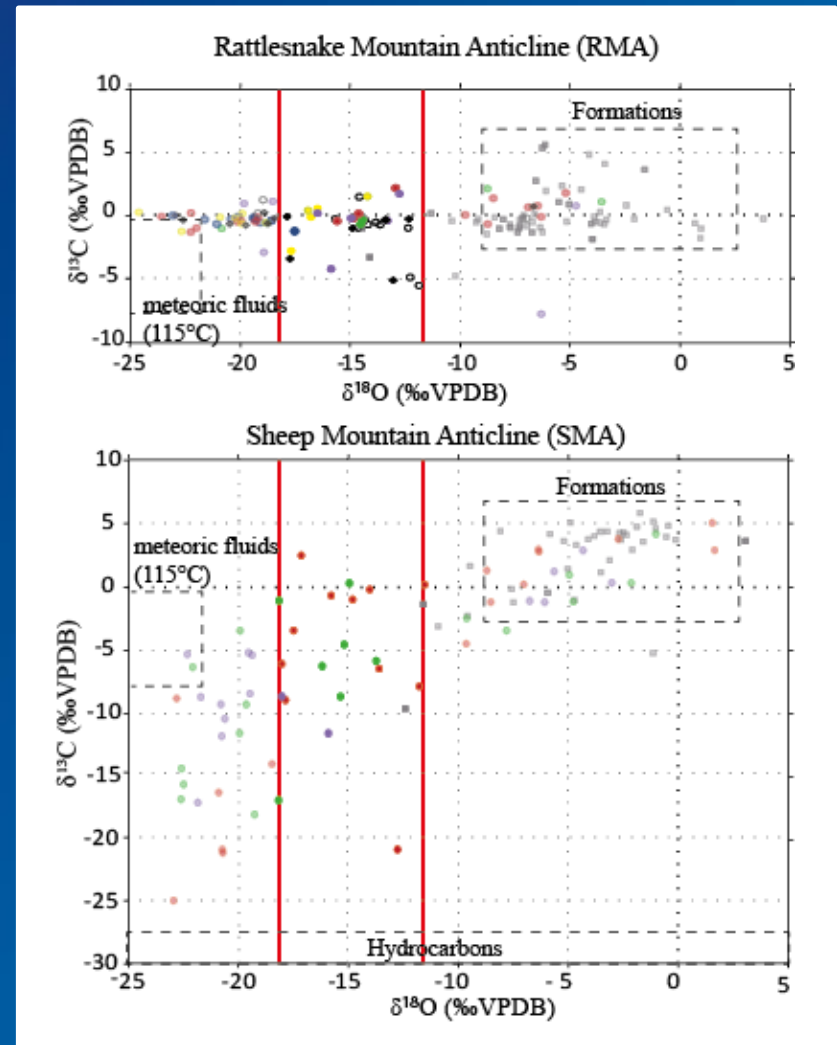
Defining the fluid system

* Total isotopic and thermal equilibrium with host-rock

* $\delta^{18}O$ depletion but thermal equilibrium with host-rock

* High $\delta^{18}O$ depletion and thermal disequilibrium with host-rock

Evolution of fluid system in SMA and RMA
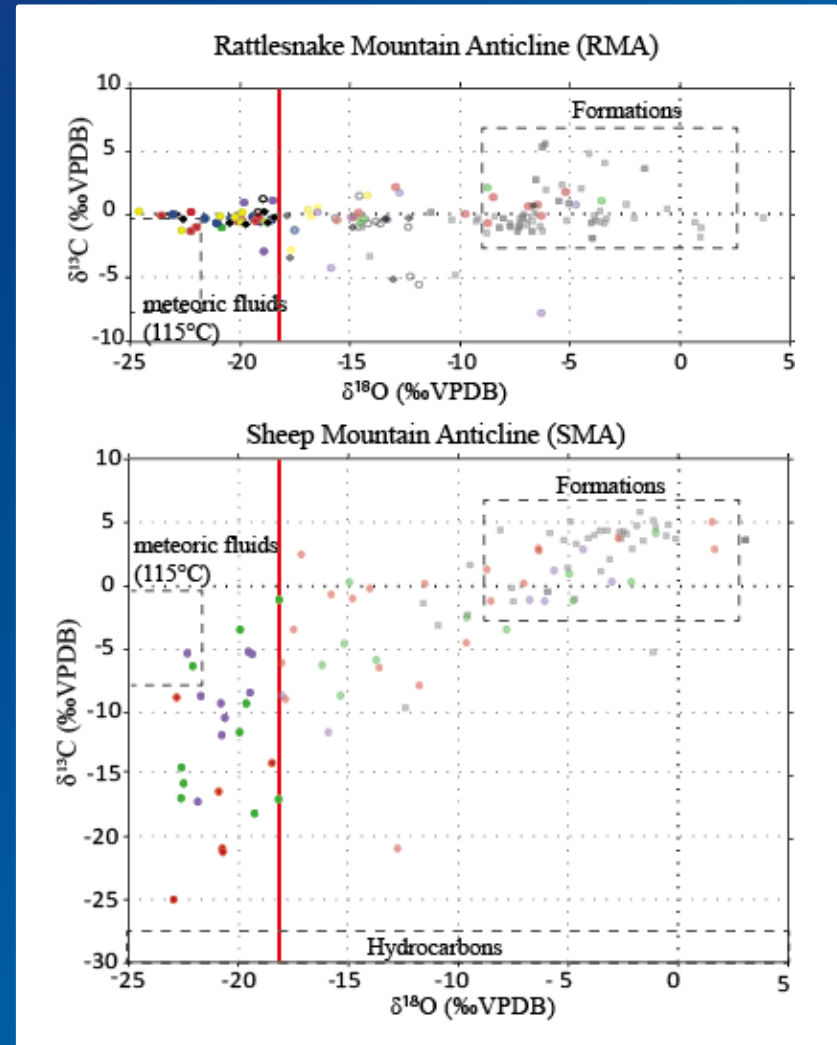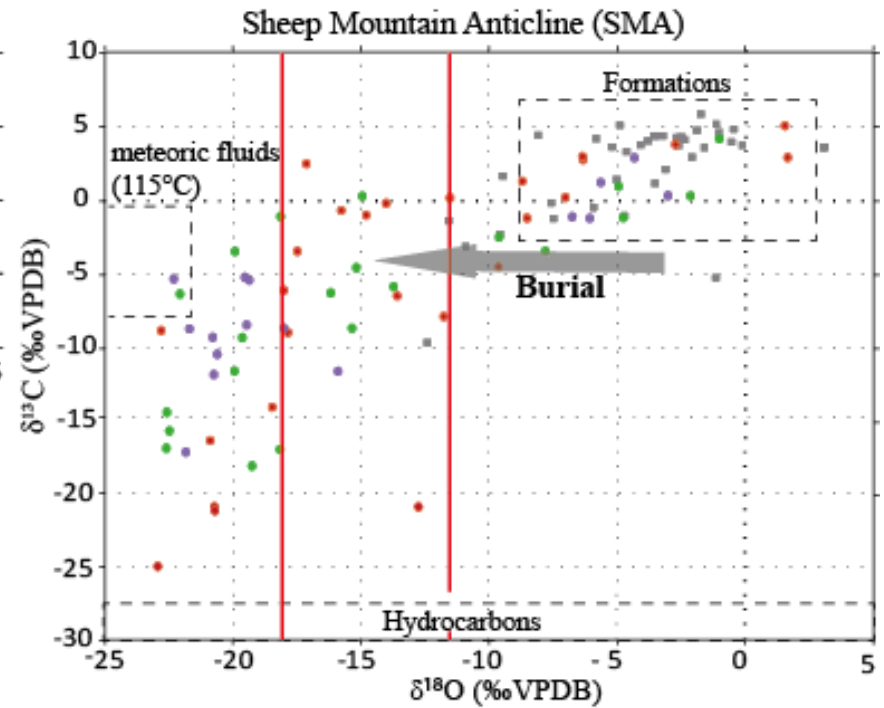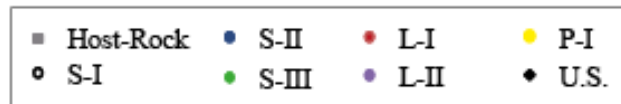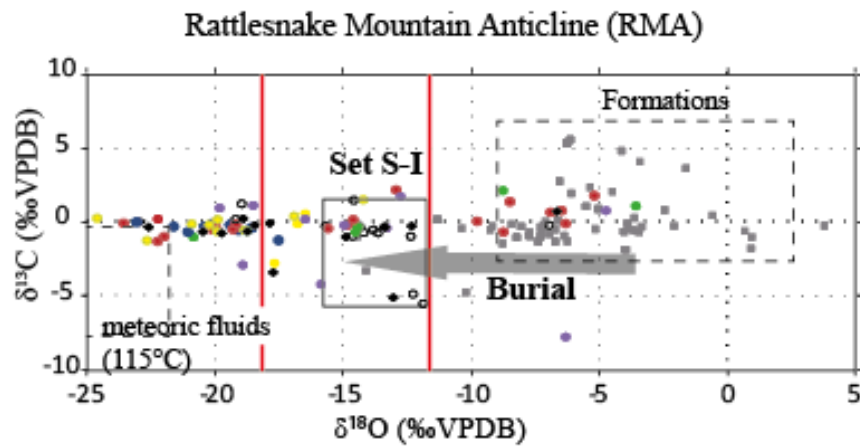
Evolution of fluid system in SMA and RMA
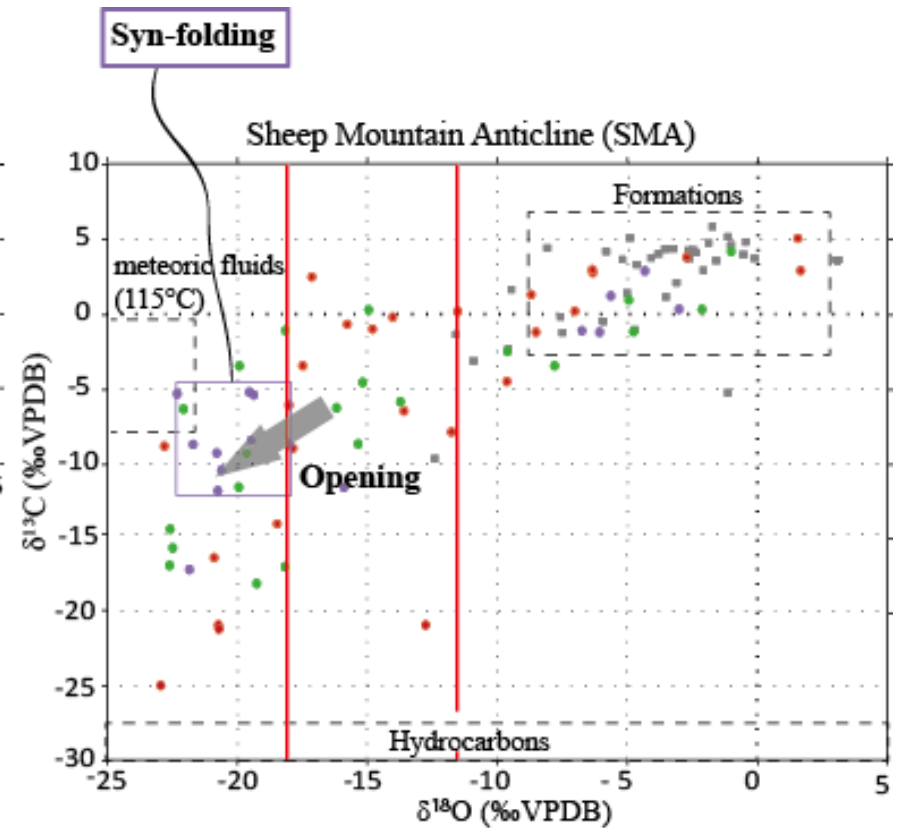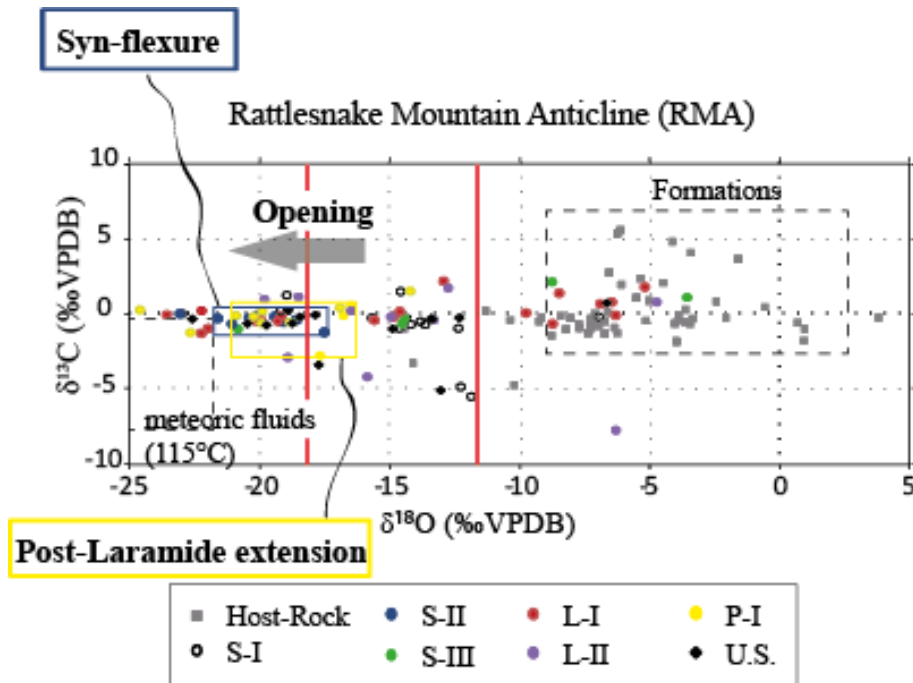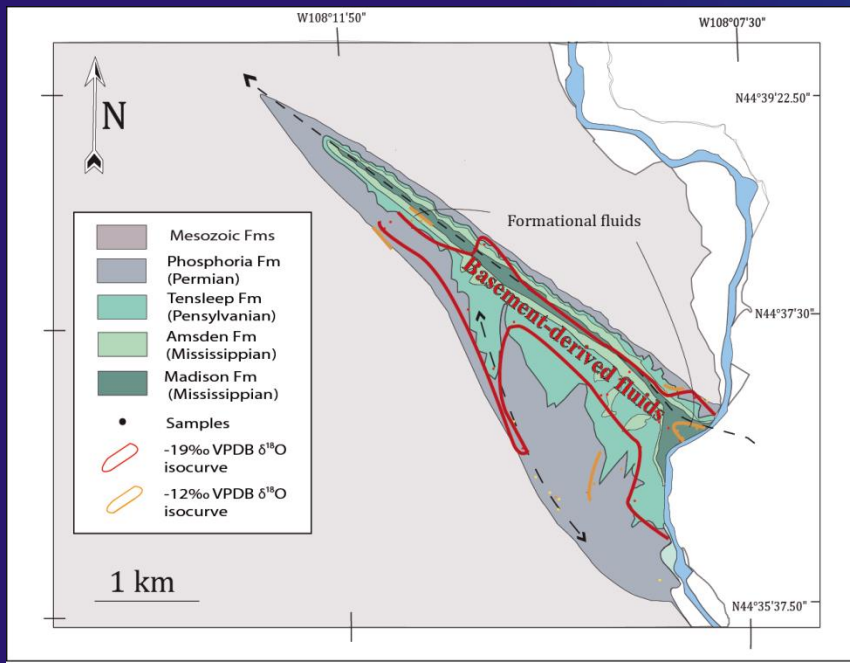
Localization of basement-derived hydrothermal fluid pulse at SMA

Vertical migration of deeper radiogenic hot fluids within the sedimentary cover explained by the development of curvature-related fractures that enhance the hydraulic permeability of the reservoir and break fluid compartmentalization by stratigraphy.

Link with structural style

(Beaudoin et al, G3, 2011; Evans and Fischer, 2012)
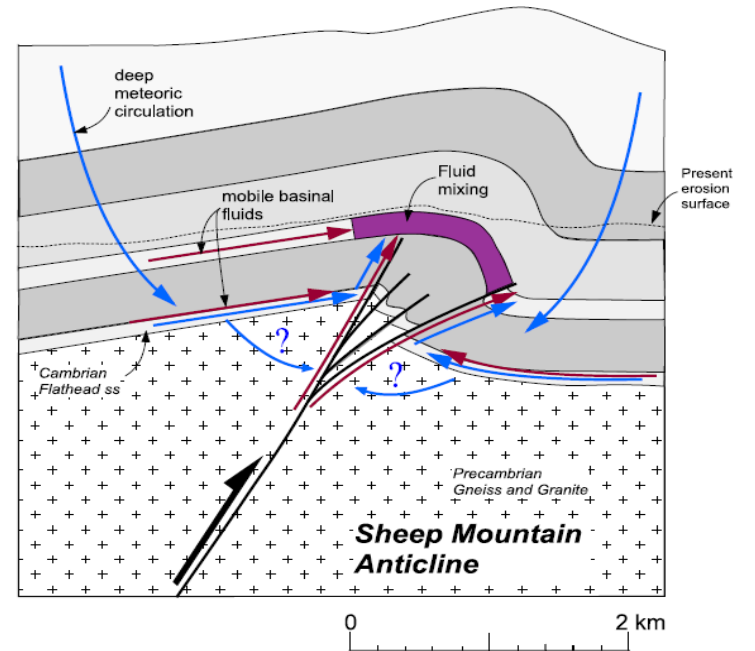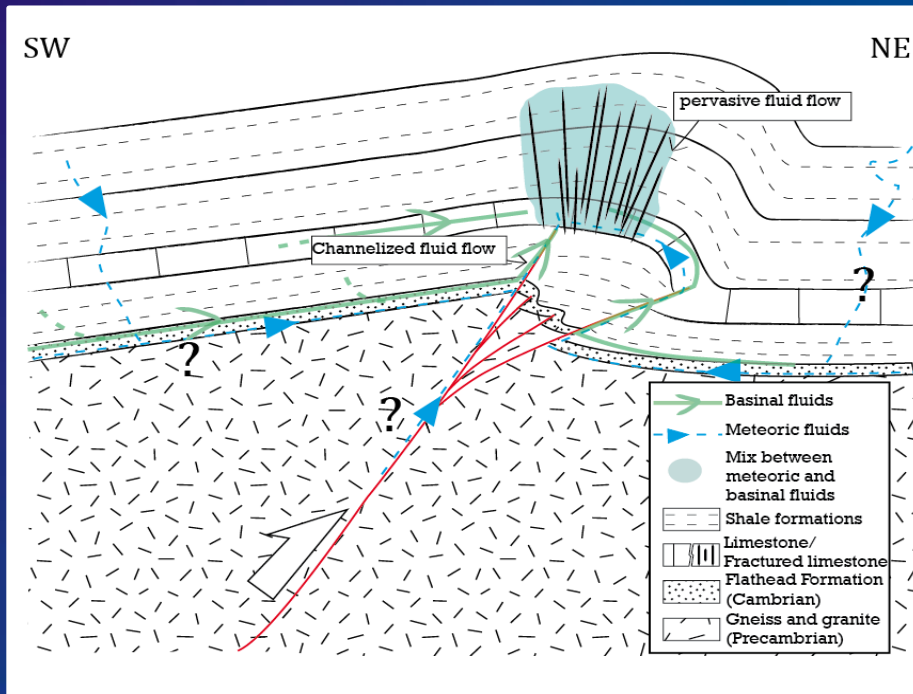
Paleo-hydrogeology of the Bighorn basin
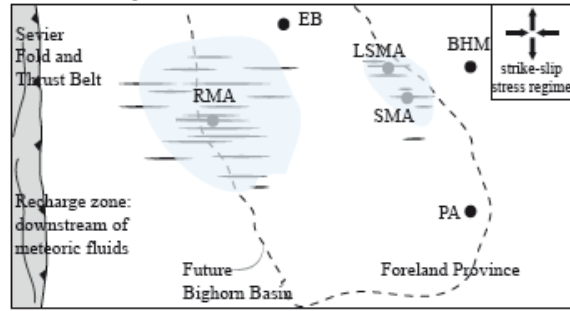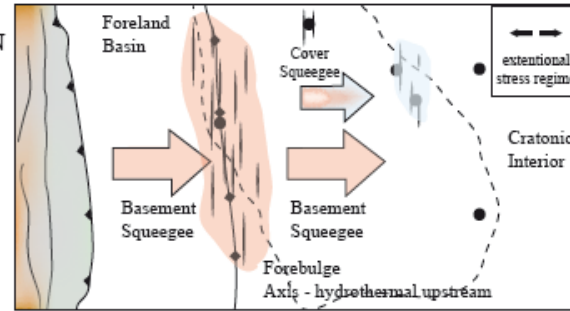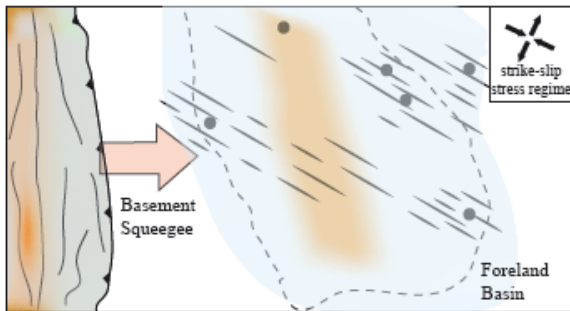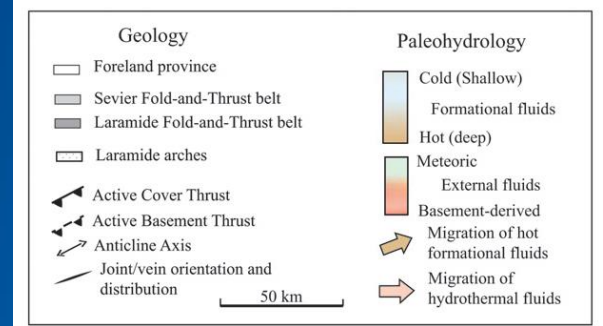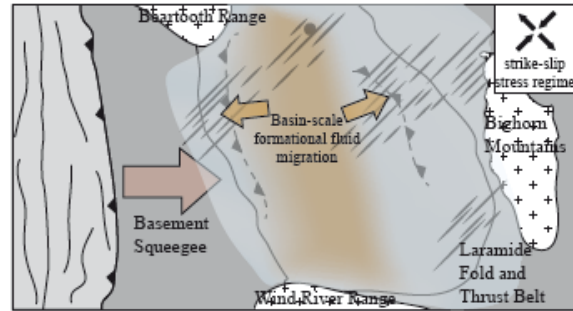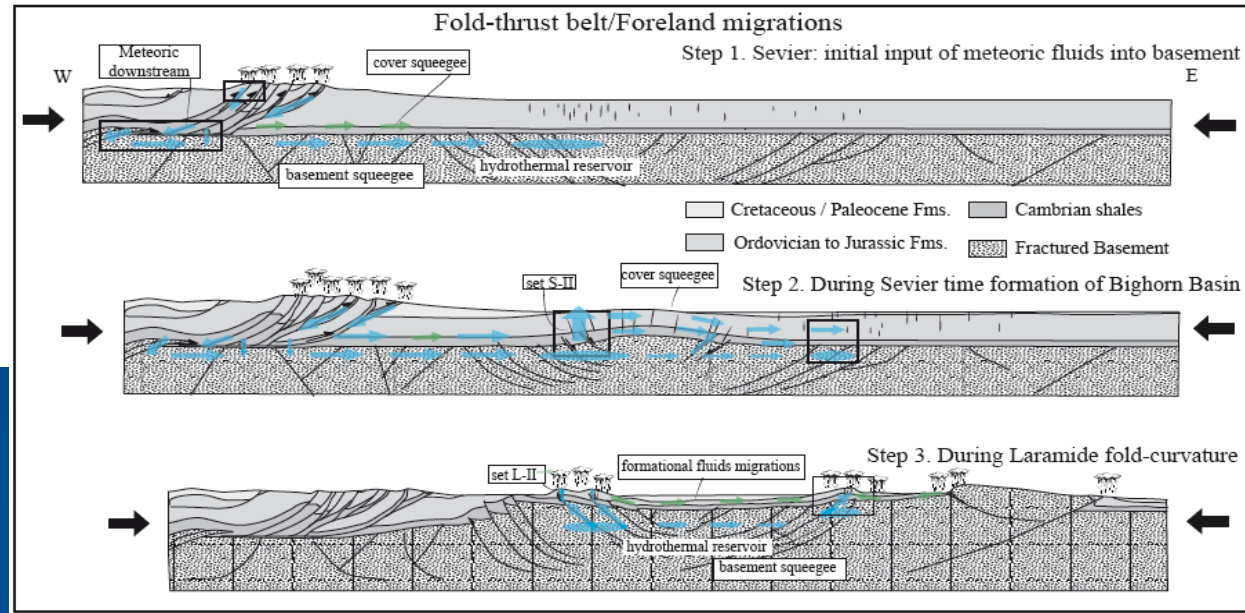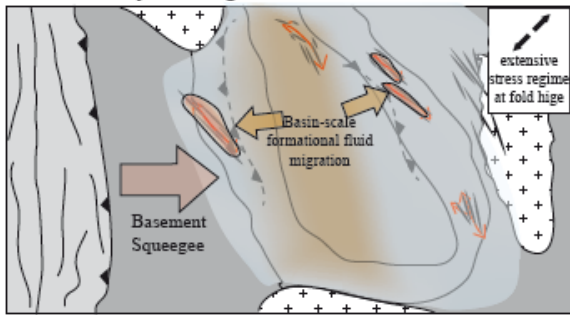
(Beaudoin et al., Basin Research, 2014)

Quantification of principal stress magnitudes and fluid (over)pressures at Sheep Mountain and Rattlesnake Mountain anticlines

Quantifying principal stress magnitudes

Finding for each deformation step, using a simple Mohr construction, the values of σ_1, σ_2 and σ_3 required for consistency between differential stresses estimated from calcite twinning, frictional sliding along preexisting planes (i.e., Byerlee's law) and newly formed faulting/fracturing.

(Lacombe and Laurent, 1992; Lacombe, 2001)

a

b
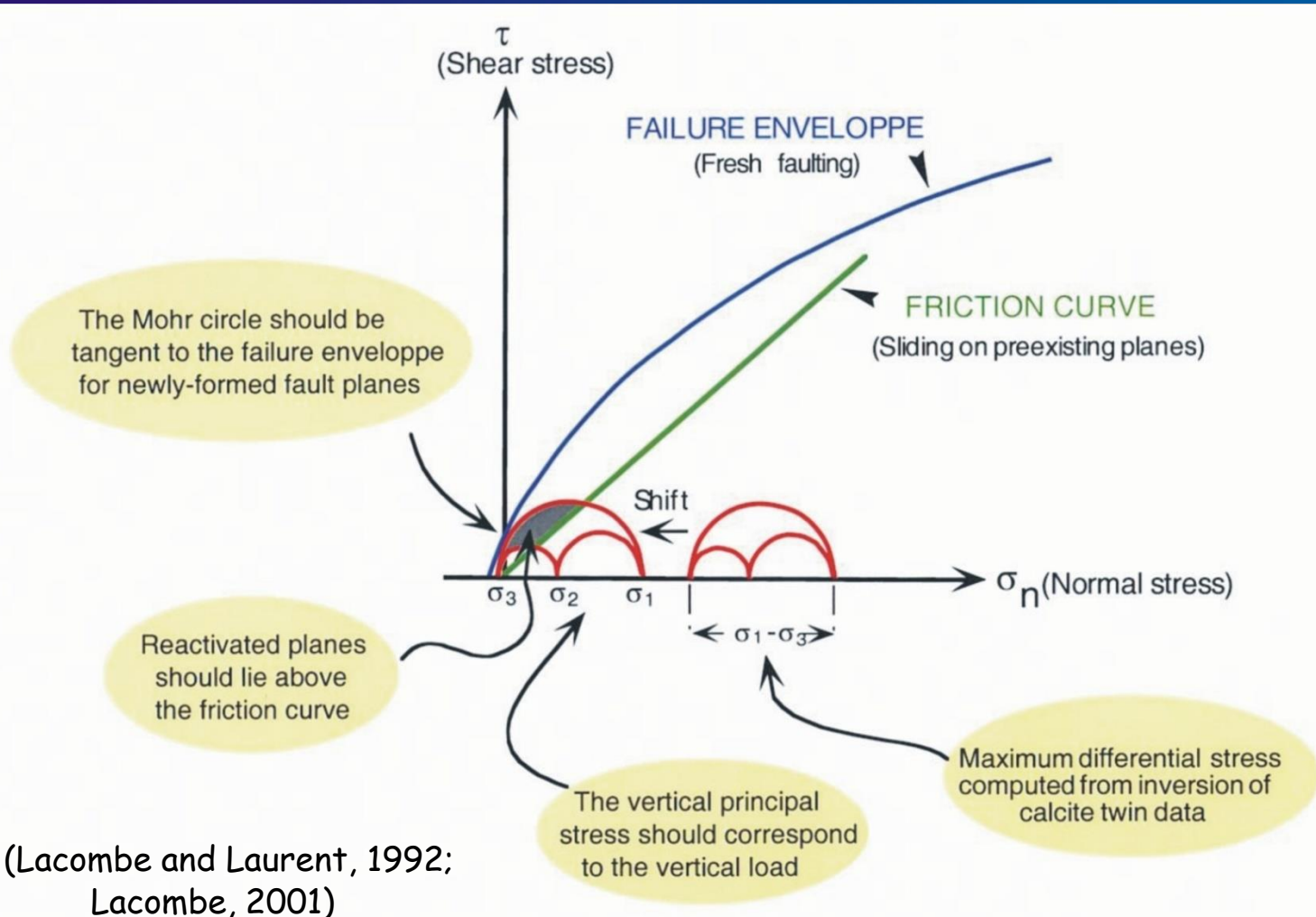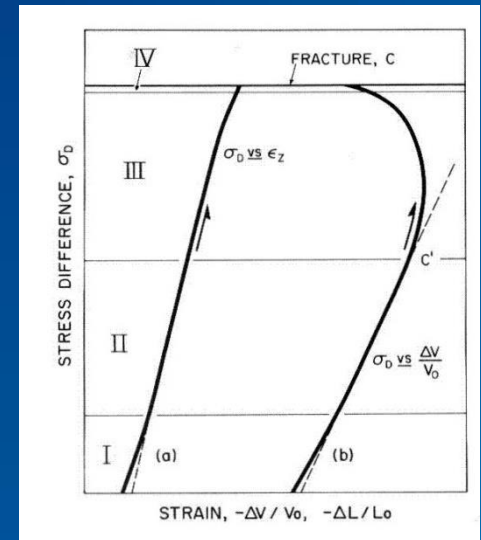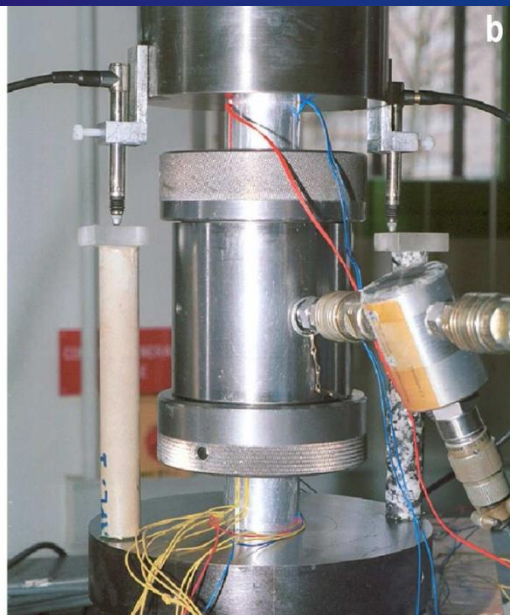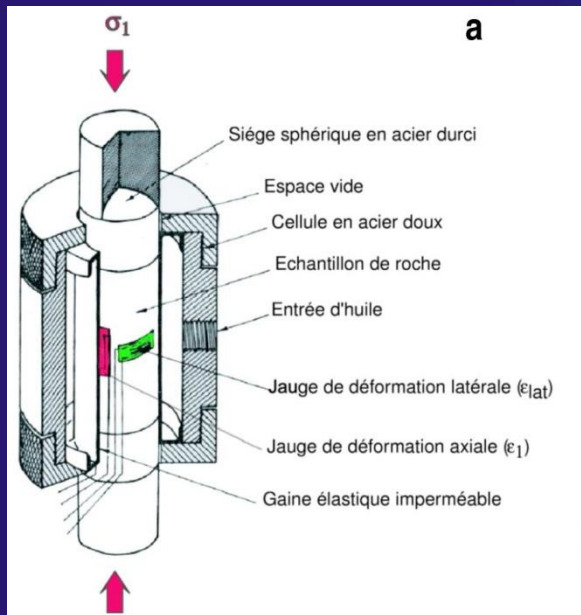
Experimental determination of the intrinsic failure envelopes of the
Phosphoria and Madison formations
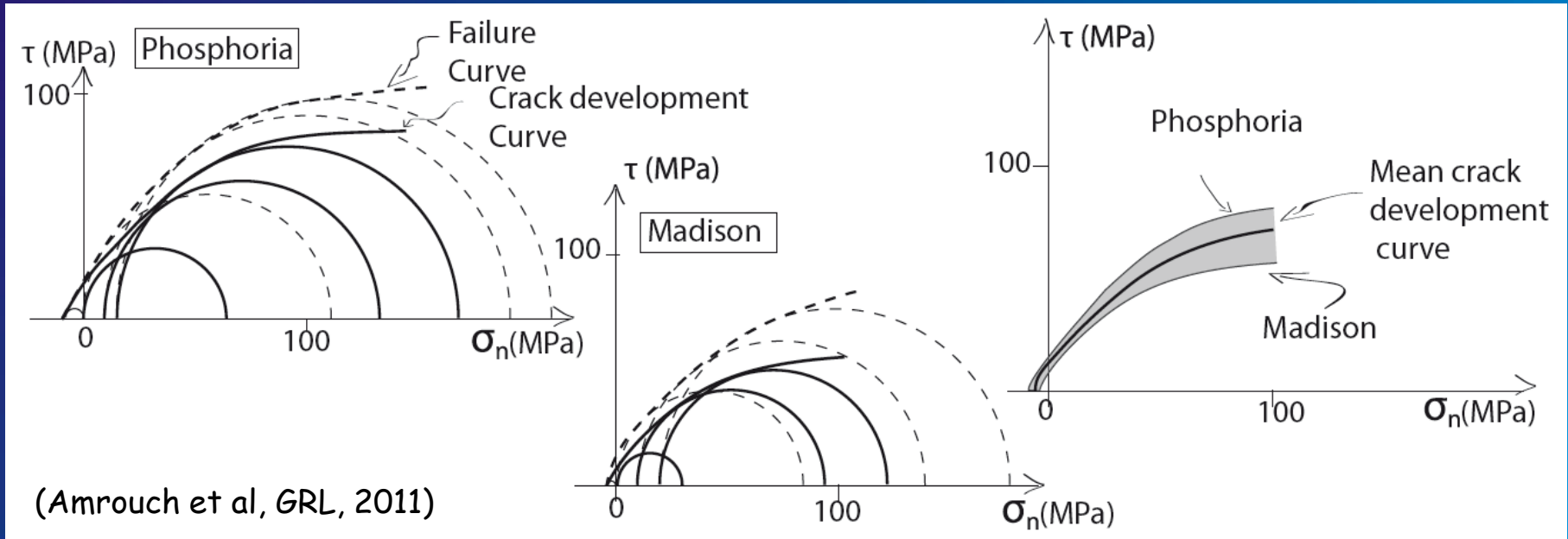
(Amrouch et al, GRL, 2011)
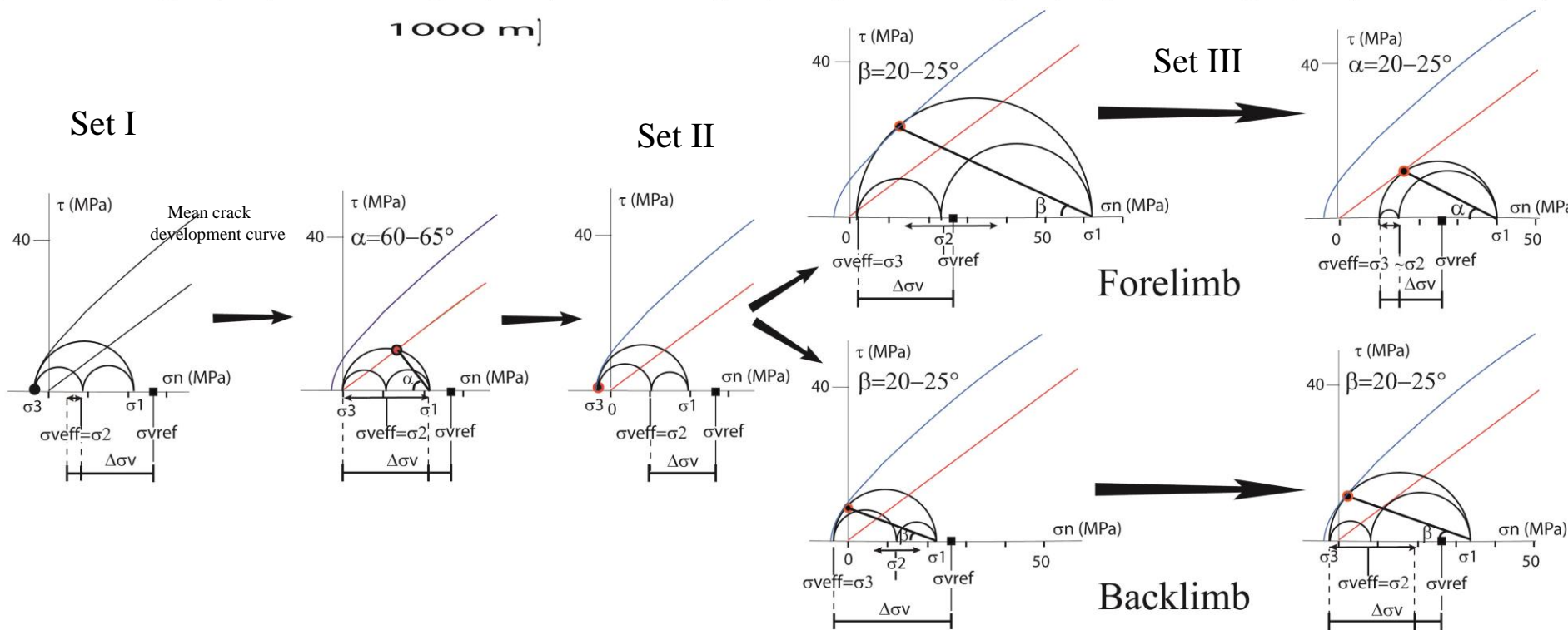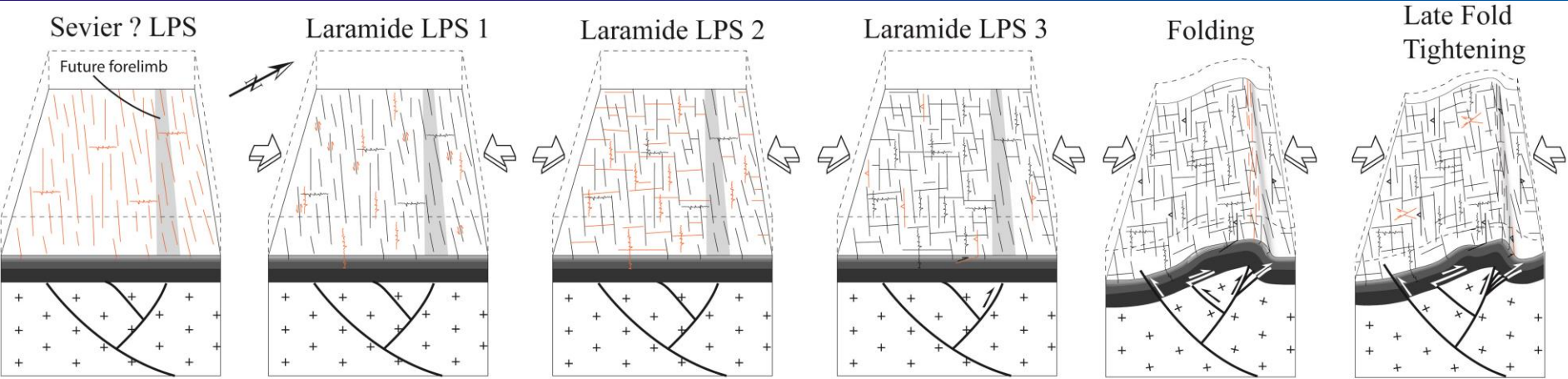
Determination of principal stress magnitudes using simple Mohr constructions (SMA)

(Amrouch et al, GRL, 2011)

The estimated paleo- principal stress magnitudes are in the range of 20-60 MPa for $\sigma 1$ and -3-10 MPa for $\sigma 3$ in the limestone rocks deformed at 1000-2000m depth.

These estimates are amongst the very few ones available for upper crustal paleo-stresses at the particular time of tectonic deformation (e.g. Taiwan, Lacombe, 2001).

Quantifying paleo fluid (over)pressure
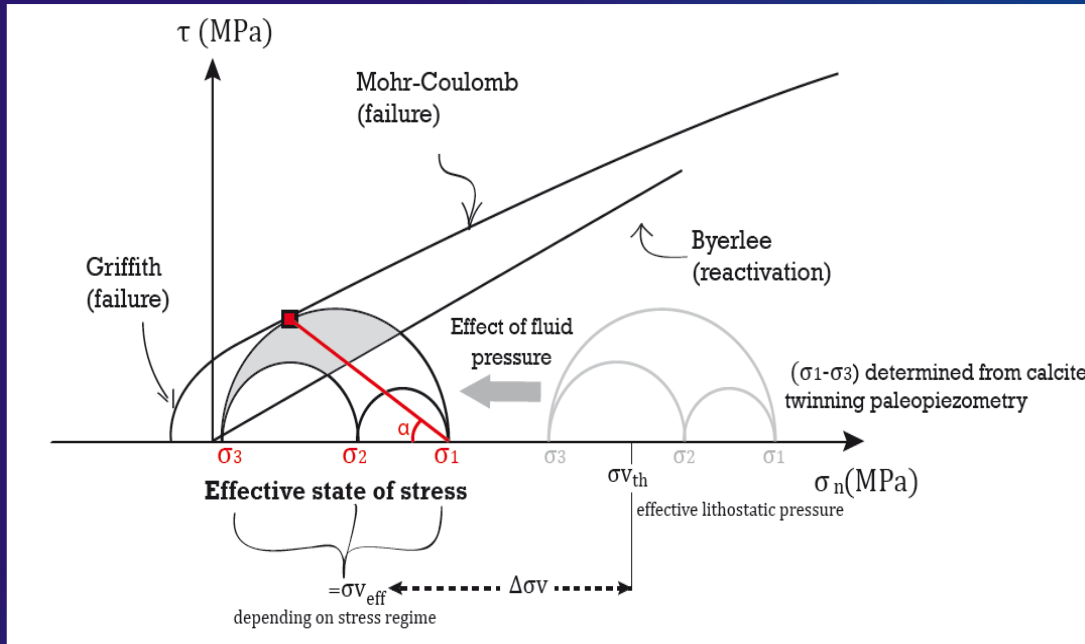
Assumption of a vertical principal stress equal to the effective weight of overburden

Theoretical effective vertical principal stress calculated considering lithostatic pressure corrected from hydrostatic fluid pressure:

$$\sigma_{vref} = (\rho - \rho_w).g.h$$

Comparison between σ_{vref} and the reconstructed effective vertical principal stress σ_{veff} :

$$\Delta\sigma_v = \sigma_{vref} - \sigma_{veff}$$

A non-zero $\Delta\sigma_v$ reflects either fluid over- or under-pressure or burial changes (sedimentation or erosion): when $\Delta\sigma_v$ is positive, either the burial depth was less than the value considered for the calculation of σ_{vref}, or the system was overpressured.
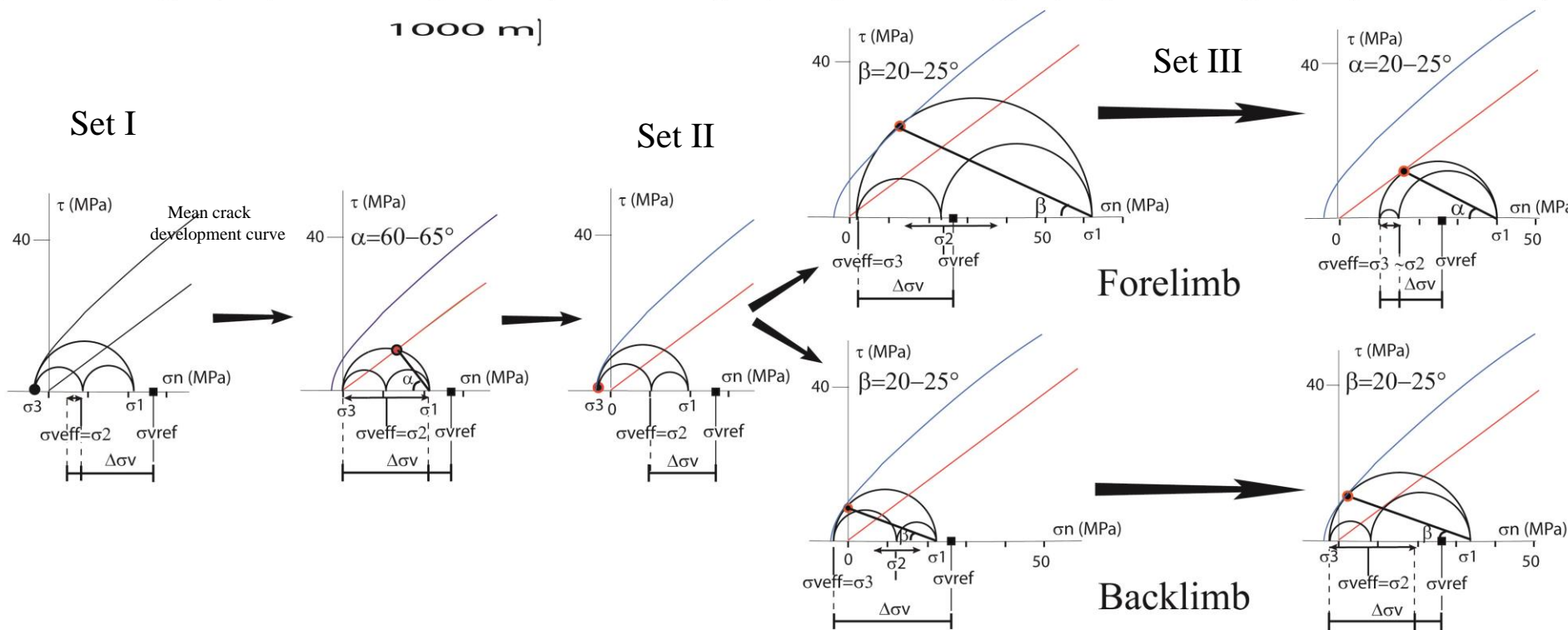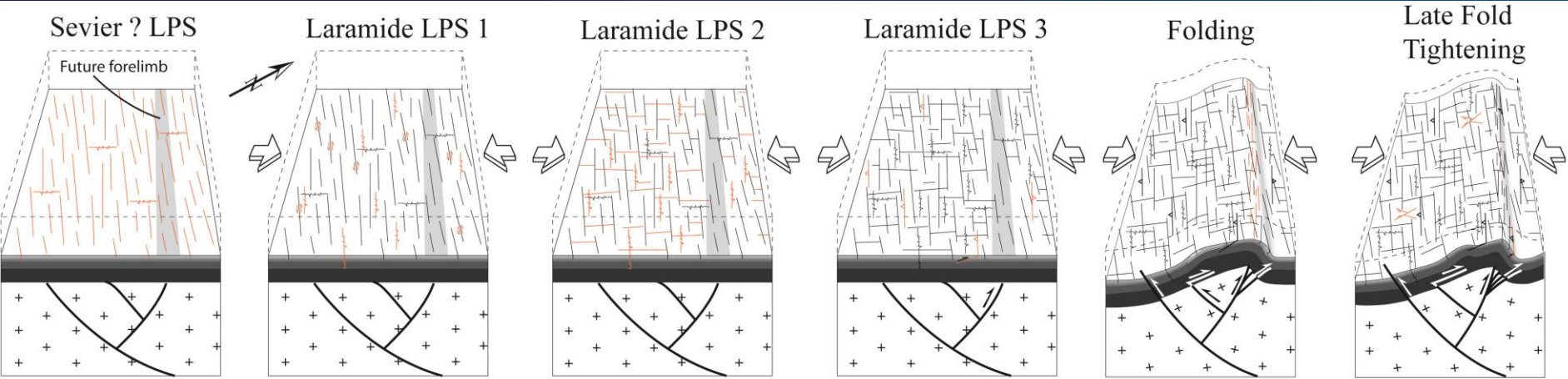
Determination of $\Delta\sigma_v$

(Amrouch et al, GRL, 2011)

(Beaudoin et al., MPG, 2014)

Comparison of $\Delta\sigma_v$ evolution
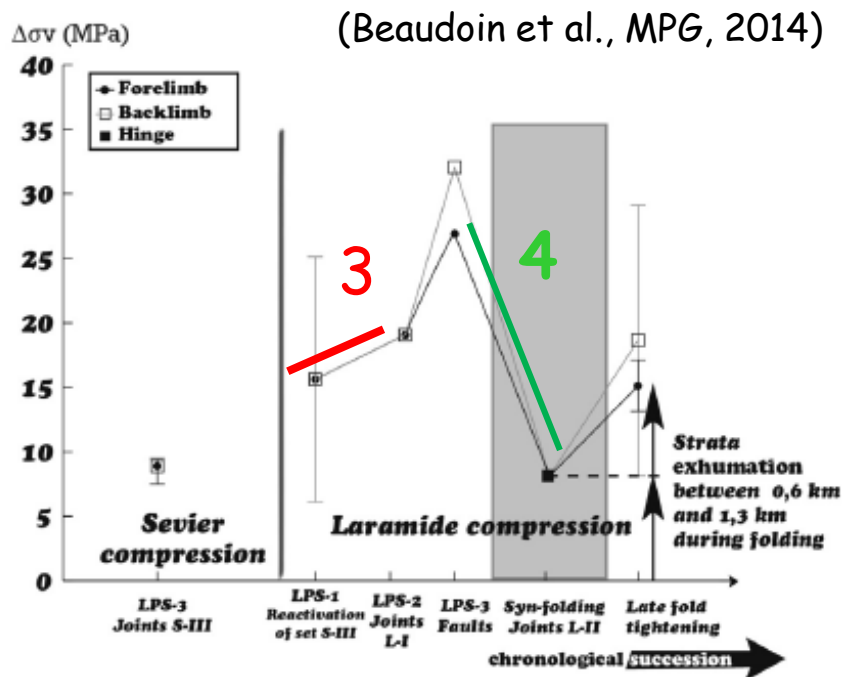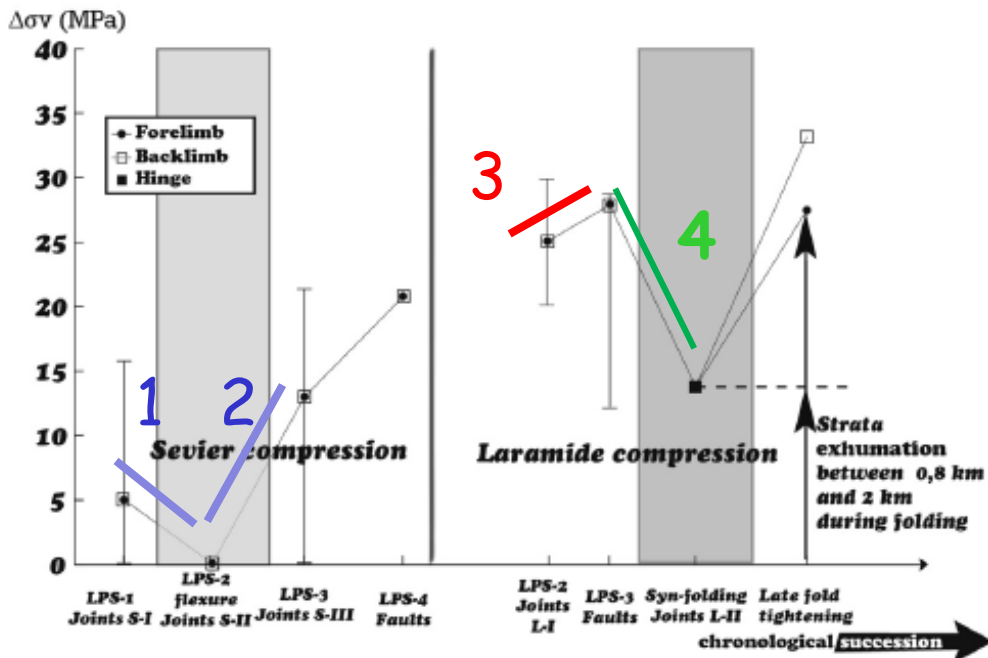
1. Decrease in fluid overpressure from early Sevier LPS to Sevier foreland flexure due to enhanced permeability by flexure-related extensional fractures.

2. Increase during late Sevier-LPS by input of exotic fluids as supported by geochemistry of vein cements.

3. Increase during Laramide LPS due to porosity reduction by pressure-solution/poor hydraulic permeability of fracture sets due to low vertical persistence or to their fast healing/strong increase in horizontal stress magnitude / input of exotic fluids into the reservoir in response to a large-scale fluid migration.

4. Drop due to development of curvature-related fractures that enhanced the hydraulic permeability of the reservoir. Break of fluid compartmentalization within the Madison-Phosphoria core consistent with geochemistry of syn-folding vein cements that suggests a vertical migration of deeper radiogenic hot fluids within the sedimentary cover.

Estimates of syn-folding erosion

a) Sheep Mountain Anticline

$\Delta\sigma v$ (MPa)

— Forelimb
□ Backlimb
■ Hinge

Sevier compression

Laramide compression

Strata exhumation between 0,6 km and 1,3 km during folding

LPS-3 Joints S-III | LPS-1 Reactivation of set S-III | LPS-2 Joints L-I | LPS-3 Faults | Syn-folding Joints L-II | Late fold tightening

chronological succession

b) Rattlesnake Mountain Anticline

$\Delta\sigma v$ (MPa)

— Forelimb
□ Backlimb
■ Hinge

Sevier compression

Laramide compression

Strata exhumation between 0,8 km and 2 km during folding

LPS-1 Joints S-I | LPS-2 flexure Joints S-II | LPS-3 Joints S-III | LPS-4 Faults | LPS-2 Joints L-I | LPS-3 Faults | Syn-folding Joints L-II | Late fold tightening

chronological succession

The post-folding Δ_{sv} value can be used to calculate the eroded/ burial thickness E as well as the post-folding overburden thickness H

$$E = \Delta_{sv} / [(\rho_{rock} - \rho_{water})g]$$
$$H = [\sigma_{vth} - \Delta_{sv}] / [(\rho_{rock} - \rho_{water})g]$$

The high Δ_{sv} value recorded during the LSFT suggests exhumation of the strata, consistent with the development of topography during folding.

Drastic drop in fluid pressure during folding :
-either a hydrostatic fluid pressure prevailed in the reservoir → exhumation :1.3/ 2km at SMA/RMA
-or a supra-hydrostatic fluid pressure still persisted after folding (overpressure not totally released) → syn-folding value of Δ_{sv} reflects the remaining fluid overpressure
→ exhumation : 0.6/0.8 km at SMA/RMA

Assuming a syn-folding erosion of 0.6-2.0 km and a duration of folding of 5-20 Ma → exhumation rate by folding of 0.03-0.40 mm/yr, consistent with exhumation/rock uplift rates in other Laramide arches derived from LT thermochronology and paleoelevation/basin analyses.

Comparison with values of fluid overpressures in sedimentary basins
derived from paleo-pressure reconstructions based on gas composition in hydrocarbon fluid inclusions or from direct measurements in limestone or shale/sandstone reservoirs.

(Beaudoin et al., MPG, 2014)
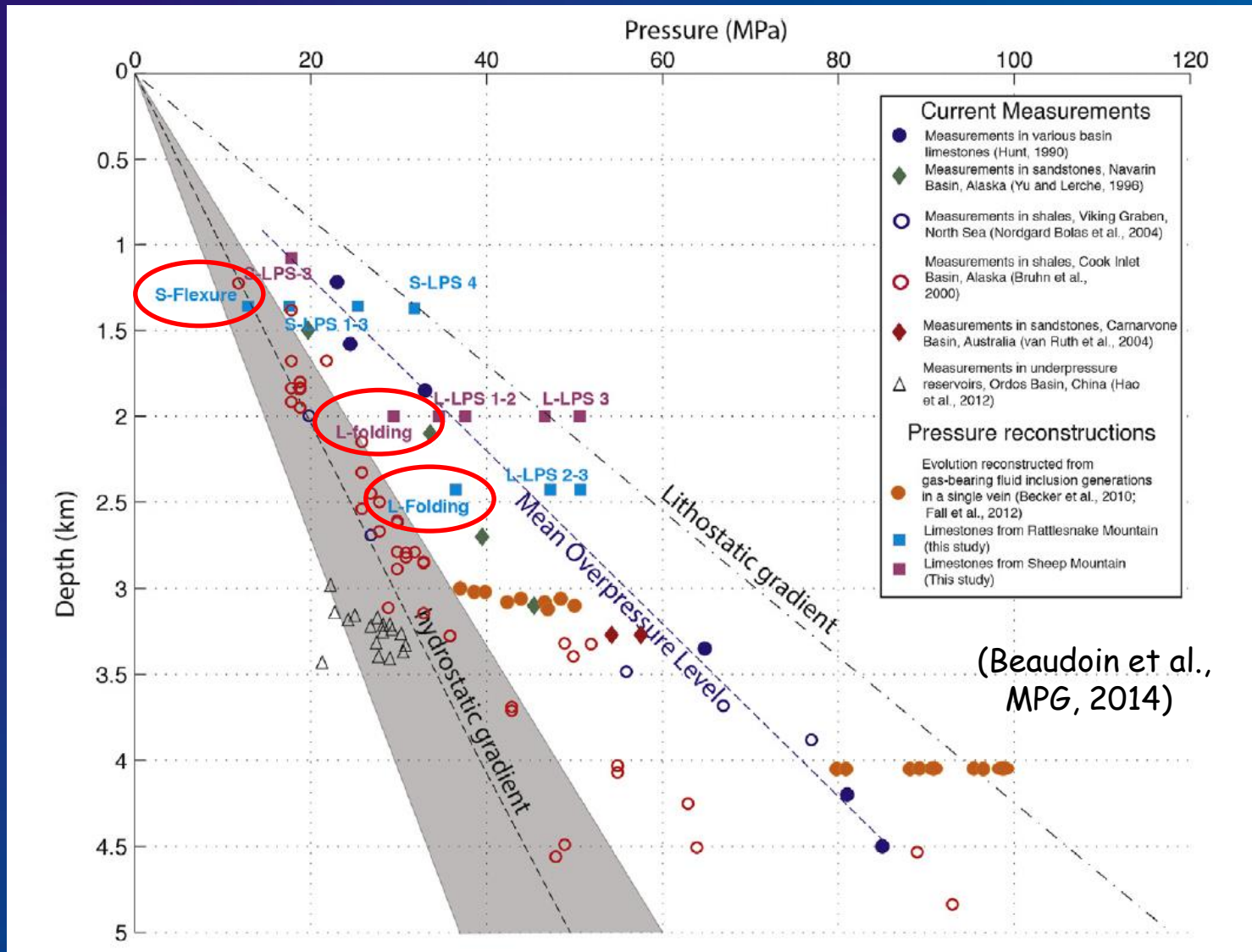
Overall conclusions

First integrated picture of stress and strain in folded strata at different scales, and operating mechanisms of deformation

First picture of the evolution of stress magnitudes and pore fluid (over) pressure through time.
Development of fluid overpressure in carbonate strata largely controlled by vertical hydraulic permeability of fractures;
Fractures formed under an extensional stress regime more efficiently trigger fluid exhaust.

Changes in P-T-X conditions, fluid flow, fluid (over)pressure and fracture development as well as stress and strain pattern within folded strata linked to the geometric/kinematic macroscopic evolution of folds → key to a better characterisation of folded-fractured reservoir behaviour

Reliability and power of studies of sub-seismic fracture populations for paleo-hydrological reconstructions Complement fault zone studies

Feedbacks between deformation, tectonic style and paleo-hydrology

Thank you